ASSESSMENT OF ACUTE RADIATION OUTSIDE LOW EARTH ORBIT: LIKELIHOOD AND INTEGRATION FOR MISSION RISKS

A Dissertation

by

SARAH ELIZABETH OVER

Submitted to the Office of Graduate and Professional Studies of
Texas A&M University
in partial fulfillment of the requirements for the degree of

DOCTOR OF PHILOSOPHY

Chair of Committee,	John Ford
Co-Chair of Committee,	Leslie A. Braby
Committee Members,	John W. Poston, Sr.
	Robert R. Lucchese
Head of Department,	Yassin A. Hassan

May 2017

Major Subject: Nuclear Engineering

ABSTRACT

For human spaceflight missions outside low Earth orbit, there is an increased risk to astronaut health due to space radiation. Solar particle events are one of the components of space radiation that constitute this risk due to their probabilistic nature in occurrence and severity. From 30 years of solar particle data, an analysis of solar particle events was conducted to derive model components for a probabilistic risk model. After generating fluence spectra from the data analysis, dose from each event was calculated through the use of one of NASA's online space radiation assessment tools, OLTARIS. To form the final model, a combination of the fluence and dose distributions with a literature occurrence rate model were integrated. Finally, an orbital scaling factor was applied to reduce event fluence further from the Sun and increase event fluence closer to the Sun.

After verification and validation, the solar particle probabilistic risk model was used to generate the number of expected solar particle event numbers for a spacecraft with 5 g/cm^2 of aluminum shielding for different Mars transits. The transit with the highest risk was a Mars to Earth Venus swing-by transfer, which had approximately triple the number of expected solar particle events and four times the total expected transit dose compared to the other Mars transits. This result was expected since the Mars-Venus-Earth has the longest transit, and brings the spacecraft closest to the Sun, increasing exposure time and intensity. The average expected doses, even for the highest risk transit, are not likely to cause major astronaut health or mission impacts, but may need to be accounted for during mission planning and design. Future work on this model may include development of different shielding levels, application of more complex orbital scaling factors, and organ specific dose studies.

ACKNOWLEDGEMENTS

First thanks go to everyone at Texas A&M who have helped make this document possible. Those in the Nuclear Engineering Department include: John Ford, Leslie Braby, and John Poston for being part of my committee and working with me throughout this process, Robb Jensen for all of his programmatic help, the department head Yassin Hassan for his assistance in securing another year of departmental funding, my former officemate David Saucier for being a sounding board, and Debbie Greer for all things HR.

Outside of my home department, thanks go to those in the Space Life Sciences program including Nancy Turner and Sue Bloomfield for their advice and feedback throughout my studies, Robin Lucchese for taking a break from chemistry to sit on my committee, and Paul Sikes, formerly part of the TAMU Bands program for our discussions about all things science and music including famous orchestral works and my dissertation research.

Other thanks to those in the College Station area include those who have supported me at my church and all of the medical professionals who helped me to understand how graduate school and having a chronic illness are not incompatible. Also, thanks to my roommates this past year for listening and being understanding whether my research was going slowly or efficiently.

Finally, thanks to everyone around the country who gave me support of all kinds during my doctoral program. These include the Integrated Medical Model team at NASA Glenn Research Center and Johnson Space Center, especially my NASA mentor Jerry Myers, and DeVon Griffin and Millennia Foy for their contributions to making my research possible. Last, thanks to my family for all of their support

and help including my aunt Julie, my grandparents, Stan and Judy, my brother and sister-in-law Ryan and Erin, my “little” sister Molly, and my parents Ann and Randy, who have always let me find my own path and gave me encouragement on the way.

CONTRIBUTORS AND FUNDING SOURCES

Contributors

This work was supported by a dissertation committee consisting of Professors John Ford (Chair), Leslie Braby (Co-Chair), and John Poston from the Department of Nuclear Engineering with Professor Robert Lucchese of the Department of Chemistry.

MATLAB code implemented in the risk assessment model for frequency of solar events was adapted from work by Millennia Foy of Wyle Laboratories, NASA Johnson Space Center. Jerry Myers of NASA Glenn Research Center also served as a collaborator for the original iteration (Summer of 2014) of the risk assessment model for application into the NASA Integrated Medical Model.

All other work conducted for the dissertation was completed independently.

Funding Sources

Graduate study was supported through funding from inside and outside the university. Two years of study were funded through the Nuclear Engineering Department's graduate teaching assistantships, through providing support to laboratory courses. Another two years of study were supported through the National Space Biomedical Research Institute's Mentored Research Program in Space Life Sciences (NCC 9-58), which included funding for a summer research project at a NASA center and travel to NASA's yearly Human Research Program workshop. Last, supplemental funding for one year was provided through the Texas Space Grant Consortium through their Graduate Fellowship Program.

NOMENCLATURE

ACE	Advanced Composition Explorer
ALARA	As Low As Reasonably Achievable
ARRBOD	Acute Radiation Risk and BRYNTRN Organ Dose (Projection)
ARS	Acute Radiation Sickness
BRYNTRN	BaRYoN TRaNsport (code)
CAF/CAM	Computerized Anatomical Female/Male
CI	Confidence Interval
CME	Coronal Mass Ejection
CNS	Central Nervous System
COSTEP	Comprehensive Suprathermal and Energetic Particle Analyzer
CRaTER	Cosmic Ray Telescope for the Effects of Radiation
CREME	Cosmic Ray Effects on Micro-Electronics
DRA	Design Reference Architecture
Dst	Disturbance Storm Time
EDE	Effective Dose Equivalent
EMMREM	Earth-Moon-Mars Radiation Environment Module
EPEAD	Energetic Proton, Electron, and Alpha Detector(s)
EPS	Energetic Particle Sensor
ESA	European Space Agency
ESP	Emission of Solar Protons
EVA	Extra-Vehicular Activity
ExMC	Exploration Medical Capabilities
GCR	Galactic Cosmic Ray (Radiation)

GEANT	GEometry And Tracking
GEO	Geostationary/Geosynchronous Earth Orbit
GLE	Ground Level Enhancement
GOES	Geostationary Operational Environmental Satellite(s)
HEPAD	High Energy Proton and Alpha Detector
HSRB	Human System Risk Board
HZETRN	High charge (Z) and Energy TRaNsport
IMF	Interplanetary Magnetic Field
IMM	Integrated Medical Model
IMP	International Monitoring Platform
IRIS	Interface Region Imaging Spectrograph
ISS	International Space Station
JPL	Jet Propulsion Laboratory
LEO	Low Earth Orbit
LOC	Loss of Crew
LOM	Loss of Mission
NASA	National Aeronautics and Space Administration
NOAA	National Oceanic and Atmospheric Administration
OLTARIS	On-Line Tool for the Assessment of Radiation In Space
pfu	Particle Flux Unit
PREDICCS	Predictions of radiation from REleASE, EMMREM, and Data Incorporating CRaTER, COSTEP, and other SEP measurements
PSYCHIC	Prediction of Solar particle Yields for CHaracterizing Integrated Circuits

RAD	Radiation Assessment Detector
REleASE	Relativistic Electron Alert System for Exploration
SDO	Solar Dynamics Observatory
SEM	Space Environment Monitor
SEP	Solar Energetic Particle(s)
SEPEM	Solar Energetic Particle Environment Modeling
SOHO	SOlar and Heliospheric Observatory
SPE	Solar Particle Event (historical: Solar Proton Event)
SPENVIS	SPace ENVironment Information System
SPP	Solar Probe Plus
STEREO	Solar TErrestrial RElations Observatory
SWPC	Space Weather Prediction Center

TABLE OF CONTENTS

Page

ABSTRACT ii

ACKNOWLEDGEMENTS iii

CONTRIBUTORS AND FUNDING SOURCES v

NOMENCLATURE vi

TABLE OF CONTENTS ix

LIST OF FIGURES xii

LIST OF TABLES xiii

1. INTRODUCTION: SPACEFLIGHT RADIATION RISK ASSESSMENT . 1

    1.1 Space Radiation Overview 2
        1.1.1 Radiation Environment 2
        1.1.2 Exposure Effects and Mission Consequences 5
        1.1.3 Strategies and Countermeasures 8
    1.2 Alignment with Agency Level Risk Assessment 11

2. SOLAR ACTIVITY 13

    2.1 Historical Observations and Trends 13
        2.1.1 Quiescent Behavior 13
            2.1.1.1 Cycles 14
            2.1.1.2 Solar wind and the IMF 18
        2.1.2 Energetic Events 19
            2.1.2.1 Pre-space age data 22
            2.1.2.2 Space age data 24
    2.2 Modeling 28
        2.2.1 Solar Event Spectra 29
        2.2.2 Mission Analysis 31
    2.3 Prediction 35
        2.3.1 Cycle Progression 35
        2.3.2 Individual Event Arrival 38

2.4 Literature Summary . . . 42

3. HISTORICAL EVENT DATA ANALYSIS . . . 44

3.1 Data Sources . . . 44
3.1.1 Neutron Monitors . . . 44
3.1.2 Satellites . . . 46
3.1.2.1 IMP program . . . 46
3.1.2.2 GOES program . . . 48
3.2 GOES Data Selection . . . 52
3.3 Event Resolution . . . 55
3.3.1 Constraints Development . . . 55
3.3.2 Characterization . . . 59
3.3.3 Code Results . . . 61
3.4 Data Summary . . . 62

4. EVENT RISK CODE DEVELOPMENT . . . 64

4.1 Earth Orbit Model Basis . . . 65
4.1.1 Kim Occurrence Model . . . 66
4.1.2 Data Classification by Risk . . . 67
4.2 Dose from Transport . . . 68
4.2.1 Fluence Spectra Fits . . . 68
4.2.2 OLTARIS . . . 74
4.2.3 Dose Distribution Fit . . . 76
4.3 Orbital Location Adjustment . . . 79
4.4 Application of NASA Risk Assessment Methods . . . 81
4.4.1 Verification . . . 82
4.4.2 Validation . . . 84
4.4.3 Sources of Uncertainty . . . 86
4.4.4 Results Robustness . . . 91
4.5 SPE Risk Model Overview . . . 93

5. RISK PROFILES FOR LONG-DURATION MISSIONS . . . 96

5.1 Mars Design Reference Missions . . . 96
5.2 Event Likelihood and Consequences . . . 97
5.3 Mission Transit Risk Assessments . . . 99
5.3.1 180-Day GEO . . . 101
5.3.2 Mars Long-Stay . . . 102
5.3.2.1 Outbound . . . 103
5.3.2.2 Inbound . . . 104
5.3.3 Mars Short-Stay . . . 105
5.3.3.1 Outbound . . . 106

5.3.3.2 Inbound . . . 107
5.4 Discussion . . . 109

6. CONCLUSIONS AND IMPLICATIONS FOR FUTURE RESEARCH . . . 113

6.1 SPE Risk Model Outside LEO . . . 113
6.2 Opportunities for Further SPE Risk Assessment . . . 115

REFERENCES . . . 119

APPENDIX A. FULL SOLAR PARTICLE EVENT LISTING . . . 136

A.1 Integrated Fluences . . . 136
A.2 Filled Flux Points . . . 138

APPENDIX B. MATLAB CODE FILES . . . 139

B.1 Data Processing . . . 140
B.1.1 Primary SPE Calculation and Output . . . 141
B.1.2 Satellite Data Setup . . . 162
B.1.3 Special Cases . . . 170
B.2 Probabilistic Risk Code Files Content . . . 181

LIST OF FIGURES

FIGURE Page

2.1 Sunspot progression starting in 1870 15

2.2 Solar cycle progression since January 2000 17

2.3 Comparison of solar flares and CMEs 20

2.4 Record solar flare and CME from 2003 20

2.5 Sunspot predictions for Cycle 24 given in 2007 37

2.6 Sigmoid shaped magnetic region on the Sun 40

3.1 October 1989 event progression 56

3.2 Data analysis flowchart for MATLAB code 59

4.1 Fluence distribution curve fits for selected SPEs from 2001 70

4.2 Relationship of >60 MeV fluence and effective dose equivalent 77

4.3 Possible distributions for >60 MeV fluence 78

4.4 SPE probability variation over a non-specific solar cycle 83

4.5 Curiosity transit simulation SPE number distribution 86

4.6 Convergence of average number of events for 1 Sv 90

4.7 SPE risk model flowchart 94

5.1 Mars design reference architecture proposed mission orbital transfers 97

5.2 NASA risk matrix for consequence and likelihood 98

5.3 Short-stay return 1 Sv distribution 110

5.4 Short-stay return dose distribution 111

LIST OF TABLES

TABLE Page

2.1 Top SPEs since 1955 27

5.1 Mission transit risk assessment results for all cases at solar maximum 100

5.2 180-day GEO SPE number and dose results 101

5.3 Mars long-stay outbound SPE number and dose results 103

5.4 Mars long-stay inbound SPE number and dose results 104

5.5 Mars short-stay outbound SPE number and dose results 106

5.6 Mars short-stay inbound SPE number and dose results 108

5.7 Probability of 1 Sv or higher events during transit 109

1. INTRODUCTION: SPACEFLIGHT RADIATION RISK ASSESSMENT

As space agencies all over the world seek to expand human spaceflight outside of low Earth orbit to Mars and beyond, there is an increased need to understand the risks present for these long-duration missions, especially those risks due to the unique radiation environment of space. For humans to survive and thrive for years away from Earth, risks need to be characterized and mitigated or accepted before these missions take place. To fully evaluate risk from the environment in space, physical, physiological, and psychosocial risks need to be considered both individually and as an integrated system. Radiation risks include aspects of all three of these areas, in that radiation can cause damage to electronics on the spacecraft, cause acute or chronic health effects to astronauts, and in a storm scenario, astronauts might be confined to a small part of the spacecraft for days for protection causing psychosocial risk. Additionally, radiation effects can work synergistically with other risk areas such as microgravity, possibly impacting the rate and type of bone and muscle loss. Some risks can be characterized through the use of ground experiments (specific biological endpoints) and analogs for psychosocial risks (Antarctic missions), but not all, and the remainder need computational modeling approaches followed by testing during missions to determine the level of risk. The research presented here uses this latter approach through utilization of data garnered over decades of space exploration paired with probabilistic risk assessment techniques to examine risks specifically associated with solar events.

1.1 Space Radiation Overview

Space radiation has been called a possible "show-stopper" for future missions beyond Earth orbit. The National Aeronautics and Space Administration (NASA) has categorized space radiation risks by their effects into the focus areas of: radiation carcinogenesis, acute radiation syndromes, acute or late central nervous system effects, and degenerative tissue or other health effects [*McPhee and J. B. Charles, eds.*, 2009]. Research into these risk areas answers questions such as "How much will an astronaut's chance of having (an exposure induced) cancer increase by completing this mission" or "What central nervous system effects will the radiation found in space induce?"

1.1.1 Radiation Environment

For any mission to space, but especially those outside low Earth orbit (LEO), there are three main components plus secondary particles of the space radiation environment that need to be considered. The first component that astronauts will encounter as they travel beyond LEO is trapped radiation - the Van Allen Belts and other particles trapped by the Earths magnetic field. Traversal of the belts takes only a short time during a long-duration mission, and so this exposure does not contribute significantly to a long-duration mission dose. Once through the radiation belts, astronauts will be out of the partial protection of Earth's magnetic field and be exposed to a higher level of radiation from the latter two radiation sources: galactic cosmic rays (GCRs) and solar particle events (SPEs). Finally, from all of these radiation sources, secondary particles such as neutrons and various ions can also be produced, further complicating the space radiation environment.

The trapped radiation astronauts will encounter during the transit from LEO to higher orbits is composed mostly of protons and electrons. Trapped radiation

particles move in spiral motions about the magnetic field lines, bouncing back and forth between mirror points and eventually falling into the upper atmosphere after losing enough energy. These particles persist throughout the Earth's magnetosphere, but are concentrated into two regions, one at an altitude of around 3,200 km and another at 16,000 km [*Knipp et al.*, 2011c]. The lower/inner belt and South Atlantic Anomaly are mostly composed of protons produced through interactions between GCRs and the atmosphere. The higher/outer belt is composed of more electrons, picked up from GCRs and solar energetic particles [*Knipp et al.*, 2011c]. Other than the two Van Allen Belts, additional belts can also appear during solar storm conditions or human produced particle injections such as nuclear explosions (as shown through the STARFISH project in 1962 [*Knipp et al.*, 2011d]).

GCRs are the low fluence rate (flux) background particle radiation, modulated by the solar cycles that stream into the solar system from the galaxy and intergalactic space. These particles are ions likely produced by the acceleration of particles generated in events such as supernovas, bringing them to energies of 1 GeV/nucleon (and higher) while stripping the particles of their electrons in the process [*NCRP*, 2006]. The relative abundance of GCR ions is similar to the natural elemental abundance found in the solar system, with hydrogen ions being the most prevalent (around 90 percent) and uranium ions being the most rare. Although the energies are quite high compared to terrestrial radiation, the fluence rate is quite low compared to other aspects of the space radiation environment, meaning that the highest energy and heaviest particles hit objects the size of a biological cell quite infrequently (some less than once a year). Finally, depending on the location of a long-duration mission, astronauts will experience a lowered fluence rate if a destination has an atmosphere or a global magnetic field. Mars for example does not have a global magnetic field, but does have an atmosphere that will provide some shielding.

Radiation from the Sun includes a variety of waves and particles including the solar wind and SPEs. These sources vary throughout the solar cycle with SPEs becoming more frequent as solar maximum approaches and then falling off again approaching solar minimum. The solar wind is the result of plasma outflow from the Sun's atmosphere, bringing with it the solar magnetic field lines along which active eruptions travel. Solar wind particles are generally protons and electrons with fairly low energies compared to GCR ions and have a lower ion density [*Knipp et al.*, 2011e]. As the active part of solar radiation, SPEs can vary widely with the types of particles involved and energies of each event. Research is still ongoing into the generation of SPEs by different research disciplines, so there are various terms and classifications depending on the source [*Knipp et al.*, 2011h; *NCRP*, 2006; *National Research Council*, 2008]. Generally though, it is agreed that events can be impulsive or gradual with wide variations in the number of particles, frequency of waves, and magnitude of energies involved in each class. The more impulsive events can include flares, where the particles travel along a fairly narrow group of magnetic field lines from the Sun, arriving at the Earth on the order of minutes to hours. More gradual events can include those SPEs of higher concern for human spaceflight in that these can be spread over a larger part of the solar longitude and have shock enhancements producing a wide swath of energetic particles. These gradual events are also associated with coronal mass ejections, which can last for days with higher levels of particle radiation than impulsive events. There are other various processes that produce energetic particle radiation output from the Sun, but the ones listed above are the most relevant for understanding the generation and propagation of solar radiation sources.

The final aspects of the space radiation environment that astronauts might encounter on a long-duration mission depend on destination and vehicle design. If

traveling to the Moon, the radiation environment will be similar to free space and the transit will be short. But, if traveling to Mars, the transit will be long, but further from the Sun, and the thin atmosphere will afford a measure of shielding, although it does not have a global magnetic field like Earth. Finally, a nuclear power or propulsion source may be used depending on the mission parameters, adding a new component to the radiation environment astronauts will face.

1.1.2 Exposure Effects and Mission Consequences

As listed above, NASA has categorized the possible detrimental effects due to radiation risk for astronauts into four categories with acute radiation syndromes and acute central nervous system (CNS) effects being of concern during extended missions. In addition, other early effects are possible such as disruptions to homeostasis, skin effects, and the well-known light flashes that occur in space could all have an impact on a mission depending on the astronaut and the timing of their duties [*NCRP*, 2006]. Radiation carcinogenesis, late CNS effects, and degenerative risks are effects that may not be seen until years after a mission takes place, and so are not generally of concern during missions other than the requirement of monitoring doses received. Factors inherent to the space environment such as microgravity, diet, and stress can also exacerbate radiation effects. Finally, outside of human risks, there are also possible detrimental effects and mission impacts to the spacecraft itself such as single-event effects and communication system disruption.

Acute effects have been studied for terrestrial radiation in humans, but there are little data for spaceflight relevant radiation. From terrestrial exposures, it is known that possible effects after a particularly large SPE could include acute radiation sickness (ARS). Depending on the dose from an SPE, effects induced could include nausea, vomiting, fatigue, and/or hematopoietic disruptions. For rare larger

events, death from acute radiation sickness is possible due to damage to hematopoietic systems impacting production of red blood cells, platelets, white blood cells, and more. Worst case scenarios generally involve extravehicular activities (EVAs) where the astronaut has limited shielding from particles and cannot get to a more shielded part of the spacecraft quickly. Medium level risks include problems posed by fatigue or gastrointestinal upset that interfere with critical mission objectives, where an astronaut cannot participate due to illness. Lower level mission impacts would be if the crew needed to rest for a day or two during a transit and did not have any priority tasks during that time, but this would possibly set the schedule back some, making minor problems later in the mission.

CNS effects are becoming more of concern for missions due to the evidence that tissue in this system is more radiation sensitive and cognitive problems may result [*McPhee and J. B. Charles, eds.*, 2009]. In a recent study investigating space relevant particles and doses, mice showed behavioral deficits in the ability to discriminate in specific situations compared to controls [*Parihar et al.*, 2015]. Additionally, past research has shown that performance decrements in motor tasks, spatial learning, and memory could be possible in space [*Kennedy*, 2014]. It is not known at this point what the time scale of these effects would be for humans, since there are differences between humans and other mammals. Any radiation-induced cognitive function deficits are of concern for spaceflight due to the risk of performance deficits already present due to the stress and lack of sleep that many astronauts suffer from during missions.

In addition to acute radiation sickness and CNS effects, radiation-induced disruptions in homeostasis, skin changes, and light flashes may become problems during extended space missions. Astronauts already are at risk of homeostasis disruptions due to the lack of a normal light-dark cycle, and it is known that certain levels of

ionizing radiation can disturb homeostasis as well [*NCRP*, 2006]. During a mission, radiation exposure can also induce skin changes such as erythema and desquamation, but prevention is possible with a feasible level of shielding and/or astronauts avoiding situations where they could damage their skin. Lastly, light flashes are a well-known occurrence in spaceflight, but are unlikely to produce any mission effect. Even if the flashes come more often than in LEO, unless the astronaut was under other stress she or he would be unlikely to be distracted enough to produce sub-standard work during a mission.

There are also some known synergistic or additive effects in that radiation combined with other space environmental factors could worsen effects. The most common interaction investigated is between microgravity and radiation that can cause changes not seen with each separately. One review by *Kennedy* [2014] discusses evidence for changes in immune function, indicating a much larger effect than with SPEs alone. In addition, although nutrition is not specifically part of the inherent space environment, astronauts tend to have increased iron stores due to their diets, which can increase development of oxidative stress and possibly harmful immune system responses [*Morgan et al.*, 2014]. These effects could prove to be problematic for extended missions due to bacteria and other microorganisms becoming more pathogenic and able to survive after exposures to microgravity [*Rosenzweig et al.*, 2010]. If astronauts have enhanced changes in their immune systems due to the combination of microgravity and radiation (and the stress of spaceflight), the presence of bacteria that are better able to survive could pose mission and health risks.

Outside of human health impacts, there are also possible mission impacts from radiation affecting the electronics on board spacecraft. Although spacecraft elements are generally designed to withstand high levels of radiation, there is still a risk of GCRs damaging microelectronics in single-event effects. These can be simple bit flips

or as bad as a high-current state where the device ceases to function [*Knipp et al.*, 2011d]. Depending on the severity of the damage, mission impacts could certainly be possible especially if occurring during a critical phase such as a propulsion maneuver or landing on the Moon or Mars. Possible minor mission impacts could include temporary loss of communications during radiation storm conditions.

For all of the effects mentioned above, there are different possible mission impacts depending on the timing and severity of such an effect. Most likely there would be few if any mission effects during an extended space mission, but due to the length of such missions, small effects could accumulate over time and the probability of a significant effect due to a larger SPE is also increased. A trip to Mars for instance generally would take on the order of two to three years to complete with over 400 days in deep space. Since humans have not undertaken such a mission before, it is unknown whether or how the effects of radiation and other stressors would interact to produce an increase in risk or not. Through careful planning and research these individual stressors can be minimized and therefore reduce the impact of additive mechanisms. This will reduce the risk of high-priority tasks lost due to radiation, or worse mission failure such that the crew would be unable to complete their primary objective.

1.1.3 Strategies and Countermeasures

In planning spaceflight missions there are many approaches to take to mitigate radiation risks. These mitigation strategies are generally used in combination, as there is not a single countermeasure feasible for space that will prevent all radiation effects to humans or their spacecraft. Biological countermeasures currently include maintenance of good health, use of vitamins/antioxidants, and anti-emesis drugs [*Kennedy*, 2014; *Buckey*, 2006]. Physical countermeasures include shielding, use of

radiation-hardened spacecraft components as necessary, and software resets to help correct issues such as bit flips. Besides these countermeasures, there are various strategies that are employed with respect to mission design, dose limits, and good practices such as ALARA.

Research is still ongoing into different pharmacological agents and antioxidants to help in cases of radiation exposure, but certain countermeasures are used to help maintain good health in astronauts such that radiation may not have as much of a detrimental effect while on long-duration missions [*McPhee and J. B. Charles, eds.*, 2009; *Kennedy*, 2014]. For instance, astronauts on the International Space Station (ISS) have healthy diets and generally ample exercise, which can promote decreased oxidative stress, helping to mitigate the production of damage due to radiation. Additionally, vitamins and antioxidants are recommended for risk mitigation, although optimal levels are not known currently, but they are still available on the ISS such as beta carotene (for use in deficiency cases or radiation exposure) [*NASA*, 2001]. One pharmacological agent kept on the ISS that could help in cases of radiation exposure is Zofran, which is used for prevention or mitigation of nausea and vomiting (and has some proven success in the ferret model) [*Kennedy*, 2014]. Overall, there is still research needed to evaluate the use of pharmacological agents and antioxidants for potential use in spaceflight, but early research has shown some benefits in animal models.

Shielding is used as a primary physical countermeasure for long-duration missions. But, due to the nature of space radiation, shielding is not completely effective for astronauts and the spacecraft. The level of shielding that would be needed to completely mitigate effects is highly impractical from a spacecraft design perspective. A practical level of shielding although can produce small to moderate reductions in dose levels. Unique approaches to take advantage of available shielding are also used

by astronauts during missions. For instance, astronauts have slept in the same module on the ISS that held water stores, which reduced the radiation exposure. The countermeasures to mitigate and/or prevent possible hardware and software issues due to single-event effects are currently adequate. The most frequently used countermeasures for these effects are using radiation-hardened devices and performing software resets to keep errors from propagating. Physical countermeasures, as with biological countermeasures, require more research. But, biological countermeasures may have a larger impact for future long-duration missions unless there is development of a new game-changing technology such as active shielding or new materials development.

Finally there are different strategies with respect to mission design and "good practices" that are currently used for long-duration missions to help mitigate the effects of radiation. Currently these strategies are used in the context of the various dose limits astronauts have for missions, careers, and short acute doses. For example, some astronauts might not qualify to go on a long-duration mission during solar minimum conditions (when GCRs are at the maximal dose rate), but would still qualify for a mission during solar maximum conditions due to the reduced likelihood of exceeding their career dose in a specific category (lens, skin, cancer risk, etc.). In addition, astronauts use the principle of "As Low As Reasonably Achievable" (ALARA) in the case of a known SPE imminent arrival, where if practical, astronauts move to a more shielded part of their spacecraft to help reduce exposure and avoid approaching career dose limits. Finally, although partially inadvertent, astronauts chosen for long-duration missions tend to be older and therefore at lower risk from radiation exposures for cancer development in their lifetime. In the future, the mission design and dose limits strategies will likely change as more is known about the space radiation environment and researchers become better able to predict events.

Countermeasures and strategies used for long-duration missions during spaceflight still require additional research. There are promising studies involving different radioprotective agents and antioxidants that may help reduce the detrimental effects of radiation for future missions. Additionally, there is more research being done to better predict and understand solar and extra-solar radiation activity. But, for long-duration missions further away from Earth, additional improvements in mission architecture are needed to be able to implement the current strategy. Another aspect of radiation risk analysis that could use further study is the use of atomic bomb survivor data for estimating space radiation risks. Since there are significant differences between the populations and radiations involved, it may not be appropriate to use those data to predict space radiation risks. But, without significant human data for space radiation effects, this is currently the only source for understanding possible spaceflight effects. For the level of long-duration missions currently undertaken, the countermeasures and strategies used are adequate, but future research is targeted to use the ISS as a test bed for long-duration missions outside LEO.

1.2 Alignment with Agency Level Risk Assessment

As NASA prepares to once again expand human spaceflight beyond LEO for future long-duration missions, there are still significant research questions that need to be answered and NASA has categorized risks into the following areas [*McPhee and J. B. Charles, eds.*, 2009]:

- Behavior Health and Performance
- Space Radiation
- Exploration Medical Capabilities
- Space Human Factors and Habitability
- Exercise and Extravehicular Activity

The research presented here intersects with both the "Space Radiation" and "Exploration Medical Capabilities" (ExMC) risk areas in assessing the medical risks associated with radiation exposure in spaceflight outside of LEO. Specifically, this research will tie in with the development of NASA's Integrated Medical Model (IMM), which is a part of ExMC that uses probabilistic risk analysis to evaluate high consequence, rare medical events such as hip fracture, kidney stones, and now ARS [*Myers et al.*, 2011].

For human spaceflight missions beyond LEO, ARS becomes of concern due to reduced natural radiation protection (outside the Earth's magnetic field) and longer mission duration, meaning that likelihood and magnitude of SPEs is increased. From historical analysis of larger rare SPEs such as the August 1972 or October 1989, doses are high enough to be of concern for astronaut safety and mission success, prompting further risk studies involving SPEs. Now that there have been decades of study covering SPEs occurrences with satellite data, it becomes possible to take a probabilistic view, determining not only what the consequences of a rare larger event would be, but also the chances of its occurrence based on mission parameters. The information gleaned from this type of study can be utilized by NASA and others to inform decisions for all design phases, adding the capability to appropriately plan mitigation procedures and determine levels of acceptable risk, allowing future missions to be safer and more productive as humans travel beyond the Earth-Moon system.

2. SOLAR ACTIVITY

In the context of space radiation risk assessment, solar activity governs the dose levels expected both from galactic cosmic rays (GCRs) and solar particle events (SPEs), making it important to understand how the Sun changes over time and what might be expected in the future. Even with modern satellite and computational investigations, there are still many questions to be answered, which makes prediction and future mission planning difficult. In the text below, the history of solar activity is presented, highlighting energetic events and how they are observed, characterized, modeled, and possibly predicted, demonstrating the progress being made in this research field and what still remains to be investigated.

2.1 Historical Observations and Trends

For hundreds of years the Sun has been investigated by scientists, showing both long- and short-term activity trends. Long-term activity is most frequently characterized through the changes in sunspots and magnetic field polarity shifts in the well-known 11-year cycle. Short-term activity refers to energetic events that cause eruptions from the Sun's surface resulting in a release of particle and electromagnetic radiation. Additionally, since long-term activity impacts the frequency and progression of energetic events, both must be considered in making a radiation assessment.

2.1.1 Quiescent Behavior

The Sun is fairly stable as an astronomical object, only varying over time about 0.1% in the radiative flux from the Sun's lower atmosphere. The upper atmosphere, where events generally originate, is much more variable, but as it only contributes 2% to radiative output, there is little impact on overall solar activity [*Knipp et al.*,

2011f]. The primary aspects of the Sun's quiescent behavior that are relevant to risk assessment are the different solar cycles, the solar wind, and their interaction with the interplanetary magnetic field (IMF). These aspects of the Sun not only provide the framework from which energetic events develop, but also determine how the events propagate through the solar system.

2.1.1.1 Cycles

The most well known solar cycle is the Sun's 11/22-year cycle, with the most recent maximum occurring in 2013 for cycle number 24. Two metrics frequently used to describe this cycle are the sunspot number and solar 10.7 cm radio flux. Other cycles have also been investigated, which attempt to describe longer-term cycle variations in the Sun over hundreds or thousands of years, tracked through the use of ground proxies.

Starting in the 1700's the sunspot number has been used to track solar cycles, with observations of sunspots going back as far as 3000 years ago [*Knipp et al.*, 2011g]. Sunspots peak every 11 years and numbers are assigned depending on whether they occur individually or in groups (i.e. a different number is assigned for five individual sunspots versus five sunspots in a group). Sunspots themselves are dark blemishes on the Sun that are areas where the magnetic fields are especially concentrated, inhibiting the rise of heat, causing them to be darker and cooler than areas around them. Sunspots are also useful in tracking the progression of the magnetic field polarity switch that occurs every cycle, with a return to the same polarity orientation every 22 years. Early in a cycle (solar minimum), sunspots form at higher latitudes and gradually shift lower, nearly to the equator by the end of the cycle as can be seen in Figure 2.1.

The second method mentioned here for solar cycle tracking is the solar 10.7 cm

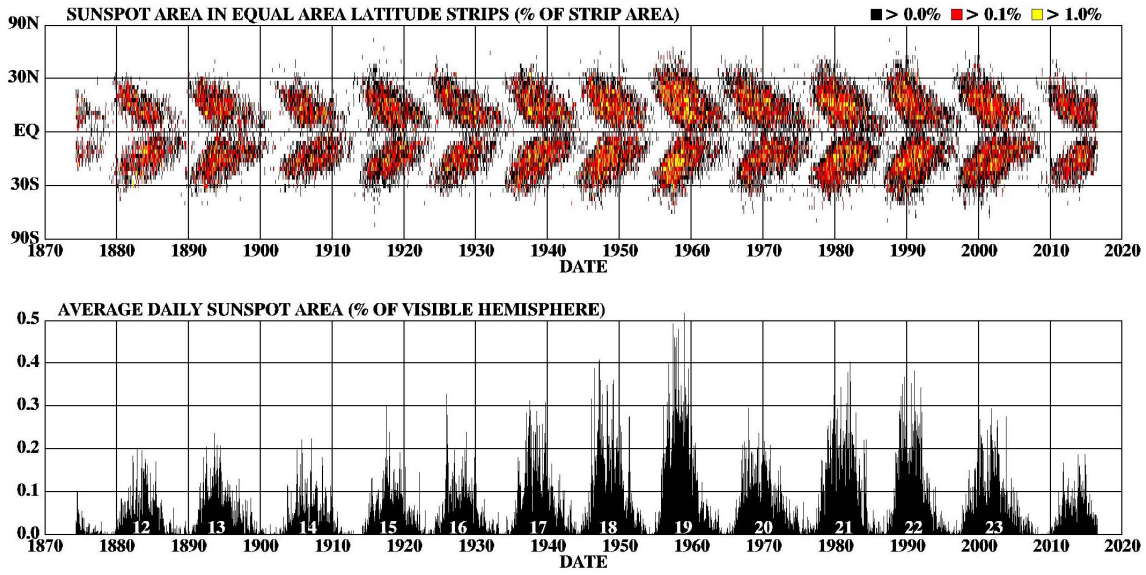

Figure 2.1: Sunspot progression starting in 1870. Top figure is called a butterfly diagram, which plots sunspot area on the solar surface by latitude. The lower figure shows this information by percent of the total visible hemisphere. Source: NASA Solar Science [*Hathaway*, 2016b].

radio flux measurement. Commonly called the F10.7 index for flux at 10.7 cm, measurement of this index began during World War II when centimetric radar systems were in use and operators noticed increased noise associated with the Sun's position on the horizon [*Tapping*, 2013]. Unlike a sunspot count, this index is not a count of total activity over a day, but a measurement of the total emission at the 10.7 cm wavelength (2.8 GHz frequency), made over a one-hour period, integrated over the solar disk [*Tapping*, 2013; *Knipp et al.*, 2011f].

The advantage of the radio flux measurement is that the 2.8 GHz frequency can easily penetrate the Earth's atmosphere, making it possible to observe even in the worst conditions. But, as the measurement does not go back further than 1947, it is not possible to study longer-term variations as with sunspots [*Knipp et al.*, 2011f]. In spite of these differences, these two indices correlate well with each other as shown

in Figure 2.2. These two indices should not be used interchangeably though, with the choice of index dependent on application.

To investigate longer-term variations in the Sun's activity (grand minima and maxima), cosmogenic isotopes (radionuclides) such as ^{14}C and ^{10}Be can be used as indirect proxies [*Usoskin*, 2013]. These isotope proxies can be evaluated through the use of terrestrial reservoirs such as tree trunks, ice sheets, and even lunar soil, searching for variations in the isotopes produced from GCRs, which are modulated by the solar cycle [*Lockwood*, 2013; *Miroshnichenko and Nymmik*, 2014]. *Usoskin et al.* [2007] present evidence from cosmogenic isotopes for both short- and long-grand minima with indications of both stochastic and deterministic processes. The short minimum is thought to be of the "Maunder" type, with durations of 30-90 years and the long minimum of the "Spörer" type, with durations over 110 years. Maunder refers to the well-known minimum that occurred in the late 17th century, sometimes called the "Little Ice age," and Spörer refers to a more prolonged minimum from around 1420 to 1550, which had decreased global temperatures and consequences for food production at the time [*Usoskin et al.*, 2007; *Hathaway*, 2016b; *Camenisch et al.*, 2016]. Grand maxima do not seem to have a clear cyclical variation, but instead seem to be related to the occurrence of grand minima, meaning that the variability is more of a stochastic process than a deterministic one. There is also a weak 2400-year quasi-periodic behavior for clustering of grand minima, with evidence that the Sun is currently in a grand maximum with a return to minimum possible as evidenced with the low solar maximum in the current solar cycle (see Figure 2.2) [*Usoskin et al.*, 2007]. If this is the case, future space missions may have higher flux from GCRs and less chance of SPEs due to the inverse relationship between solar activity and GCR dose, which could increase risks of cancer development and late central nervous system effects for astronauts.

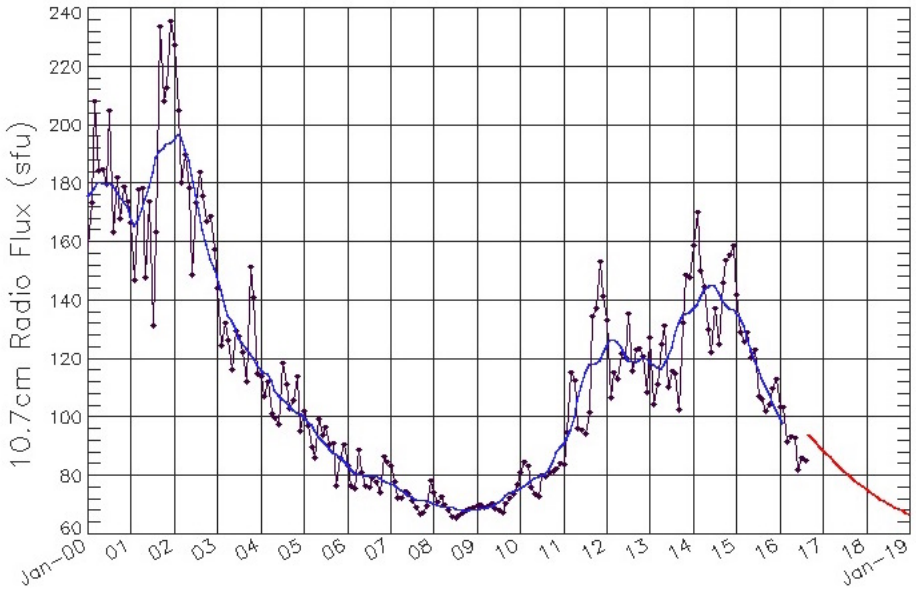

(a) 10.7 Radio flux progression

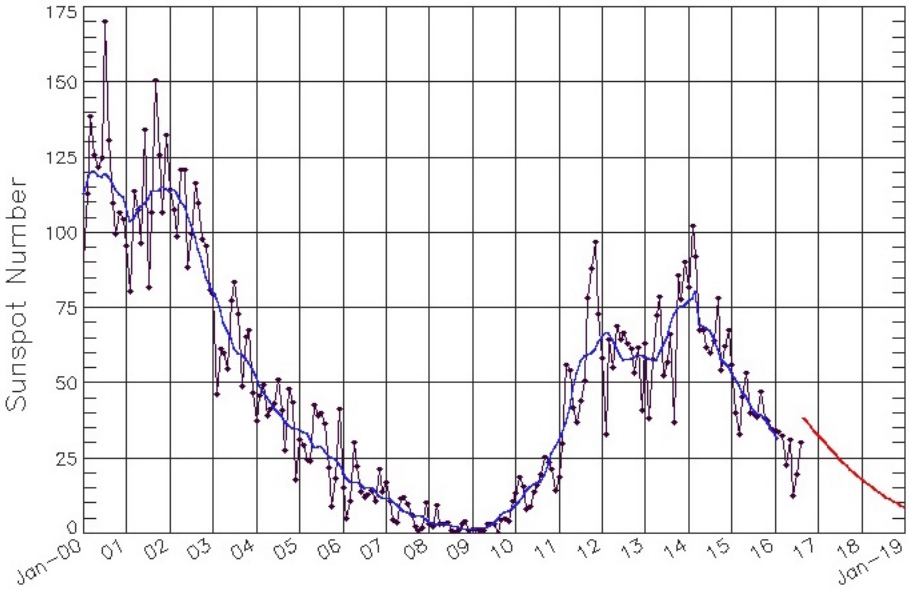

(b) Sunspot number progression

Figure 2.2: Solar cycle progression since January 2000. The blue lines represent smoothed monthly values, the black dots and lines monthly values, and the red lines predicted values till the end of the current solar cycle. Source: NOAA Space Weather Prediction Center, last updated September 5, 2016 [*NOAA*, 2016e].

2.1.1.2 Solar wind and the IMF

Since charged particles can be bounded by and travel along magnetic field lines, the development and properties of the IMF and its source, the solar wind are important in understanding how events travel through the heliosphere. The plasma outflow of the solar wind carries with it the lines and knots in the solar magnetic field, with open field lines traveling outward in a spiral formation until reaching the termination of the Sun's influence far beyond the outer planets [*Knipp et al.*, 2011e].

The solar wind is comprised of fast and slow flow type plasma that are from the outflow from coronal holes and streamer boundaries respectively. The fast type can reach speeds about double the slow type and contributes to a larger magnetic component in the IMF [*Knipp et al.*, 2011e]. Evidence of these two types of plasma can be seen in comets with two tails due to the ions, which are separated based on their weight and charge. The solar wind can also have an extreme speed version, which is a result from coronal mass ejections (CMEs). But, as this is highly variable and can depend on the event, it is not considered to be part of quiescent solar activities. Additionally, since magnetic field lines are within this plasma, the orientation can impact aurorae formation, with an oppositely directed magnetic field producing the common aurorae seen on Earth except during solar minimum [*Knipp et al.*, 2011c].

Once the solar wind begins to branch out from the Sun, the IMF is formed, with variable lines and currents dependent on the Sun's solar wind type at each formation location. Faster flow can also overtake slower flow, creating compressed magnetic field lines, further complicating the IMF's progression through the heliosphere. From the combination of the Sun's rotation and the "frozen-in" aspect of the magnetic field, a spiral is formed, frequently called the "Parker spiral" after the scientist responsible for the solar wind theory that predicted this feature (for further details see *Knipp et al.*

[2011e]). This spiral feature makes it more difficult to predict energetic events since it is possible that particle events emanating from the Sun seen by satellites between the Earth and Sun can miss Earth, while the X-rays and other electromagnetic radiation would still arrive at Earth.

2.1.2 Energetic Events

The "Parker spiral" is the final relevant feature of the quiescent Sun, allowing for understanding of the framework from which energetic events develop. In contrast to the slowly changing solar cycles and constancy of the solar wind and IMF, the Sun releases a variety of energetic events with different combinations of radiation types, energies, and spectral shape [*Gerontidou et al.*, 2002; *Meyer et al.*, 1993]. Depending on the field of the researcher, these events can be called SPEs, solar energetic particles (SEPs), solar proton events (historically and given the same SPE acronym), CMEs, solar flares, and more. The initial event causing a SPE is generally separated into solar flares and CMEs, both of which can cause different impacts to satellites and humans in space.

Solar flares and CMEs are distinct events that originate from the Sun, with differing progression paths through the heliosphere (see Figures 2.3 and 2.4), and cause different consequences for spaceflight activities.

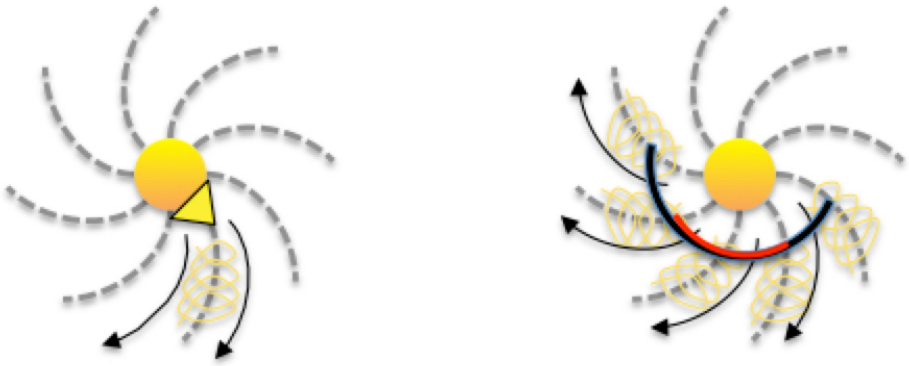

(a) Solar flare **(b)** Coronal mass ejection

Figure 2.3: Comparison of solar flares and CMEs. CMEs tend to be broader, taking up more radial space in the heliosphere, while flares are more impulsive and tightly bounded. The red and black arc represents the acceleration shocks that are also associated with CMEs. Adapted from: *Reames* [1999].

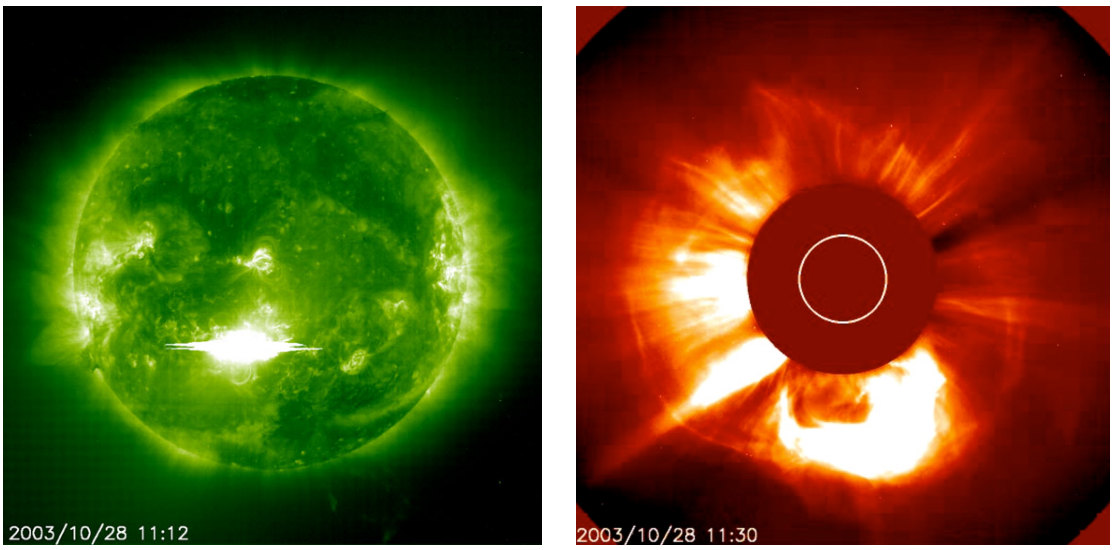

(a) Solar flare associated with event **(b)** CME associated with event

Figure 2.4: Record solar flare and CME from 2003. The flare shown in (a) was recorded as an X17 event and the CME shown in (b) reached a maximum proton flux of 29,500 protons per cm^2 s sr [*NOAA*, 2011b]. The CME also had an associated halo, which is the faint ring around the edges of the eruption. Source: NASA Goddard Space Flight Center and NOAA [*NASA*, 2003b].

Both solar flares and CMEs develop out of rearrangement of magnetic field lines in the Sun, but differ in their development and the spectra present for each event. Solar flares are more impulsive with sharp onset and quick arrival with primarily electromagnetic radiation, while CMEs are typically more gradual in onset and move slower, but primarily contain particle radiation that is accelerated by shocks [*Knipp et al.*, 2011b]. As a result, different classification systems were developed with solar flares categorized by flare class based on X-ray flux levels, and CMEs by the proton flux and/or magnetic storm levels [*NOAA*, 2016e]. An example of an X-class solar flare (highest flare class) is shown in Figure 2.4a from October of 2003, which was the third strongest solar flare ever observed (as of 2003) [*NASA*, 2003b]. This event also had an associated CME that was the fifth largest by proton flux at 30 MeV since 1960 (as of 2009) [*Kim et al.*, 2009]. The resulting solar storm from these events was intense enough for aurorae as far south as Texas to be seen [*NASA*, 2003b].

Beyond the knowledge that solar flares and CMEs result from changes in the magnetic flux ropes of the Sun, exact processes are still unknown and under investigation [*Cooper*, 2013]. As mentioned above with the solar wind and IMF, ionized particles also carry magnetic fields with them. If the magnetic field is oriented southward, a solar storm reconnection scenario can result, creating the more rare aurorae that can reach far from the poles and cause significant communications disruptions [*Knipp et al.*, 2011c].

Historically, solar events have been tracked for hundreds of years with especially large events causing notable effects on Earth even before the space age. The most well known pre-space age event is the Carrington Storm that occurred in early September 1859, where aurorae were visible as far south as Hawaii and newspapers could be read in the southern United States from the auroral lights alone. Telegraph services were also disrupted due to the severity of the storm, where telegraphs even worked

without power and some others emitted sparks, shocking operators [*Knipp et al.*, 2011g]. More recently in May of 1967 there was a solar storm (and associated SPE) that disrupted communications for the US military, almost leading to rash decisions due to the tensions of the Cold War [*Knipp et al.*, 2016].

2.1.2.1 Pre-space age data

Prior to the space age, data about solar events could only be gathered through the use of ground observations and eventually vehicles such as high-altitude balloons. Aerospace vehicles are still used today in the atmosphere, but as these vehicles in the past were generally designed for short-term measurements (hours to weeks), scientists have generally looked to ground measurements for pre-space age data.

Ground observations include telescopic observations of the Sun, isotope analysis, nitrate ice core samples, and particle detectors. Telescopic observations with proper protective equipment were primarily used to see features on the Sun's surface (sunspots), but scientists would sometimes see events take place. Richard Carrington observed the event named after him through this process, seeing an extraordinary sparkle from a group of sunspots, which proceeded to brighten and stay illuminated for approximately five minutes [*Knipp et al.*, 2011g].

Isotopes and nitrate ice cores are both indirect proxies, requiring calibration and cross correlation with other known events to be able to infer past events. While these indirect proxies are imperfect, some knowledge about past SPEs can generally be deduced. Isotopes commonly used are ^{14}C and ^{10}Be as mentioned in the discussion of solar cycles. In a more recent work by *Usoskin and Kovaltsov* [2012], the cosmogenic isotope data does not seem to support the premise of a massive SPE related to the Carrington Storm. Cosmogenic isotopes can show correlation with other events, allowing for identification of 19 SPEs in the last 11,400 years with integrated

event fluences at 1-3 x 10^{10} protons per cm^2 at the energy of 30 MeV [*Usoskin and Kovaltsov*, 2012]. In comparison, the highest event in the space age was estimated to be 9 x 10^9 protons per cm^2 at the energy of 30 MeV [*Kim et al.*, 2009].

In the past there has been significant support for utilizing nitrate ice core samples as the primary indirect proxy for SPEs, but new studies have now recommended that this proxy no longer be used [*Duderstadt et al.*, 2016; *Carnell et al.*, 2016]. The theory behind utilizing nitrate levels in ice core samples is that the ionization present when events occur leads to the production of NO and from it other oxidized nitrogen compounds. These compounds have been found in some polar ice cores in spikes thought to be associated with SPEs [*Wolff et al.*, 2012]. In the 1990's and early 2000's initial published data showed that ice cores from Greenland and Antarctica showed spikes in nitrate levels aligning with larger SPEs, including the Carrington Storm [*Dreschhoff and Zeller*, 1990; *McCracken et al.*, 2001b,a]. As investigations of other ice core sites began, it became clear that the same events were not always shown in the data between different sites. In one study by *Wolff et al.* [2012], evidence for the Carrington Storm was only present in the data for 1/14 of ice core sites in Greenland and none from Antarctica. Additionally, *Schrijver et al.* [2012] recommend measurements of SPEs from space and not to use the ice core nitrate levels or isotope data as proxies since isotope data can also be unusable, as it must be calibrated with the use of even less reliable data. In summary, although ice core and isotope proxies may provide valuable information in some specific cases or more general solar activity levels, these proxies should not be included in a historical list of SPEs at this time.

Finally, ground particle detectors have also been investigated as a source of pre-space age data. Through measurement of particles generated in the atmosphere from GCRs, researchers were able to discover long-term changes in GCRs including

short-term spikes and/or depressions in the data corresponding to solar events. One of the first instances in which scientists identified the Sun as the responsible agent was in 1942 when events were detected through the use of ionization chambers [*Shea and Smart*, 1990]. As technology advanced, it became clear that the spikes, now called ground level enhancements (GLEs) in the data were associated with solar events. One of the largest GLEs recorded by neutron monitors occurred in 1956 from a SPE with a particularly large magnitude, with large fluxes even out to the highest energies [*Kim et al.*, 2009; *Shea and Smart*, 1990]. Some events do not exhibit GLEs, but instead only show depressions in the data, called Forbush decreases that result from magnetic fields in a CME causing a deflection of charged particles, lowering the number of neutrons produced in the atmosphere [*Knipp et al.*, 2011a]. Other ground measurements have not continued significantly into the space age and therefore neutron monitors form the primary ground comparison for SPEs.

2.1.2.2 Space age data

Neutron monitors have continued operation into the space age, allowing for some comparisons to satellite data and confirmation of events. After the development of neutron monitors, rapid technological development for space continued, leading to today's plethora of satellites, bringing much more detailed and accurate information about SPEs. Together, NASA and the National Oceanic and Atmospheric Administration (NOAA) along with other agencies have a fleet of space weather satellites, many of which are solely dedicated to increasing knowledge and collecting data about the interactions between the Sun and Earth. Listed below are satellites that have been used in the past or currently in use to gather information about solar activity. Additionally, two more satellites are going to be added to this fleet: the Solar Probe Plus (SPP) and Solar Orbiter, which will investigate coronal heating and solar wind,

and the generation and maintenance of the heliosphere respectively [*Zell, H., ed.*, 2016].

- ACE - Advanced Composition Explorer: measures particles in the energies of 0.1 keV to 0.5 GeV, gathering data to better understand the solar wind, IMF, and acceleration mechanisms [*Christian and Davis*, 2012]
- Hinode (Solar-B): studies the generation and dissipation of magnetic fields for both energetic and quiescent solar activity [*Zell, H., ed.*, 2016]
- GOES - Geostationary Operational Environmental Satellite: network of satellites that measure multiple weather parameters including energetic particles (protons, electrons, and alphas) and electromagnetic radiation outside the Earth's radiation belts [*NOAA*, 2016c]
- IMP - International Monitoring Platform: some satellites still exist in orbit, but were primary for event resolution in the 1970's and 1980's before the GOES program was as prominent and measured similar particles and energies [*McGuire*, 2002]
- IRIS - Interface Region Imaging Spectrograph: utilizes UV radiation to investigate the movement of solar material, including the solar wind and CMEs through the Sun's lower atmosphere [*Zell, H., ed.*, 2016]
- SDO - Solar Dynamics Observatory: investigates movement within the Sun's atmosphere associated with magnetic field generation and structure, and how stored energy is converted and released into the heliosphere [*NASA*, 2016a]
- SOHO - SOlar and Heliospheric Observatory: studies internal and external solar structure to determine the origin of the solar wind [*NASA*, 2016g]
- STEREO A & B - Solar TErrestrial RElations Observatory: observes the Sun-Earth system with one satellite ahead of Earth and one behind (radially) to examine the 3-dimensional aspects of CMEs, and provides alerts and arrival

times for events headed towards Earth [*Zell, H., ed.*, 2016]

- Wind: measures the solar wind before it interacts with Earth's magnetosphere [*Zell, H., ed.*, 2016]

Out of the data produced by the satellites listed above, there have been many studies documenting SPEs, creating event databases just as with events before the space age. Most well known are those studies by Shea and Smart that compile space and ground data from around 1955 through the 1980's, providing a listing of SPEs by solar cycle and year [*Shea and Smart*, 1990, 1993, 1994, 1995; *Smart and Shea*, 2002]. Others contributing to this documentation have included *Goswami et al.* [1988]; *Feynman et al.* [1990]; *Jun et al.* [2007], with the work by *Jun et al.* [2007] detailing SPE fluence and time interval analysis from 1977 to 1997. Further research has given rise to a listing of the major solar events through 2009 documented in work by *Kim et al.* [2009]. From these studies, the top ten major SPEs since 1955 are listed in Table 2.1 by fluence at 30 MeV (source: *Kim et al.* [2009]). The SPEs below were recorded by ground instruments or satellites in various orbits around Earth. Even in this short list, it can be seen that certain active portions of the solar cycle had more than one large SPE such as the years 1989-1991.

Of the events listed in Table 2.1, the August 1972 and October 1989 events are most frequently utilized in worst-case event scenarios since their spectra were fully measured through use of satellites at the time. The 1960 event was detected and measured by neutron monitors, which later resulted in questions about the validity of its use in models and other studies since there are "large differences" in the derived fluence between researchers at the time [*Shea and Smart*, 1990; *Freier and Webber*, 1963].

Finally, there have been some limited studies into solar events outside of near-Earth space, including analysis for the lunar surface and a Mars transit. *Adams*

Table 2.1: Top SPEs since 1955.

Event Start Date	Integrated fluence (protons cm^{-2})
1960-11-12	9.00 x 10^9
1972-08-02	8.10 x 10^9
1989-10-19	4.23 x 10^9
2000-07-14	3.74 x 10^9
2003-10-26	3.25 x 10^9
2001-11-04	2.92 x 10^9
2000-11-08	2.27 x 10^9
1991-03-23	1.74 x 10^9
1989-08-12	1.51 x 10^9
1989-09-29	1.35 x 10^9

et al. [2007] investigated the ionizing radiation environment on the Moon, comparing neutron production from different radiation sources between data (Lunar Prospector) and models (GEANT4, GEometry And Tracking 4). From these investigations, *Adams et al.* [2007] found that neutron production has little impact on dose from SPEs. Recently, the Mars Radiation Assessment Detector (RAD) on the Curiosity rover made measurements both during transit to Mars and on the surface [*Hassler et al.*, 2014]. During the transit from Earth to Mars, RAD recorded five SPEs and also found differences in the time progression of the events compared to the events recorded by GOES-11 at Earth [*Zeitlin et al.*, 2013]. These studies indicate that there are differences between low-Earth orbit (LEO) and missions to the Moon or Mars in event progression.

Together all of these data provide approximately 60 years of energetic particle data, but little of it can be directly used for missions outside of LEO. As of the time of this document's preparation, there are few data sources for SPEs outside the near-Earth space (further away than the Moon) with the exception of the recent

RAD data. Without further data, modeling must be used in conjunction with known quiescent and energetic solar data from near-Earth space, to produce risk models and aid in further predictions of SPEs.

2.2 Modeling

To predict and understand the mechanisms that generate solar events, the data from satellites and ground measurements have been used to develop a variety of models. Most models are designed to generate event fluences and some include inputs to assess dose for missions as well.

Generally, the most common issues are relying on ice core data (as explained above), separating the solar cycle into "active" and "inactive" phases, separating events into "ordinary" and "anomalously large," and only allowing single historical SPE spectra inputs. Splitting the solar cycle into two parts can be an issue since it is a simplification of the likelihood in that there is less chance of larger events (such as the October 1989 event) only due to there being less chance any event during minimum parts of the solar cycle [*Kim et al.*, 2009]. Since reliable recording of events with the space age, there have been too few larger SPEs to determine if this is correct approach or not. Therefore at this time it is not a valid assumption to split the solar cycle into active and inactive parts, although may be justifiable in certain cases or when a simplification is acceptable. In the case of the ordinary and large event classification, acquisitions of more data have shown that SPEs are more diverse than this classification allows [*Kim et al.*, 2009; *Miroshnichenko and Nymmik*, 2014]. The last issue mentioned is more of a limitation than a problem since for mission analysis, it is important not just to model one historical event, but all expected dose inputs from SPEs and GCRs. This modeling allows the determination of total mission exposures and what countermeasures need to be implemented for keeping

within limits and minimizing dose exposure. If the goal is to only determine a worst-case single-event scenario, then the models with single historical event inputs can be quite useful. The models are described below with their capabilities as of their reference year, with information as to what endpoints and limitations each model has. Models chosen for use in this research are further discussed in the sections covering code and implementation (4.1-4.5).

2.2.1 Solar Event Spectra

- *Adams* [2011]: The model developed by this research group, which is based out of NASA, includes both the JPL and King models. It also uses the concepts of active and inactive parts of the solar cycle to generate a worst-case environment. SPE data sources include GOES and IMP spacecraft, and SPEs are defined to be statistically independent before being incorporated into a Monte Carlo model for calculating probability distributions.
- ESP [*Xapsos et al.*, 1999]: The ESP (Emission of Solar Protons) model at the time of publication was intended to be an update to research conducted by King and others on Solar Cycles 20 and 21, adding data from Cycle 22. Compared to the JPL model, the ESP model showed similar results for cumulative and worst-case event models based on the active/inactive solar cycle concept. This model has additional features such as calculations for solar cell degradation, total ionizing dose degradation, and other electronics damage.
- JPL [*Feynman et al.*, 1993, 2002]: Also called the "Interplanetary Proton Fluence Model," the JPL (Jet Propulsion Laboratory) model was first developed in the 1980's with the goal of calculating the fluence expected over an exposure time at a given confidence interval. Data inputs to the model include early IMP satellites and outputs are mission-integrated fluences with confidence lev-

els. The JPL model uses the active/inactive solar activity assumption based on sunspots to characterize overall activity to generate events.

- *Kim et al.* [2009]: The Kim model takes a probabilistic modeling approach to predicting radiation exposure from SPEs based on data from the last five solar cycles and some corrected ice core data. Outputs include an expected number of events for a non-specific solar cycle and an additional option for an SPE exceeding a given threshold fluence. The Kim model does not rely on any other models and the only shortcoming is inclusion of ice core data for the additional SPE fluence threshold.
- *King* [1974]: The King model was one of the earliest attempts to generate a probabilistic model for a proton fluence exceeding a given fluence during a mission. This model only used data from 1966-1972 (IMP data) and separated events into ordinary and anomalously large events, with the large events given the same spectrum as the August 1972 and the ordinary events assumed to have a lognormal distribution. Besides the quality of data (in comparison with modern standards), the primary disadvantage of this model was the separation of events into two specific categories.
- *Miroshnichenko and Nymmik* [2014]: This model is based on all available data (ice cores, IMP, and GOES) from 1561 to 2014, generating a SPE distribution function with emphasis on extreme SPE probabilistic distributions (in the updated 2014 version). The most useful part of this model is the distribution function, which would still be usable without the ice core data, allowing for generation of SPE probabilities for fluence at 30 MeV. Other than the ice core data, another disadvantage of this model is the use of double power-laws for event spectrum shape. Since the use of exponential or Weibull fits can be more accurate and are more commonly used, the double power-laws make it more

difficult to compare results between this model and others.

2.2.2 Mission Analysis

These models are excellent tools for a variety of applications, especially if investigating radiation risk alone, as most of the models are stand-alone, web-based models. Some of these models are quite customizable and can even take mission parameters or materials as inputs. In the case of integrated risk, these stand-alone models are not as useful since they do not take inputs unrelated to radiation such as bone or nutrition impacts. The largest advantage to the following models is that they are more rigorously verified and validated than many of the models listed above, since they are designed for use during mission development and have been verified for spaceflight modeling use.

- *Adamczyk et al.* [2011]: This analysis combines GCR and SPE environment models with OLTARIS (see below) to enable generation of estimated mission doses for future lunar missions. Inputs to the model include the 1977 solar minimum GCR environment at 1 AU, ACE satellite data, and the King August 1972 event model, which allow for calculation of worst-case mission scenarios. The disadvantages to this tool are that it utilizes a very specific set of data (1970's environment) and that the data included may not be as accurate as those collected within the last couple of decades.
- ARRBOD [*Kim et al.*, 2010; *NASA*, 2016e]: ARRBOD (Acute Radiation Risk and BRYNTRN Organ Dose, BRYNTRN - BaRYoN TRaNsport code) is part of the NASA Space Radiation Program Element's Integrative Risk Models Toolkit, available for free in both web and disk versions (authorization required by a NASA official). ARRBOD includes different endpoints for acute radiation impacts such as gastrointestinal effects, fatigue and weakness ratings, red

blood cell and lymphocyte changes, and total event doses for whole body and specific organs. Inputs include selection of a historical event, spectrum, vehicles, shielding levels, and event statistical parameters with options for an EVA during the selected SPE. It is not possible to integrate this model with others, but it can serve as a reference with which to compare other models to for well researched historical events, assisting in the validation and verification process. To access, see instructions at: https://spaceradiation.jsc.nasa.gov/irModels/.

- EMMREM [*Schwadron et al.*, 2010, 2006]: The development of EMMREM (Earth-Moon-Mars Radiation Environment Module) was developed at the University of New Hampshire with additional support from NASA. This mission analysis tool is a combination of many other models, and EMMREM even has a model for event propagation through the inner heliosphere for a catalogued or user-defined event. After including orbital location, shocks, and planetary shadowing factors, particle histories are generated in radiation transport codes (including BRYNTRN), dose profiles created based on location, and results are given for the scenario. The only disadvantage to this model besides the computational time and complexity inherent, is that it has yet to integrate a probabilistic component to the solar event inputs at the start. Access can be obtained for interested researchers through the University of New Hampshire: http://emmrem.unh.edu/contacts.html.
- MIRACAL [*Nealy et al.*, 1992]: MIRACAL (MIssion Radiation Calculation Program for Analysis of Lunar and Interplanetary Missions) was an early tool developed by NASA researchers to determine the risks associated with the radiation environment in space for missions outside LEO. This analysis tool takes trajectory information, shield thickness, a statistical or continuum model for ordinary SPEs, selection of large SPEs, and desired spectral data as inputs for

the risk metrics output. MIRACAL was originally designed as a stand-alone model or sub-routine for trajectory codes with the goal of mission optimization with respect to multiple considerations. Disadvantages to this model include the age of the data, lack of updates since first development, and the separation of SPEs into ordinary or large classifications, which are likely due to the postponement of missions for which it was designed.

- OLTARIS [*Singleterry et al.*, 2010]: OLTARIS (On-Line Tool for the Assessment of Radiation In Space) is another web-based tool that is part of the NASA's Integrative Risk Models Toolkit, and like ARRBOD is available for free, but users must register and gain approval before use. OLTARIS offers similar options as EMMREM with respect to radiation transport, but does not have the extra environment event modifications such as shocks and shadowing. In addition, OLTARIS offers either historical SPE spectra or a user-customizable SPE input function (exponential in rigidity or energy, three-parameter Weibull, or Band fits). Outputs are user specified and include dose, dose equivalent, and effective dose equivalent for each simulation case. Compared to other stand-alone models, OLTARIS offers many more options for analysis such as user-specified inputs, but is still not as useful for integrated models. OLTARIS webpage: https://oltaris.nasa.gov.
- SEPEM [*Jiggens et al.*, 2011; *Crosby et al.*, 2015]: The SEPEM (Solar Energetic Particle Environment Modeling) website is a joint ESA (European Space Agency) and member state universities project, which is available to researchers with a free registration. SEPEM is designed to generate event maximum flux and integrated fluence along with the calculation of single-event, upset rates and radiation doses. The model was recently updated to include values from 0.2 AU to 1.6 AU for the environment instead of just near-Earth. This tool

additionally relies on the JPL model for Monte Carlo analysis and ESP worst-case model plus cumulative analysis (as described above), which means that it includes the disadvantage of the active/inactive solar cycle concept. SEPEM webpage: http://dev.sepem.oma.be.

- SPENVIS [*Kruglanski*, 2013; *Kruglanski et al.*, 2009; *Heynderickx et al.*, 2004]: The SPENVIS (SPace ENVironment Information System) is another ESA tool freely available with registration. SPENVIS does more mission analysis and less focus on SPEs compared to SEPEM, and additionally includes support for the radiation belts, Mars, and Jupiter radiation environments. SPENVIS relies on the King, JPL, Rosenqvist, ESP, and PSYCHIC models for fluence, and CREME86, CREME96, and Xapsos (2000) models for solar particle flux within the tool. Of the fluence models not already described above, Rosenqvist's model is based on the JPL-91 model with updates to account for underestimation of the fluence, and PSYCHIC (Prediction of Solar particle Yields for CHaracterizing Integrated Circuits) is a model for heavier ions. The flux models are intended for single event upset rates near Earth with the CREME (Cosmic Ray Effects on Micro-Electronics) model containing GCR environment models, and the Xapsos model contains Weibull spectra for the October 1989 spectrum [Vanderbilt University, School of Engineering, 2016]. SPENVIS webpage: https://www.spenvis.oma.be.

As described in this section, there are numerous options for space radiation modeling currently and although not all can be used for all applications, between these options a general radiation risk assessment for a specific mission is possible. For more advanced uses such as integration of mission risks including those outside of radiation, selection of a tool or model will depend on the application and other mission parameters.

2.3 Prediction

The final sources for space radiation risk assessment are prediction tools and models, which seek to anticipate solar activity based on theories, previous data, and current activity levels, providing live predictions. With today's reliance on technology for space and ground applications, risk assessment is critical to prevent future complications related to solar activity such as satellite outages or even ground transformer damage in the case of a Carrington level event [*Knipp*, 2015]. In addition, the combination of event possibilities and unpredictability is a concern for future space missions, which creates the risk about which NASA is concerned for acute radiation events [*National Research Council*, 2008].

There have been difficulties in implementing this approach in all areas: theories, data, and current activity levels. The first will diminish with more research, but currently, there is still little known about the exact processes that cause events to occur or for the overall solar activity to progress from maximum to minimum and back. Second, as discussed earlier, more data are needed to understand the variations in solar activity (active/inactive parts, ordinary/anomalously large events), as pre-space age data cannot always be relied upon. The final area of monitoring current activity levels is mostly mitigated today with the constellation of satellites observing the Sun and returning data to Earth for analysis, but will be of concern for missions outside of near-Earth space. Discussed below is an overview of some of the more prominent and/or successful tools and models to predict solar cycle progression and the onset of solar events.

2.3.1 Cycle Progression

Solar cycle progression is important to consider in radiation risk for spaceflight since as mentioned earlier, it is one of the factors that determines future dose levels

and event probabilities. Predicting the cycle progression allows for calculation of expected mission doses or satellite degradation due to space radiation. Currently, the primary provider of the cycle progression in the United States is NOAA's Space Weather Prediction Center (SWPC). SWPC maintains a current prediction of cycle progression and releases predictions of the next cycle during minimum [*NOAA*, 2016d]. The information used in this prediction comes from both indirect and direct approaches for solar cycle progression, including the use of sunspot numbers, geomagnetic indices, and polar magnetic field strength.

In the case of sunspot numbers, *Hathaway* [2016a] states that prediction of a solar cycle through sunspots is fairly certain after about three years into the cycle, which means that early on the cycle progression is more uncertain. This was especially true for the original predictions for Cycle 24 (the current cycle) as shown in Figure 2.5 as compared with the actual cycle progression (Figure 2.2b). The current cycle was predicted to be low or moderately strong with NOAA's panel divided between the two predictions, and progressed to be the smallest sunspot maximum since Cycle 14 (maximum in 1906) [*NOAA*, 2016d; *Hathaway*, 2016a].

Hathaway [2010] outlines the approaches for solar cycle prediction through measurement of previous cycle sunspot numbers, geomagnetic current levels, and dynamo theory. One approach is to use a benchmark such as the mean of the last known sunspot amplitudes, and then consider the longer-term variations in cycles to improve on this benchmark. One implementation of sunspot amplitudes is discussed in *Kim et al.* [2004], which is a self-correcting model based on treating even and odd numbered solar cycles separately in addition to the rise and fall portions of solar cycles. From these data the statistical model is created, including predictions for the coming cycle with projection errors that can be corrected as the cycle progresses.

A more reliable and wider used prediction method is to utilize geomagnetic pre-

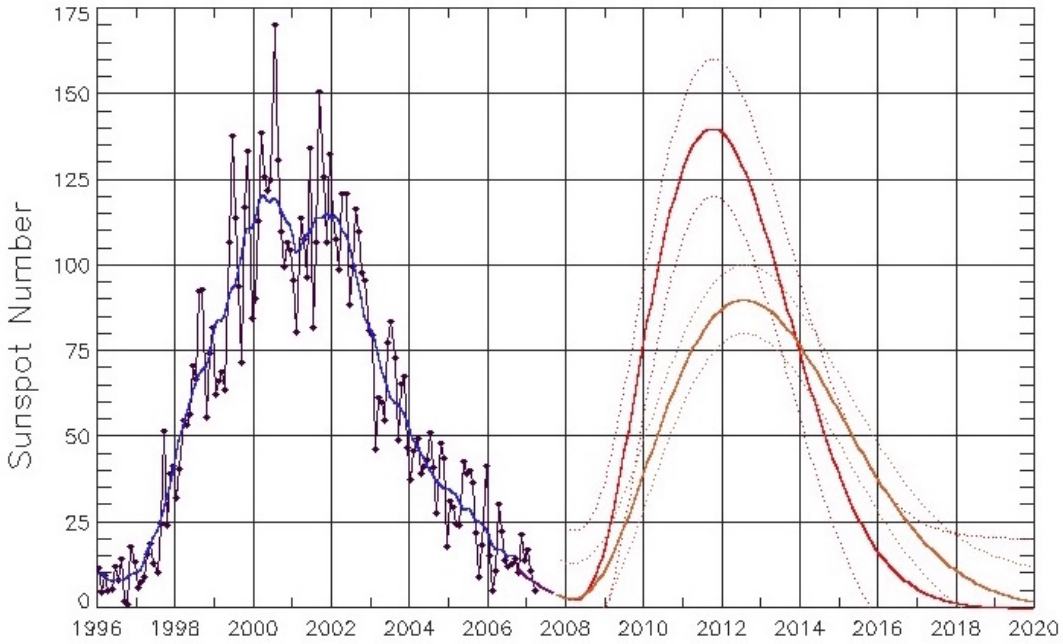

Figure 2.5: Sunspot prediction for Cycle 24 given in 2007. The two solid lines represent the high and low predictions for this cycle while the dotted lines are 1-sigma error bands. As this cycle progressed, it became clear that the lower sunspot prediction was correct. Source: NOAA Space Weather Prediction Center [*NOAA*, 2016d].

cursor indices, some of which extend back to 1844 [*Hathaway*, 2010]. These indices include the *aa* index, which measures the variability in the geomagnetic field in three-hour intervals from two higher latitude stations. Specifically, the *aa* index measured after solar minimum can be a decent predictor for the amplitude of the coming maximum, but can sometimes be late, not giving much of an advanced prediction. Another approach is to separate the geomagnetic component from the "interplanetary" component through observation of high-speed solar wind components that vary with the solar cycle. The physics that causes the phenomena of geomagnetic indices is still unknown, but these indices remain useful predictors for solar cycle progression and prediction [*Hathaway*, 2010].

Models of the Sun's magnetic field through the use of dynamo theory can also predict solar activity levels, through measurement of the Sun's polar field and the variations through the cycles. Although accurate measurements can be difficult to obtain, measurements have been made since 1976 at the Wilcox Solar Observatory that correlate well with sunspot variations. Although it is unknown when the optimal time to make prediction measurements is, again these measurements are more reliable as a cycle progresses for creating predictions [*Hathaway*, 2010].

Further applications of the solar dynamo can also be used to make measurements including flux-transport methods, but many researchers are critical of this use stating that the solar dynamo is too unpredictable to use in this context [*Hathaway*, 2010]. Although not all are as critical of these approaches, it is clear that there is still much research to be done in order to understand the mechanisms behind solar activity variations, enabling more accurate future predictions and better risk assessment for future space missions.

2.3.2 Individual Event Arrival

Within the context of a solar cycle, individual event occurrence can be somewhat predicted in that historically the Sun releases more events during solar maximum than solar minimum. In addition, event development can sometimes be predicted through observation of particles emitted from the Sun or features on the Sun's surface that are known to precede events. Also, there are prediction tools that use a combination of models similar to the approach discussed above. Finally, there has been some research into event propagation through the inner heliosphere between Earth and the Sun, and the Earth and Mars that is relevant to missions outside the near-Earth environment.

One example of a model that gives a probability prediction for event occurrence

within the solar cycle was developed by *Kim et al.* [2009]. This statistical model uses SPE data from the last five solar cycles to determine event occurrence probabilities for anytime during a generic 4,000-day solar cycle. Another model described by *Nichols* [2009] takes a locally weighted regression approach to forecasting total dose from an event based on early event dose rates. When tested against past data, this approach produced greater than 80% of forecasts within uncertainty bounds for events less than about 1.5 Gy, however the uncertainty was large in these predictions.

Models that seek to use precursors generally utilize electrons, other current particle data, or identification of active regions to forecast events that have already begun at the sun and project their impact at a site of interest (i.e. satellite, Earth, Mars, etc.). Research conducted by *Posner* [2007] demonstrates that electron signatures can help provide short-term forecasting for SPEs in arrival time and intensity. Relativistic electrons in events arrive before heavier protons and ionized helium, allowing for warning of imminent event arrival. *Posner* [2007] uses GOES 8 data to derive the forecasting method and warning electron data can be obtained from SOHO, allowing for prediction up to one hour before an event arrives. Further research has also been done by *Steward et al.* [2011] in flare prediction to automatically identify solar active regions through solar magnetic field components. This approach, when tested produced greater than 80% correct prediction of flare class C or greater with a false alarm rate under 10%. A combination of CME and flare forecasting has also been investigated by *Núñez* [2011], who sought to predict the time interval that the flux is expected to meet or exceed SWPC's threshold for 10 MeV protons. The model was tested against events from the past two solar cycles (22 and 23), producing a detection rate of about 80% and a false alarm rate of about 30%, with prediction times of an hour or greater depending on event type and magnetic connection with Earth. Other than looking for specific particle and magnetic signatures, there are

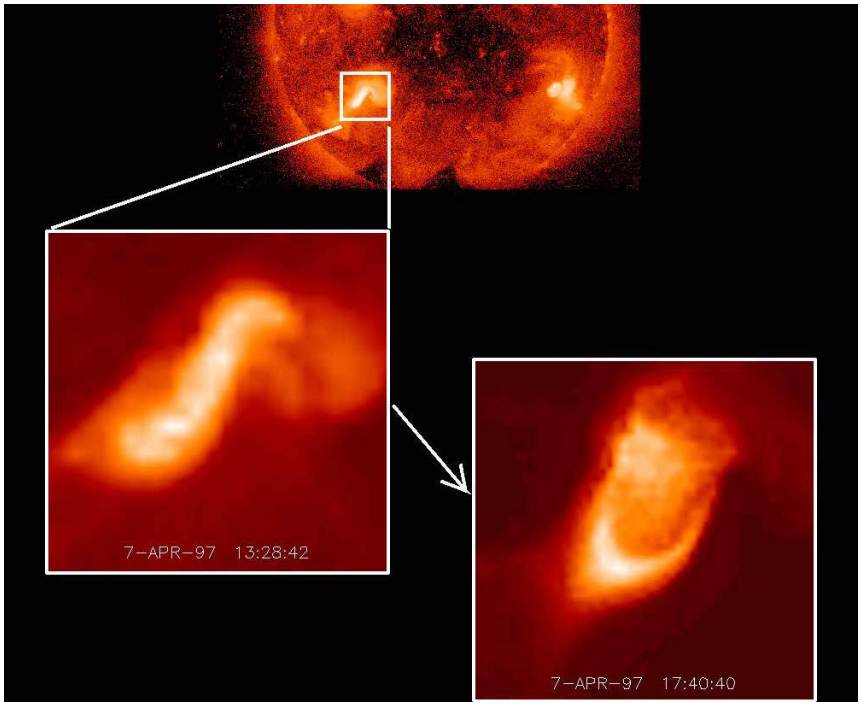

Figure 2.6: Sigmoid shaped magnetic region on the Sun. The sigmoid region is bright in the X-ray spectrum and in 1997 this region erupted soon after, releasing a CME. Source: NASA Astronomy Pictures of the Day [*Nemiroff and Bonnell*, 1999].

also visible signatures of CMEs such as the "sigmoid" appearance in the soft X-ray portion of the electromagnetic spectrum (see Figure 2.6). This sigmoid shape is produced from extreme twisting of the magnetic fields and is connected with high eruption probability, especially for CMEs, which in theory relieve the twist, but if it returns another CME could erupt from the same site in the future [*Knipp et al.*, 2011b].

The third approach to prediction includes the development of tools similar to ARRBOD or EMMREM, which integrate multiple models to better forecast and possibly predict events. One model developed by those who created EMMREM is PREDICCS - Predictions of radiation from REleASE, EMMREM, and Data Incorporating CRaTER, COSTEP, and other SEP measurements. PREDICCS is a

web-based system that is designed to forecast the radiation environment at Earth, the Moon, and Mars through integration of models and data (listed below) to generate the space radiation environment over time [*The University of New Hampshire Space Science Center*, 2016].

- REleASE - Relativistic Electron Alert System for Exploration: forecast model utilizing electron signatures to predict events up to 90 minutes before an event.
- EMMREM: provides a framework for the radiation environment, combining SPEs and GCRs inputs for dose over time.
- CRaTER - Cosmic Ray Telescope for the Effects of Radiation: instrument present on the Lunar Reconnaissance Orbiter that provides solar particle measurements, and
- COSTEP - Comprehensive Suprathermal and Energetic Particle Analyzer: experiment on SOHO that provides energetic electron and ion measurements that may impact the near-Earth and Moon environments.

Another approach under this category is by *Falconer et al.* [2011], which describes a software tool developed for NASA's Space Radiation Analysis Group to help forecast astronaut doses from SPEs. This tool uses an empirical relationship between event rate and the free magnetic energy of an active region to develop an algorithm based on historical active region data.

Although some of the models and tools listed above include particle forecasting outside of the near-Earth environment, there are also a few researchers who specifically target forecasting in this area for future space missions. One model developed by a joint US-Spain group examines the prediction of flux between Earth and the Sun (less than 1 AU distances) through the use of a database with pre-calculated

particle flux profiles [*Sanahuja et al.*, 2008]. The database includes nearly 700,000 possible combinations of heliocentric distance, shock speed, and other SPE parameters available for quick forecasting. Another joint group (US-German) examined the Hohmann-Parker effect for Mars missions or other missions greater than 1 AU from the Sun [*Posner et al.*, 2013]. Through applying common propulsion transfers from closer to the Sun to further from the Sun, *Posner et al.* [2013] were able to show that many of these transits remain within the same magnetic field lines from the Sun. The opposite transits depend more on solar wind speed and do not remain within the same magnetic field lines until approaching closer to the destination.

Models for prediction and forecasting of solar activity are less advanced than other areas of research discussed in the previous sections, but research is promising for future capabilities. Future astronauts will likely be able to forecast events if equipped with detectors and advanced software processing capabilities, allowing for optimal countermeasure usage and safe travel to Mars and beyond.

2.4 Literature Summary

The above sections have presented an overview of solar activity and the current state of research in understanding, modeling, and predicting SPEs, which is especially relevant for future human spaceflight radiation risk assessment. During solar minimum, events are less likely to occur, but severity is not necessarily associated with solar activity as events develop out of magnetic reconnections within the Sun's upper layers. Historical event data are most accurate when taken from space-age satellites, but other sources such as ground neutron monitors can be of use depending on application. Finally, models and simulations demonstrate integration of data and theories, allowing for increasingly accurate predictions and dose profiles for future missions.

Gaps in this research area include questions about solar activity generation that drive solar cycles, event occurrences, and integrated models. The solar cycle has been well observed through sunspots since the 1700's, but predictions are still uncertain for coming cycles. This gap may be filled through the continued collection of data and discoveries in solar activity theories, allowing for better understanding of the mechanisms that cause solar cycles. Next, historical data for SPEs have been noted for decades, but data before the 1950's are generally not accurate enough to determine event occurrence and magnitude (with the possible exception of extremely large events). Additionally, there are sometimes measurable precursor signatures for events, but with the diversity of events, these are only useful in short-term warning (on the order of an hour) and only for near-Earth space (or locations magnetically connected with Earth in the IMF). This gap may also be filled through acquiring more data from future solar cycles and through understanding of event generation, but also through greater satellite or detector capabilities for future space missions. Finally, models and simulations have existed for various aspects of solar activity for decades and depending on the application, can be quite useful. There are gaps in this area because some models use outdated information and cannot easily be integrated with other mission risks outside of space radiation.

The research presented in this document aims to help fill the gaps highlighted in the last area - modeling and simulation studies. The next sections in this document cover the development of a SPE risk model that integrates GOES data and NASA tools, and its application to future human spaceflight missions. Although solar activity is complex, it is hoped that research presented herein will help further the development of this research area, enabling safe travel beyond the near-Earth environment to Mars and beyond.

3. HISTORICAL EVENT DATA ANALYSIS

Out of the possible SPE data sources, the joint NOAA-NASA GOES program was chosen for this research due to the decades of data and similar systems used throughout each generation of satellites. The information gained from the analysis presented below of GOES data provides SPE probabilities and spectra, which form the basis for a Monte Carlo model and dose assessment for radiation risk.

3.1 Data Sources

Of the energetic particle data sources discussed in Section 2.1.2, neutron monitors, GOES, and IMP provide space age proton flux data that can be used to generate SPE occurrences and magnitudes for risk assessments. Other ground-derived data (relying on radionuclides/isotopes) are not currently usable due to high uncertainties, while other satellites do not provide accessible and relevant data for proton flux through out the past few decades.

3.1.1 Neutron Monitors

Currently the most reliable ground observations for solar events are from neutron monitors through GLE measurement. Researchers that have analyzed GLEs to obtain SPE data include those by *Bieber and Evenson* [1991], *Smart and Shea* [1989], *Stoker* [1995], and *Tylka and Dietrich* [2009]. Some of these sources also contain joint data sets between satellite and neutron monitors with comparisons between the two. Since the data from neutron monitors starts in the 1950's, there are advantages to using the plethora of data for SPE research, but also disadvantages compared to SPE satellite data.

The measurement of GLEs with a neutron monitor occurs through detection of

secondary particles created by solar or galactic particles above a threshold. This threshold is a measure of geomagnetic rigidity cutoff (GV), which varies based on latitude with some neutron monitors having lower thresholds and some higher based on the strength of the Earth's magnetic field at that location [*Shea and Smart*, 2006]. Based on the particles that exceed this threshold, SPE spectra can be back calculated from a GLE.

Current neutron monitor data can be found through the University of Delaware's Bartol Research Institute [*Bieber*, 2014]. This research institute provides real-time data and a six-month history plot for seven different neutron monitors, including data from Inuvik (North West Territories) and McMurdo (Antarctica). Additionally, older data can be accessed online for many of the monitors, with data as far back as 1957 from McMurdo, Swarthmore/Newark (Delaware), South Pole, and Thule (Greenland). Finally, SPE probabilities can be derived through the combination of GLEs and Forbush decreases.

Aside from any possible problems associated with converting GV values to particle measurements and the calibrations required to do so, the primary drawback to using neutron monitor data is that only particles of extremely high energy exceed the thresholds producing GLEs. The result is that satellites are a better data source for SPE likelihood and/or frequency compared to neutron monitors. Compared to the data accessible from satellites, this means that it is more difficult to determine likelihood for SPEs if many are not detected. Although the SPEs that are not detected may not impact missions, they are still important to consider in the context of total mission dose.

In addition, neutron monitor data can even be questionable for larger well-known SPEs such as those from 1956 and 1960. The 1956 SPE was early in the development of neutron monitors and did not have as much data supporting it as later SPEs

did with the implementation of more detectors. The 1960 SPE did not have the disadvantage of sparse data, but still there have been large differences in estimates of integrated fluence between researchers [*Shea and Smart*, 1990]. These early SPEs were prior to accurate satellite coverage, but more recent SPE comparisons between GOES and neutron monitor data have shown better agreement [*Mottl and Nymmik*, 2007; *Shea and Smart*, 1990].

With these limitations and drawbacks, neutron monitor data were not selected for use in this research at this time and data are drawn from the satellite sources listed below. Satellites come the closest to the ideal data source for this research at this time as they provide both likelihood and magnitude for SPEs. Satellites also contain data from MeV level protons directly, limiting the amount of correction and/or extrapolation needed. Neutron monitors may be of use in this research field in the future for investigations into the higher energy portions of SPEs.

3.1.2 Satellites

The largest body of relevant data for SPEs is derived from the IMP and the GOES satellite sets. It was from these satellites that NOAA developed cutoffs for SPEs based on the 10 MeV proton data. Other satellites such as SOHO or SDO are useful for monitoring other radiation types such as X-rays for solar flares. A description of both the IMP and GOES programs is given below, including their capabilities, years of data collection, and the advantages and disadvantages to using data from each.

3.1.2.1 IMP program

The IMP satellites were used in determining SPE occurrence from data in starting in the early 1970's. These data are sourced most commonly from IMP-8, which launched in 1973 to monitor space weather with both magnetic activity and particle

detectors. The orbit of IMP-8 was fairly high, ranging from around 130,000 to 280,000 km, placing it well out of the radiation belts of Earth [*Grayzeck*, 2016]. IMP-8 was also known as IMP-J or Explorer 50, which was the last of the satellites in that program. IMP-8 originally provided coverage rates of over 90%, but was reduced in the 1980's and early 1990's with a return to the higher coverage till it was discontinued as an independent mission in 2001. After 2001, coverage was as low as 30% at times due to multiple issues including acquisition problems. IMP-8 continued to provide scientific data up till 2006, after which data are not reliable for scientific purposes [*Grayzeck*, 2016].

Earlier IMP satellites included IMP-6 and IMP-7, which were primarily designated as gamma-ray monitors to detect bursts in the space environment originating from multiple sources (Sun, stars, novae, etc.) [*NASA*, 2003a]. IMP-6 was launched in 1971 and IMP-7 followed in 1972. These satellites also had particle detectors and were capable of measuring the enhancements in the proton spectrum that signify SPEs as with IMP-8. Overall these satellites provided just under three decades of data covering the space radiation environment in high altitude orbits [*NASA*, 2003a; *McGuire*, 2002].

The IMP program's particle measurements included protons (0.5-500 MeV), helium ions (1.2-500 MeV/nucleon), heavier ions (carbon through iron, 1.5-40 MeV/nucleon), and relativistic electrons (3-18 MeV) [*McGuire*, 2002]. Data can be downloaded for specific times of interest for these satellites through the Coordinated Data Analysis Web (CDAWeb), which is managed by NASA Goddard Space Flight Center [*NASA*, 2016b].

The IMP program provides a wealth of possible data for use in measuring SPEs, but has a few disadvantages to using these data compared to the GOES program. The main disadvantage is the high amount of processing needed if not utilizing a previous

researcher's work with the data set. As provided through online data repositories, the data are not corrected for background counts or any other possible issues that may make it less accurate. Originally the GOES data were similar in availability, but as it became the primary data set for researchers, new averages were calculated and data going back 30 years is now available in the newer format, mitigating these data availability issues and decreased errors in the data. Also, the data points are less frequent for IMP with particle data given in 30-minute fluxes, not 5-minute fluxes as GOES program data are. In addition, IMP-8 had years that it was less than full in its coverage, meaning that there are times when a SPE occurred and the satellite may have not recorded it. In comparison, GOES generally had two or more satellites measuring particle fluxes at any time and so did not have as frequent gaps in coverage. Despite these disadvantages to utilizing IMP data, there were a number of SPE analyses, which can be helpful in comparison of larger events from multiple detectors (IMP, GOES, and neutron monitors) [*Goswami et al.*, 1988; *Jun et al.*, 2007; *McGuire*, 2002; *Sandberg et al.*, 2014].

For analysis of SPEs over multiple years, IMP data were not selected to be included due to the possible data issues from coverage and corrections. In other research contexts the IMP data may be useful, especially for single event analyses from the 1970's while coverage was still over 90% or in comparison with other data sources (neutron monitors) to derive more accurate early SPE data.

3.1.2.2 GOES program

The GOES program has become the primary data source for SPE measurements at 1 AU and is utilized in a variety of research applications. The first GOES satellite started to measure the space weather environment in 1976 and new generations of this program continue to the present day [*NOAA*, 2011a, 2016b; *NASA*, 1996].

The most recent satellite in this program is GOES-15, with new data coming soon from GOES-R, which launched in November 2016 [*NOAA*, 2016b]. GOES primarily measures the space weather environment from GEO, which is approximately 36,000 km above the Earth [*NASA*, 1996]. For space weather observations, this altitude allows measurements to be taken mostly outside Earth's radiation belts. The primary interference at this altitude is in the electron spectrum, not protons, making it an excellent location for SPE measurements for spaceflight applications outside LEO [*Knipp et al.*, 2011c].

The GOES program has been split into a few different satellite generations (series) with each containing nearly the same instrumentation for measuring space weather [*NOAA*, 2016c]:

- GOES-1 to GOES-3 (A-C): 1976-1983
- GOES-4 to GOES-7 (D-F, H): 1983-1994
- GOES-G: launch failure [*NASA*, 1999]
- GOES-8 to GOES-12 (I-M): 1995-2010
- GOES-13 to GOES-15 (N-P): 2010-present
- GOES-16 (R): launched in November 2016, data available in coming months

Data availability starts in 1986 for particle radiation with GOES-6 and GOES-7 from NOAA's database. This database includes "new averaged data that were updated since 2011 in an effort to decrease errors and apply new methods to increase reliability for this dataset [*NOAA*, 2011a, 2016c]. Other satellites after GOES-6 and GOES-7 are sometimes missing data for a SPE due to satellite errors such as with GOES-9, which was deactivated early due to hardware issues. GOES-11 and GOES-14 also had problems with data coverage relevant to SPEs. In the past, particle data prior to 1986 were available in the FITS format, but is currently not available and only magnetic field and X-ray data are available at this time. Data access is open and

free from *NOAA* [2016a] directly or through the linked FTP site, both of which also contain information about updates to the data and starting points for research related to GOES.

The GOES program has included similar measurements to the IMP program including detectors for: electrons, protons, and ionized helium (alphas) at relevant space weather energies (MeV). These measurements are from two sets of sensors that form the space environment monitor (SEM) on GOES: the energetic particle sensor (EPS) and the high energy proton and alpha detector (HEPAD) [*NASA*, 1996]. EPS (in later generations called EPEAD for energetic proton, electron, and alpha detectors) is a combination telescope and dome assembly designed to measure electrons from 0.6 to 4.0 MeV, protons from 0.8 to 500 MeV, and alphas from 4 to 500 MeV per nucleon. HEPAD measured protons at 330 MeV and above and 2.5 GeV and above for alphas [*NOAA and NASA*, 2009; *NASA*, 1996]. The SEM on GOES also includes an X-ray sensor to observe the solar X-ray output that is associated with SPEs. This sensor can be useful if a particle event list is not available, but as a list is generated from NOAA (*NOAA* [2011b]), the X-ray data were not used in this research. Specifications for these sensors are discussed briefly in the GOES data books (*NOAA and NASA* [2009]; *NASA* [1996]). The EPS/EPEAD has a band edge stability of $\leq \pm$ 3%, and a noise level of around 10 keV below 100 keV and 10% of threshold energies above 100 keV. The largest sources of possible error associated with these detectors are orbit and satellite dependent, not related to sensors as discussed in the next paragraph.

Although the satellites in GOES program are used for the primary measurement of SPEs today, there are some disadvantages in using this dataset for research related to data availability and intercalibration between satellites. Also, there are not HEPAD data for GOES-7, and GOES-14 did not provide particle data for any SPEs

so far. Comparing satellites to one another, there have been instances of unusual highs or lows between satellites of the same generation that can be related to orbital location and/or directionality. In addition, the directionality of a satellite was not always fixed, depending on whether it was spinning or three-axis stabilized, and even stabilized satellites flip their orientation once or twice a year [*Rodriguez et al.*, 2014]. Before GOES-8, the satellites were more commonly spin-stabilized, but GOES-8 through GOES-12, with the exception of GOES-10 faced westward (GOES-10 eastward) at all times and GOES-13 through GOES-15 alternate [*Rodriguez et al.*, 2010]. The sensors on GOES generally record higher fluxes when facing westwards versus eastwards, but this difference is not large during SPEs since it depends on magnetic pressure. Magnetic pressure increases during solar eruptions, which decreases the west/east difference to values similar to the baseline differences from one GOES to another. This difference can also be mitigated in the future as shown through research by *Rodriguez et al.* [2014], which shows that these differences can be reduced to less than 10% for all times, not just during SPEs, using the procedure described in their work. The data availability problems pose the larger issue for analysis since data gaps must be analyzed to determine if SPEs with missing flux points should be included or not, with guidelines set to determine if a SPE is still acceptable for analysis.

Since the GOES program is ongoing with a new satellite just launched in November of 2016, this dataset will continue to be of use into the future. Additionally, improvements to the sensors on GOES through the generations have increased the reliability of this dataset in comparison to other programs that only have one satellite that measures particle data for years without replacement parts or software. Finally, the limitations discussed above have somewhat been overcome through intercalibration research, and the remainder can be addressed through thorough data

processing. For these reasons combined with a long-standing use of GOES data in literature (*Sauer* [1993]; *Smart and Shea* [1989, 1999]; *Townsend and Zapp* [1999]; *Zapp et al.* [1999] and many more into the 2000's), these satellites were chosen to complete this research to generate the necessary input conditions and underlying probabilities for the SPE risk assessment model described later in this document.

3.2 GOES Data Selection

GOES data used in this analysis were comprised of available proton solar particle data from the NOAA database (*NOAA* [2011a]). The NOAA database includes monthly .csv and .nc formats organized by year, with one to four satellites covering a particular month that recorded particle data. The .csv files were used in this analysis and processed through the MATLAB code files listed in Appendix B for all months with SPEs as listed in the NOAA SPE list: *NOAA* [2011b] from 1986 to the present. Components of the GOES dataset that needed to be addressed during selection were HEPAD data, energies for severity cases, and choice of satellite(s).

Most data from the EPS/EPEAD were utilized, but the HEPAD data were excluded from this analysis due to data availability and its low capability for adding to the risk model. The HEPAD data were not consistently available till 1995 for all satellites, as GOES-7 did not include this part of the dataset. It was decided to start with data from 1986 without HEPAD instead of with this data in 1995, increasing the number of years of data available for analysis. In addition, the HEPAD data only add one more data point for the higher energies and is not corrected as the EPS/EPEAD, so utilizing the higher energy data will not likely add to the accuracy of the risk model. This exclusion of HEPAD still leaves the 5-minute averaged proton flux for energies of >1 to >100 MeV. No other reduction in data from *NOAA* [2011a] was undertaken at this phase of data analysis.

In past analyses, there has been a focus on either >10 or >30 MeV as a standard for integrated fluence [*Shea and Smart*, 1990; *Kim et al.*, 2009]. Both of these energies are of interest in this research area since 10 MeV is part of the NOAA definition for a SPE (defined in next section), and 30 MeV is the energy that it takes for a proton to penetrate an EVA suit [*McPhee and J. B. Charles, eds.*, 2009]. This analysis considers all energies and then focuses on specific cases as applicable to the research results. This decision was motivated in part due to the differing spectral shapes, making it difficult to choose one, as SPEs can share integrated fluence at an energy or two, but have different doses. Later after calculating doses (see Section 4.2) for a specified shielding level, it could be shown that there was the closest relationship between dose and fluence in the two highest energy bins (>60 and >100 MeV). The energies most closely correlated with dose likely depend heavily on shielding and so through use of all the energies, it is possible to adjust to use a specific energy bin as needed depending on the application.

Finally, lists of major SPEs generally use data from one satellite or another such as in *Kim et al.* [2009], which includes specific satellites and not averages or multiple satellites that covered the same event. Since this past approach may not cover all scenarios due the differing spectral shapes of SPEs, in this research, every satellite with usable data was considered. From examination of the differences between integrated fluences of satellites covering the same SPE, there are differences in spectra, even between satellites that are part of the same generation/series. A few examples of these spectra differences are discussed below, and further details can be found in the appendix material, which lists all SPE data generated from the analysis code discussed in the next section.

- 1989, September: event starting on the 13th had higher values for integrated fluence at all energies for GOES-7 compared to GOES-6, but event on the 29th

switched to higher values around 30 MeV for GOES-6.

- 1989, October: had similar trend for event starting on the 19th as with the September 29th event.
- 1991, June: for the event on the 4th GOES-7 had higher integrated fluences at 5, 10, and 30 MeV, and GOES-6 was higher for 1, 50, and 60 MeV, and the satellites were approximately equal at 100 MeV, but later events that month showed a dominance of GOES-7 for all energies.
- 1998, April: GOES-8 was approximately equal to GOES-9 for integrated fluence over all energies.
- 1998, August: GOES-8 had higher integrated fluence values compared to GOES-10, but this effect was lessened for energies of 1, 60, and 100 MeV.
- 2001, April: GOES-8 tended to have higher integrated fluence values compared to GOES-10, especially at 10 MeV and below, while GOES-11 was more likely to agree with GOES-8 instead of GOES-10.

The list above is only a small sample of the differences observed between satellites and due to lower quality data from other sources, only larger SPEs can be distinguished as to which satellite might provide the more accurate data. Additionally, these differences in spectra mean that doses can be different between SPEs that may share the same integrated 30 MeV fluence. Therefore, the 30 MeV fluence should not necessarily classify SPE severity. The solution to mitigate these differences was to average the spectra obtained from EPS/EPEAD for a SPE from all satellites that recorded the event. This prevents bias in attempting to choose one satellite over another when it is not necessarily known which provides data that have higher risk if such a SPE occurs.

Through the analysis presented here, the primary data excluded were from HEPAD due to data availability issues and data included were all energies for all satel-

lites with EPS/EPEAD data for the month of a SPE occurrence. Although this increased the time necessary to analyze the data, the final risk model will be more reliable through these data choices. The next section discusses decisions made during processing of the 30 years of solar particle data and the results of the data processing.

3.3 Event Resolution

SPE analysis was completed through the use of MATLAB, with code files written to take direct input of the GOES data from NOAA data files and resolve SPEs. Additional notes are in Appendix B regarding the operating system and version of MATLAB that was used and additional information about using this analysis code set. This section contains information related to event processing, including the assumptions and definitions applied in the process, an overview of the workflow within the code, and a summary of the results that were eventually used for risk analysis.

3.3.1 Constraints Development

To resolve events from the NOAA GOES data there were a set of constraints applied in two categories: NOAA definitions and research derived constraints. NOAA defines what a SPE is in context of the GOES data by setting a 5-minute averaged proton flux value that must be exceeded of 10 pfu (particle flux units, 1 p/cm^2-s-sr) for protons >10 MeV. In addition, this value must be equal to or exceeded for three consecutive data points for the start of a SPE. The end of a SPE is the last data point that equals or exceeds the 10 pfu criterion before dropping below this value. This definition was created by researchers based on the data to allow for multiple events and shock accelerations within rises from the baseline, which generally is on the order of 0.1 to 0.01 pfu for protons >10 MeV.

From working with the data it was clear that additional assumptions would be

needed to fully resolve SPEs based on the NOAA event list (*NOAA* [2011b]). The part of the NOAA definition that posed the most difficulty in event resolution was the ending criterion since events can rise and fall during all portions of the event, including the "tail" of a SPE. Sometimes the 5-minute flux will fall below the 10 pfu criterion and still rise above 100 pfu later while still being part of the same SPE. The rises and falls that produce this effect can be seen in Figure 3.1 below, showing the 5-minute flux at >10 MeV for the notable October 1989 event.

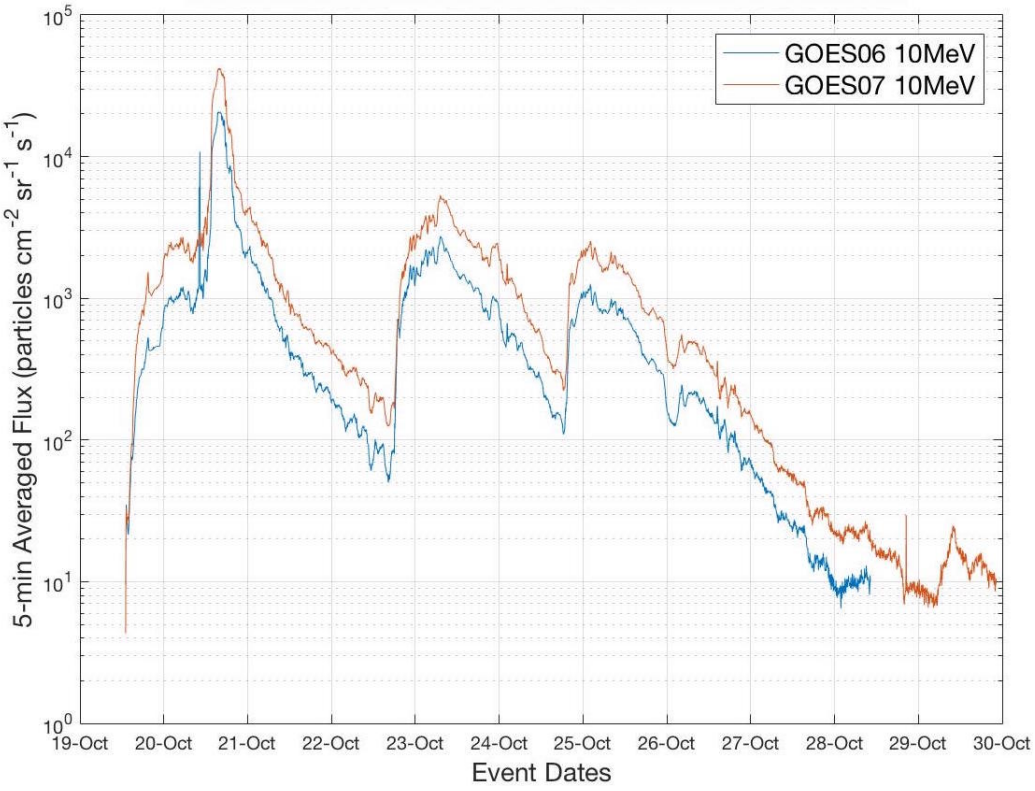

Figure 3.1: October 1989 event progression. The 5-minute flux at >10 MeV is plotted for GOES-6 and GOES-7, showing the rise and fall as the event progresses. At the end of the event for both satellites, there is a brief rise back above the 10 pfu criterion before decreasing back below.

Other events that rose and fell within an event included July 2000 and January 2014. In July 2000, GOES-10 rose to 45 pfu after about 5 hours below 10 pfu. GOES-13 in January 2014 had an initial rise, not even breaking 20 pfu and fell off for a few hours before returning to previous levels and then rising to above 100 pfu. To counter these rises and falls, a different ending criteria was developed to look for the last point $\geq$10 pfu that falls off afterwards to $<$3.33 pfu. Other values were examined such as 6.66 pfu or 5 pfu, but 3.33 pfu captures the event starts/ends better than other approaches. This was still not completely inclusive of all events and so the MATLAB code also includes a check for the user to verify that a SPE is not occurring just after another when it finds a possible end to the event, which is better captured by a 6.66 pfu criterion.

Another consideration related to the NOAA criteria is that there are sometimes smaller SPEs that do not rise to 10 pfu or above, or may only have a data point or two that do meet this criterion. It was determined that these are not important for the dose analysis since they would not contribute to dose compared to galactic cosmic ray sources present at the same time. For the MATLAB code, these months are still entered, but MATLAB returns information that an event was not present and moves on to the next month of analysis.

Besides possible loss of data through strict use of the NOAA SPE definition, there was also the question of how to approach missing data points within the files. Sometimes satellites will lose coverage or there will be a temporary loss of data during a SPE and these are reported in the files as a large negative number on the line instead of a flux value. These points cannot simply be excluded from analysis since they take away from the final integrated flux value, slightly decreasing the dose (depending on when during an event). In the past, the practice has been to interpolate between values to fill in the approximate values that the sensor would

have provided, and this approach was continued in this research [*Nichols*, 2009].

Finally, there were two criteria applied to determine if an event should be excluded due to an excess of missing data: the event must either have more than 10% of the data missing throughout the event or more than two hours in succession (24 data lines) missing. These criteria were developed from examination of the data, which showed that SPEs with over 10% missing generally were missing much more than 10%. Examples of this typically occurred in the GOES-11 data when the satellite was underperforming in 2001. This primarily occurred in March and part of April, where GOES-11 had many more missing data points than GOES-8 and GOES-10. Also, since SPEs can change dramatically over the course of two hours, the additional criterion of no more than two hours in succession missing was implemented to make sure that no rises or falls in data would be missed. Examples of these can be seen in any SPEs that have a steep initial rise such as the October 1989 event shown earlier that rose a full order of magnitude for the >10 MeV flux in about two hours. Other larger SPEs show similar trends as well in the >10 MeV flux including the early November 2001 event that rose two orders of magnitude over three hours, and the Halloween event of 2003, rising two orders of magnitude in about two hours.

In summary, the NOAA definition criteria for SPEs were used, but additional derived constraints were added to the code to fully resolve events. These cover cases such as rises and falls in the tail of an SPE and small rises not meeting NOAA's cutoff. The last area covered was the approach for missing data points where a 10% criterion was applied to limit the amount of interpolation to be used when calculating the integrated fluence for each event. The next section discusses how these criteria and constraints were implemented into the data analysis code files while giving an overview for a future user.

3.3.2 Characterization

Events were generated through a main script file that the user can call, which asks for the names of files to be analyzed and loops till the end of the number of files a user has designated (by number of months). The end result is two files in .xlsx format: a listing of event spectra (integrated fluences by energy bin) and missing data points filled through interpolation to generate the event spectra. Additional information about these output files is given in Appendix A, which gives information about specific outputs to the files. This section describes briefly from NOAA data file input to .xlsx file output what steps were taken in the code and an overview of the process is shown in Figure 3.2 below.

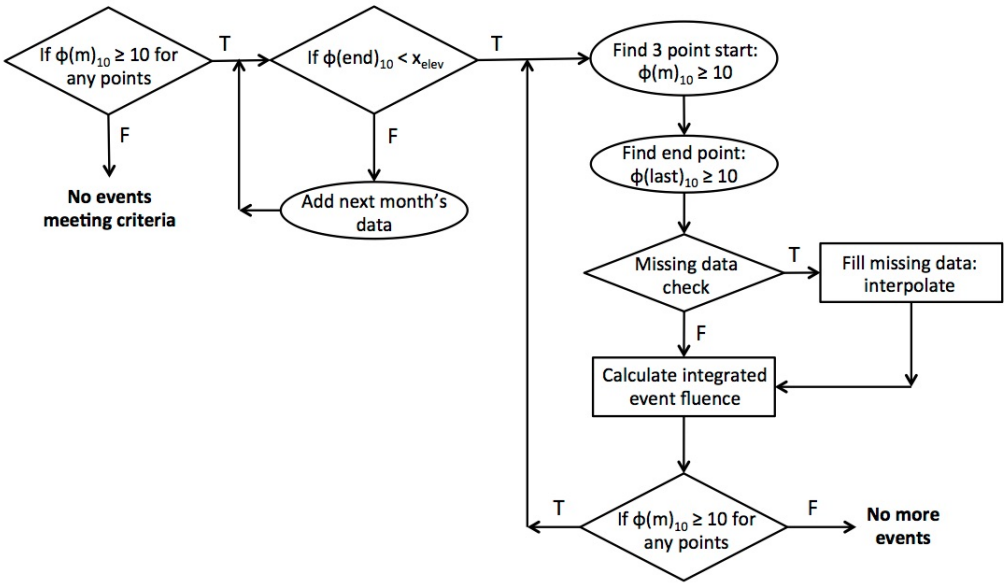

Figure 3.2: Data analysis flowchart for MATLAB code. $\phi(m)_{10}$ is flux > 10 MeV, x_{elev} is the cutoff value to check for elevated fluxes near the end of a month, and m is any point in the flux. The analysis begins in the upper left and finishes in the bottom right through checks for exceeding the 10 pfu criterion. For more details see the appendices.

Before characterizing the events themselves, it was necessary to perform a few steps to prepare the data and check for possible problems that would interfere with event analysis. The first step was to construct a function that would take the monthly inputs of NOAA data and generate usable matrices formatted for MATLAB. In addition, another step preceding individual event analysis was to check that a month did indeed have data meeting the NOAA 10 pfu criterion since there are cases where a month with an SPE in NOAA's list was not shown in the data. This can happen due to lower fluxes for one satellite compared to another (one shows an event and the other does not) or there was missing data masking the event's occurrence. After this check, the end of the data file was examined for missing data points at the end of the month that might obscure a SPE's start or end. Then the data are checked for elevated flux values (indicating a SPE occurrence soon or part of the tail) using the same criterion as mentioned above for the end of an event (3.33 pfu). If the flux values are elevated, the user is asked to enter the name of the file corresponding to the next month. Once these steps take place, individual event occurrences are determined.

The start of a SPE was determined through searching the data for the NOAA three point start, but skipping values that were missing. After finding the start of the event, the program continued to execute till a drop below 3.33 pfu was detected and the last point before that $\geq$10 pfu is counted as the end of the event, excluding missing data points again. The user is asked at this point if another SPE occurs near in time to the current SPE being analyzed and the code is designed to find a different end if so to separate out events. Next, the program checks for missing data points during the event, and fills them based on interpolation for the last non-missing data point before missing data and the next non-missing data point after the missing data. As noted above, if there was more than 10% overall or 2 hours missing, the

event was excluded since flux changes might be obscured. Finally, after recording missing data points, the integrated fluence was calculated for each energy bin in the spectra and all information recorded about the execution.

After processing the files, the resulting outputs were examined and checked for SPEs listed as separate that should be part of one event through comparison with the NOAA event list. These were combined or re-executed as necessary to insure that the events were properly processed to finalize the SPE processing.

3.3.3 Code Results

After processing all of the relevant monthly data files from NOAA through the data analysis code, there were a total of 191 SPEs resolved out of the possible 205 for 1986 to present from NOAA's event listing. The most common reason the lower number of resolved events as that the events were smaller and did not meet the three consecutive points at or above 10 pfu (such as in 1988). One SPE (July 7, 1991) also had poor data quality and was excluded due to missing too many data points over the course of the event for all satellites observing. Other cases of too many missing data points did occur, but there was at least one other satellite providing more reliable data. The only other loss of an SPE compared to NOAA's listing was for the January 6, 2014 event, which had two events occurring at nearly the same time and so were combined together since the data could not be resolved into two separate events.

Comparing these 191 SPEs to known literature examples, there were 5 events exceeding 2 x 10^9 p/cm^2 at $>$ 30 MeV fluence, which matches the events that *Kim et al.* [2009] list for 1986 to 2007 meeting this level [1]. In addition, values of the >30 MeV event fluence were compared to satellite values reported in literature for these

[1]Note: *Kim et al.* [2009] lists 2008 as one of these SPEs that exceed this limit, this should be referring to 2003 - "Halloween" event that year.

5 larger SPEs:

- October 19, 1989: the value obtained through the code is within 0.3% of the literature value for GOES-7
- July 14, 2000: values are equal between literature and code for the three significant figures reported for GOES-10
- October 28, 2003: values are within 0.3% of each other for GOES-10
- November 4, 2001: values are equal for significant figures reported for GOES-10
- November 8, 2000: values are equal for significant figures reported for GOES-10

In examining the number of SPEs per solar cycle found in literature and through the data analysis, the numbers do differ for Solar Cycles 22 and 23. Solar Cycle 22 (1986-1996) was reported to have 77 SPEs, but the code only produced 63 since 12 events listed did not meet the 10 pfu criterion. The next solar cycle was much closer with literature listing 92 and the code producing 93 [*Kim et al.*, 2009]. The differences in number are likely due to the data used in analysis since NOAA has released revised solar particle data since *Kim et al.* [2009] was published. This revised data have little impact on larger SPEs, but can easily change smaller ones that barely met the 10 pfu criterion. Overall, the results match well with values reported in literature for larger SPEs, while deviations for smaller events that did not always make the 10 pfu criterion.

3.4 Data Summary

In order to produce the background data for the risk model, three different sources of solar particle data were examined in detail. Both neutron monitors and the IMP program were not selected as data sources due to problems with measurement and data availability compared to the GOES program. Although GOES has its disadvantages as well due to differences in calibration between satellites, these effects are

lessened for this research application. The GOES dataset itself is publicly available through NOAA at *NOAA* [2011a] and is updated monthly, while a list of SPEs derived from these data can be found at *NOAA* [2011b]. In order to efficiently and consistently extract SPEs from the 5-minute flux data, a data analysis code was developed in MATLAB that will take data files as inputs for GOES-6 through GOES-15 and output event fluences and filled data points (due to missing data). This process also integrated other research derived constraints into the code besides the NOAA definition of 10 pfu at >10 MeV for event occurrence to account for rises and falls in the data, and missing data points due to satellite coverage availability problems. Finally, from processing events from 1986 to the present, there were 191 events meeting the criteria out of the 205 listed by NOAA, which for larger SPEs matched well with values reported in literature. The SPE event fluences generated from this data analysis process are used to derive the needed distributions for the SPE risk model described next.

4. EVENT RISK CODE DEVELOPMENT

This section discusses development of the SPE probabilistic risk model for outside of LEO, which contains smaller models that were integrated together from Earth orbit models, satellite-based dose distribution, and orbital location effects. In addition, NASA risk assessment methods are applied as relevant to this research. This step is taken to begin the process of credibility assessment, which will make the model ready for peer review and eventual use by NASA.

Throughout this process of code development, the primary test cases for evaluation were a combination of Earth orbit and Mars transit mission segments. For the Earth orbit case, there are no orbital location effects, allowing for isolation of other components of the model. This case is designated as GEO, for geostationary Earth orbit since this is where the satellites used in this research recorded the data. The GEO case is set to be a 180-day mission to match similar length seen in LEO with the ISS. The Mars transit cases vary and are taken from the Mars Design Reference Architecture (DRA) document (*Mars Architecture Steering Group and Drake* [2009]). The Mars DRA document includes information about two generic round-trip missions designated as "long-" and "short-stay", with outbound transits of 210 and 217 days and 210 and 403 days for the return/inbound transits respectively [*Mars Architecture Steering Group and Drake*, 2009]. The short-stay return is much longer than the other transits since it includes a Venus swing-by before returning to Earth. There are many more Mars transits possible to apply to this research (see *Burke et al.* [2010]), but the ones presented in the DRA are adequate for this research. This set of mission transits can be used in the initial model credibility assessment since it includes both Earth orbit and non-Earth orbit, including basic and complex

transits that have already been well studied. Out of the five transits, the best case from a dose perspective should be the shorter Mars transits and the worst-case the Venus swing-by with GEO as a control. Further information regarding the doses seen in these orbits can be found after discussion of the SPE risk model development.

4.1 Earth Orbit Model Basis

Since most models and data focus on Earth orbit, there are a number of usable models to apply for the first part of the model, which models the likelihood of SPEs. The model investigated for use by the IMM team is by *Kim et al.* [2009] and from a literature review, this model is the most suitable for this research. Other possible models were discussed in Section 2.2.1, including *King* [1974] and *Miroshnichenko and Nymmik* [2014], both of which take probabilistic approaches to SPEs, but have disadvantages to their use in this research. *King* [1974] has been integrated in to a number of models since it was first developed, but separates events out into "ordinary" or "anomalously large" SPEs. This assumption has been shown to be unjustified since SPEs tend to follow continuous distributions and it also raises the issue of what fluence and/or energy qualifies for "anomalous." This issue combined with older data from IMP, makes *King* [1974] a disadvantageous model to use for SPE likelihood. The other model (*Miroshnichenko and Nymmik* [2014]) takes all available data for development of a probabilistic approach, generating probabilities for >30 MeV fluence. The disadvantages of this model include that it uses ice core data in its development (contraindicated, see *Carnell et al.* [2016]) and that it assumes that SPE spectra follow double power-laws. SPE spectra are more commonly modeled with Weibull or exponential fits, and so, it is more difficult to validate and verify this model. Other models mentioned in Section 2.2.1 do not take probabilistic approaches or are not capable of being integrated directly into the risk model devel-

oped here. As a result, the model by *Kim et al.* [2009] is used as recommended by the IMM team to determine event occurrence throughout a solar cycle.

4.1.1 Kim Occurrence Model

Kim et al. [2009] used space age data to develop a model for the probability of SPE occurrence by day during a solar cycle. The model is based on a Poisson process and hazard function approach to generate the final model by goodness-of-fit. *Kim et al.* [2009] selected an adjusted beta distribution function as the optimized fit for the SPE occurrence data as shown in Equation 4.1.

$$\lambda(t) = \frac{\lambda_0}{d_{ss}} + \frac{K}{d_{ss}} \frac{\Gamma(p+q)}{\Gamma(p)\Gamma(q)} \times \left(\frac{t}{d_{ss}}\right)^{p-1} \left(1 - \frac{t}{d_{ss}}\right)^{q-1} (0 \leq t \leq d_{ss}) \tag{4.1}$$

The differences between the above equation and the standard beta distribution are in the use of the λ_0 and K parameters, which adjust for offset and scaling respectively. p and q are the standard beta parameters, sometimes called α and β, depending on the source [*Devore*, 2012]. The last variable listed in the equation, d_{ss} is the assumed length of a solar cycle, with a default value of 4,000 days used in this research. If the solar cycle is longer than this value, the probability will change in the rise and fall of the solar cycle with a lower rate for the change in SPE occurrence and the opposite for a shorter cycle (probability for a SPE increases and decreases quickly).

In the risk model, this equation is evaluated for each day of a mission, generating a probability for a SPE that day. A random number between zero and one is generated, and if the random number is less than the probability, an event occurs and if not, then no even occurs that day. This process is repeated for each day of the input mission transit till reaching the destination with another set of random numbers generated to determine the expected dose for the event.

4.1.2 Data Classification by Risk

After a SPE occurs, the next step is to generate severity cases for the event. This includes another random number and use of NASA's Human System Risk Board (HSRB) Risk Matrix to classify the risk by likelihood and consequence [*NASA*, 2014]. By setting certain doses as levels of consequences and calculating the probability of an event exceeding a set relevant risk dose, the model is setup for risk assessment.

The HSRB Risk Matrix contains probabilities (likelihoods) of occurrence at $\geq$ 1%, $<$ 1%, and $\leq$ 0.1% for high, medium, and low respectively [*NASA*, 2014]. The consequences are set at levels of impact to the mission or future consequences at none, minimal, significant, and mission endangering (loss of crew or loss of mission, LOC/LOM). The user can use these as guides or set values of interest for examination and in this research the values include: 10, 100, and 1000 mSv. The decision to use these values came from knowledge of acute radiation effects, NASA limits, and the amount of dose likely to be received from other sources (GCRs). As demonstrated from the Earth-Mars transit of Curiosity and lunar astronaut doses, the dose received from GCRs will likely be around 1-2 mSv [*Zeitlin et al.*, 2013; *National Research Council*, 2008]. Doses from SPEs alone that approach an order of magnitude above or higher than the average daily GCR dose are important to investigate as they can have impacts regarding decisions during mission. This impact is likely minimal for the 10 mSv level, but if there were enough of these SPEs, then decisions might need to be made to keep within dose limits and/or restrict less shielded mission activities. Effective dose equivalents (EDEs) above 100 mSv could significantly impact a mission as these doses start to approach the dose limits, especially with respect to the blood forming organs as depressions in these cells can occur in the range of 100 mGy to 1 Gy. The final value selected was 1000 mSv (1 Sv), which is high enough to be concerned

about the typical acute radiation effects in humans. Sensitive astronauts may have GI upset and they may already be dealing with space motion sickness, which would adversely impact the mission while effects lasted. These were the cutoffs used by this research, but other researchers may choose different EDEs depending on application, and so the code is setup to take a user-defined, upper cutoff as an input.

4.2 Dose from Transport

There are a number of transport codes for nuclear and health physics applications, and some for spaceflight have been developed by NASA as web toolkits. The toolkit selected in this research for determining does from SPEs is OLTARS due to the customizable options it includes. Another option would have been to directly execute the transport code without the use of a toolkit, but since the focus of this research is on the SPE data and characterizing the events, it was decided to use an external transport code to calculate the doses from the analyzed SPEs.

4.2.1 Fluence Spectra Fits

In order to use the transport model in OLTARIS, there was a need to generate fluence spectra curve fits to one of the fluence distributions integrated into the model. The spectral fit options for user-defined SPEs in OLTARS are exponential in energy, exponential in rigidity, Weibull, and Band [*NASA*, 2016f]. Based on the data and literature searches, the exponential in rigidity and Weibull distributions were the most likely to fit the data [*Bieber and Evenson*, 1991; *Freier and Webber*, 1963; *Kim et al.*, 2009; *Nichols*, 2009].

The equations associated with the exponential and Weibull distributions in the format given in OLTARIS are listed below in Equations 4.2 and 4.3 where Φ is fluence

with respect to rigidity, R and/or energy, E [*NASA*, 2016f].

$$\Phi(>R) = J_0 e^{-R/R_0} \quad \text{where} \quad R = \sqrt{E^2 + 2m_p E}, \quad m_p = 938\text{MeV} \tag{4.2}$$

$$\Phi(>E) = J_0 e^{(-kE^{\alpha})} \tag{4.3}$$

The variables determined through non-linear curve fits include J_0 for both functions, which is the total integral fluence parameter. The others include R_0 (spectral rigidity parameter, MV) and k and α, which are spectral parameters (dimensionless) [*NASA*, 2016f]. From evaluating these options, the Weibull distribution was the closest fit to the data from visual tests as seen in Figure 4.1. Other SPEs not shown in the figures showed similar trends, but some like the April 28, 2001 SPE reached the iteration limit in MATLAB (contraindicates usage), although these make up less than 4% of the total SPEs.

Through examining the distributions graphically and extrapolating out to 1000 MeV (1 GeV), the Weibull fit performed better than the exponential fit in most cases. Although the exponential and Weibull were similar over the lower energies, the exponential decreased rapidly as energy increased, which may result in lowered doses in the risk model.

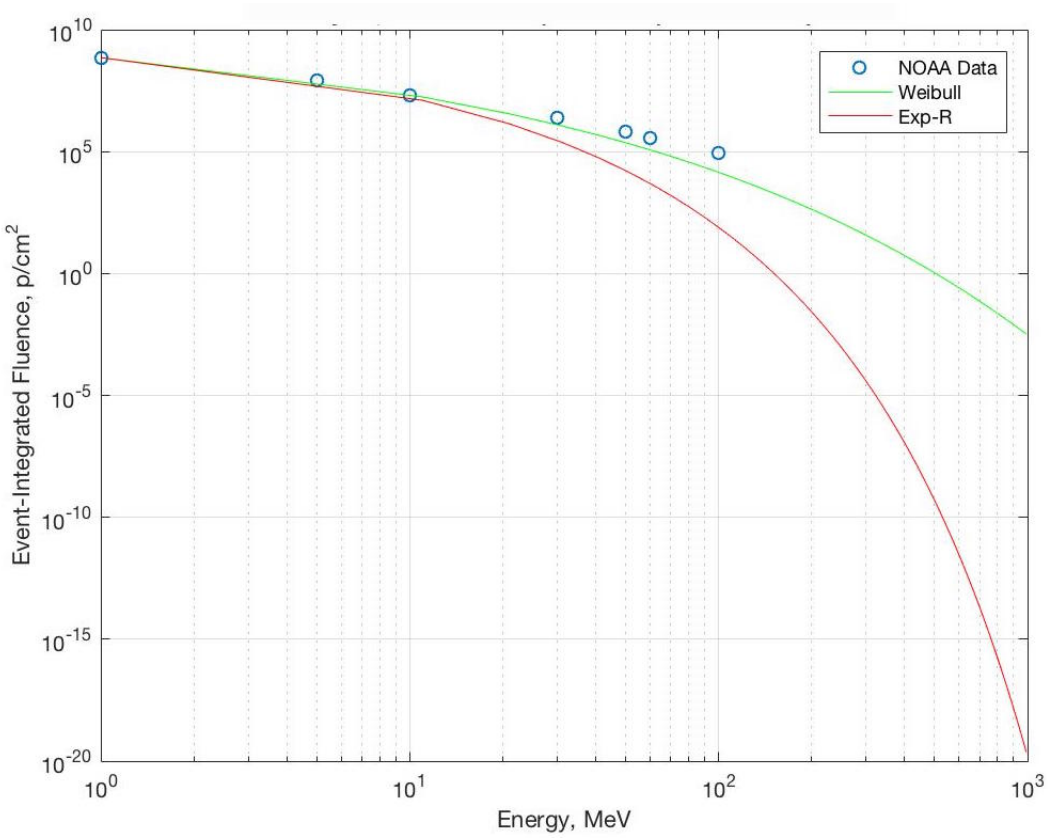

(a) January 28th SPE

Figure 4.1: Fluence distribution curve fits for selected SPEs from 2001. The data fell between the distribution fits for the August 16th SPE, but the Weibull was the closest in the middle energies.

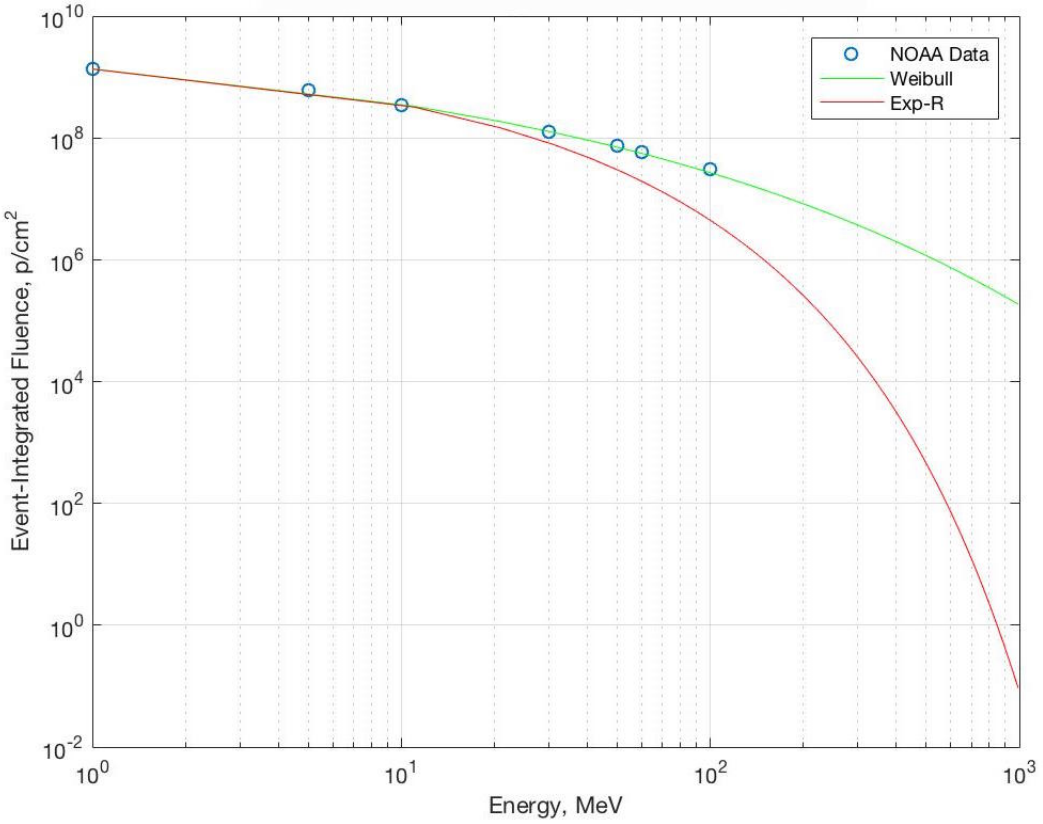

(b) April 15th SPE

Figure 4.1: Continued

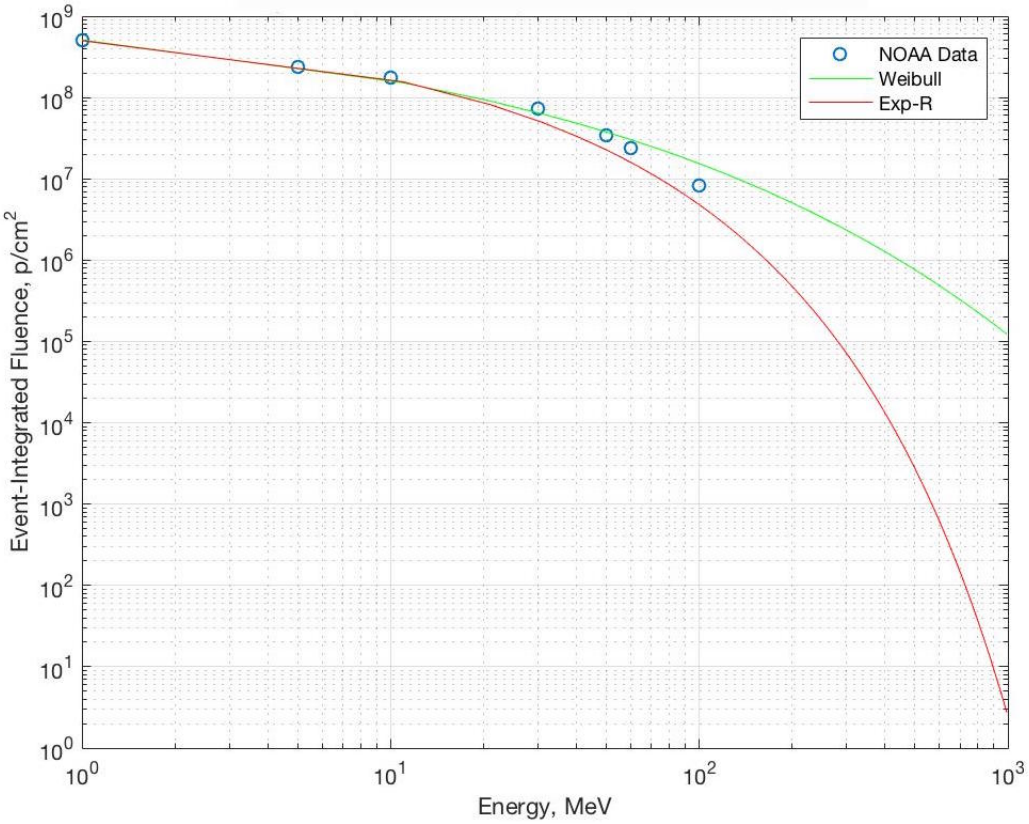

(c) August 16th SPE

Figure 4.1: Continued

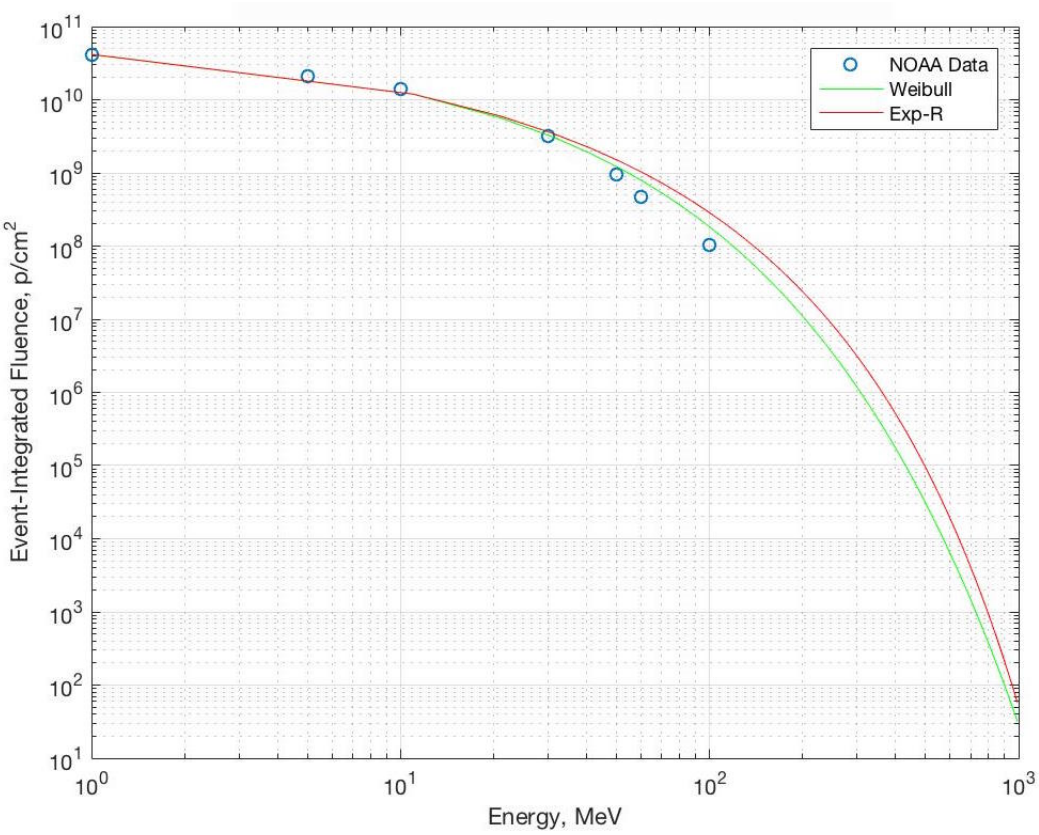

(d) November 4th SPE

Figure 4.1: Continued

In addition, some SPEs were not capable of being adequately fit to the Weibull or exponential distribution, as MATLAB could not reach the tolerance level in the number of iterations allowed for the calculation. These SPEs were excluded from the remainder of the model development leaving 184 SPEs out of the 191 found through the data analysis. These excluded events were a combination of small, short SPEs and larger, more erroneous SPEs. The former were likely inadequately fit due to there being less data to build up the trends seen in larger SPEs. The non-small SPEs that were inadequately fit generally showed unusual trends in the fluence. The values in the second half of the energy bins tended to be within the same order of magnitude instead of the gradual decrease seen in most other events. These events are likely erroneous since none of the largest historical SPEs showed this trend in the data. Further research into SPEs and their fluence spectra may clarify this in the future.

4.2.2 OLTARIS

OLTARIS is a web interface for calculating dose and other parameters through HZETRN (High charge (Z) and Energy TRaNsport), which is a NASA developed code that has been around for decades with new features added over time as computational capabilities increased [*Slaba et al.*, 2010; *Wilson et al.*, 1991]. OLTARIS has three SPE environments (free space, lunar surface, and Mars surface) that can be applied to a built-in SPE or a user-defined SPE [*Singleterry et al.*, 2010; *NASA*, 2016f]. The configuration used in this research to compute doses was the free space, user-defined SPE environment. The built-in SPE configuration was considered, but only includes spectra fits for historical worst-case events such as October 1989 or August 1972.

The Weibull spectra fits were entered into the OLTARIS web interface for execu-

tion with a selected shielding level of 5 g/cm^2 aluminum. This level is considered to be the standard "light" shielding case for NASA missions and is similar to the level of shielding for capsule operations (Apollo - 4.5 g/cm^2, *Zeitlin et al.* [2013]) [*McPhee and J. B. Charles, eds.*, 2009]. Other levels of shielding considered were that of a storm shelter (20 g/cm^2 aluminum) and an EVA suit (0.3 g/cm^2 aluminum). The storm shelter was not considered in this research since this level of shielding reduces acute radiation risk to very low levels. But, use of a storm shelter generally assumes that a more advanced warning system will be in place for interplanetary missions, which this research does not consider. For EVA levels of shielding, the risk is greatly increased, but it is assumed that astronauts will at least have some active radiation detectors on any mission. This would allow an astronaut to make a quick ingress and the selected shielding level of 5 g/cm^2 would then apply. The disadvantage of picking one shielding level is that it will possibly constrain applications until this model is integrated with a transport code or a diverse enough list of discrete shielding levels relevant to spaceflight are used. Future research may address other levels of shielding as circumstance dictates, but for this first iteration of the SPE risk model, the shielding is set to the light NASA shielding case.

Other selections made for OLTARIS executions included the use of CAF and CAM models (Computerized Anatomical Female/Man) for dose calculations and whether to calculate detector responses as well. The selected outputs included point dose, point dose equivalent, and effective dose equivalent (EDE) total and for specific organs behind the light shielding. The primary variable of interest was selected to be EDE since this research is concerned with the dose deposited in humans.

One last reduction in the number of SPEs included in this model development also occurred in this step due to Weibull spectra that had parameters outside the values that could be used in OLTARIS. Since OLTARIS was designed more for evaluation of

larger SPEs, further problems with smaller events was not unexpected. If OLTARIS is ever updated, this could be an area to include, which would further solidify SPE dose distributions for use in models such as this one. Excluding the Weibull fits that could not be used in OLTARIS, 180 SPEs remained to process for doses leading to dose distributions in this model.

4.2.3 Dose Distribution Fit

This component of the SPE risk model is a distribution for the calculated doses to use in conjunction with the occurrence probability portion. As doses varied widely and do not have a strong correlation with event probability, it was assumed that no other factors than the doses themselves needed to be considered for any distribution fit. This wide variance can be seen in the historical SPEs for which larger doses (above 100 mSv) can occur during any point in a solar cycle. For example at the end of the previous solar cycle, just before reaching minimum, the January 2005 SPE exceeded 100 mSv and out of the remaining events before minimum, three out of eight exceeded 10 mSv. Conversely 2004 did not even have any SPEs exceed 2.2 mSv, although it would have been expected to have stronger events since it was closer to solar maximum. These types of trends can be seen in other solar cycles as well such as for 1988 with no events that even exceeded 1 mSv, while the following year had some of the largest SPEs recorded in the space age.

To fit the dose distribution, all 180 SPE averaged EDEs (between female and male) for each event were used and different continuous distribution functions tested for goodness-of-fit. These EDEs were considered with respect to the input fluences as well, and it was found that the higher energy fluences have a strong logarithmic relationship with dose. As seen in Figure 4.2, this relationship has few outliers and a high R^2 value for the linear regression model for the natural log of fluence at >60

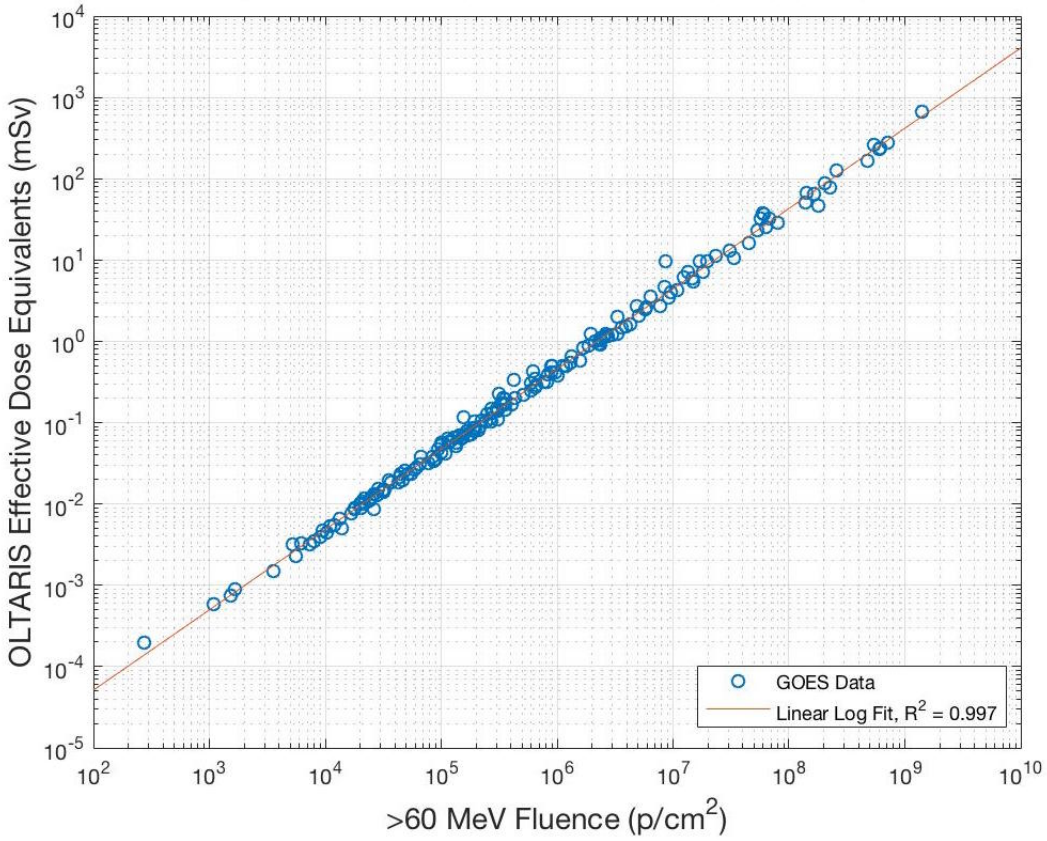

Figure 4.2: Relationship of >60 MeV fluence and effective dose equivalent. The linear equation for the line shown above is $ln(E) = 0.9872 * ln(\Phi_{60}) - 14.424$, which is overlaid in the exponential form on this log-log plot.

MeV and EDE. This relationship is likely due to the alignment between the level of shielding and where particles would stop in tissue, producing this strong correlation for this fluence. But, others such as the >1 MeV fluence do not show as strong of a correlation ($R^2 = 0.513$). This relationship was examined for this research since the scaling factor for orbital adjustments goes with flux or fluence, not dose (see discussion in next section).

From the >60 MeV data, a distribution fit is also determined for the probabilistic component of the model. Selected possible distributions included extreme value,

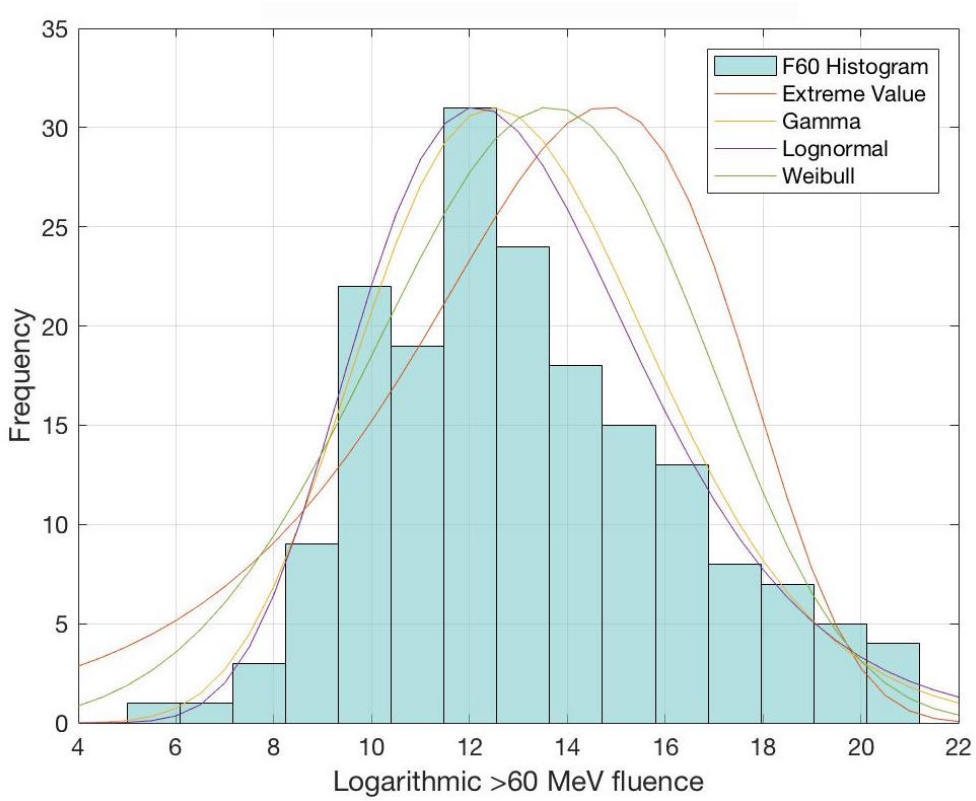

Figure 4.3: Possible distributions for >60 MeV fluence. Four of the possible distributions are shown here scaled with the histogram of the logarithmic fluence.

gamma, lognormal, and Weibull (2-parameter), of which the lognormal and Weibull were the closest fits as seen in Figure 4.3.

The lognormal and gamma are the closest by visual inspection, but Weibull and lognormal are closest when compared to distribution of historical fluences (GOES data). After the visual comparison, the confidence in the parameters was investigated with Weibull having a slightly larger confidence interval about the mean compared to the lognormal distribution parameters. Further comparisons demonstrated that the lognormal highly overestimated the probability of a SPE in the highest fluence values, by more than three times. The Weibull was less accurate within the lower fluences, but had a better fit overall compared to the lognormal distribution and so

was selected for implementation into the SPE risk model. Unlike the spectra fits discussed earlier, this Weibull is a 2-parameter probability distribution as shown in Equation 4.4 (adapted from *Devore* [2012]).

$$f(x;a,b) = \frac{a}{b^a}x^{a-1}e^{-(x/b)^a}, \text{where } a = 4.556, b = 14.4230 \tag{4.4}$$

For this case, the Weibull distribution has two instead of three parameters (a and b instead of p_0, α, and k), with both being distribution parameters instead of one fluence parameter and two spectral parameters.

This distribution function is implemented into the risk model through the use of the inverse distribution function and another random number variable to generate the probability input. This random number serves as the expected probability and from the inverse function, >60 MeV fluence can be determined, from which EDE is calculated using the log relationship described above. The disadvantage to using EDE instead of another quantity is that currently the US uses gray-equivalent, not sievert for non-cancer risks. Gy-eq was not an option in OLTARIS, but the values can still be compared with other space agencies and other risk levels [*Cucinotta*, 2010].

4.3 Orbital Location Adjustment

Although the progression of SPEs through the heliosphere can be complex, there have been approximations developed by NASA researchers and others to use for adjusting fluence based on event location. In the late 1980's workshop a group of researchers at Jet Propulsion Laboratory (JPL) set the scaling factor for fluence at $r^{-2.5}$ with variations from r^{-3} to r^{-2} for 1 AU to any other distance [*Dayeh et al.*, 2010; *Lario et al.*, 2007].

More recent research has also produced new recommendations and scaling factors

with respect to energy. *Crosby et al.* [2015] for instance recommends a scaling factor of 2 for European modeling applications (SEPEM, discussed in Section 2.2). *Dayeh et al.* [2010] also demonstrated that the scaling factors (α, where r^{α}) are 2.52 and 5.97 for 25 MeV, and 2.13 and 5.21 for 52 MeV (1 to 2.5 and 2.5 to 4.91 AU respectively). Additionally, other factors that impact the determination of a scaling factor include diffusion and transport processes, pitch-angle scattering, particle mean free paths, Parker spirals, and flux tube generation [*Dayeh et al.*, 2010; *Crosby et al.*, 2015; *Frahm et al.*, 2013; *Lario et al.*, 2007]. These other factors cannot be accounted for at this time in this risk model, but are possible considerations for future research.

From these literature sources it was determined that for this research a scaling factor for fluence of 2.5 as suggested by the JPL workshop is acceptable. The articles did not mention specifically the higher energies relevant for lightly shielded spacecraft (>60 and >100 MeV). Without adequate evidence for extrapolation from lower energies to higher ones, the more specific literature values cannot be used [*Dayeh et al.*, 2010]. The disadvantage of this approach is that it may be less accurate, but for order of magnitude dose calculations, it is likely sufficient. More data and literature studies will confirm whether using a scaling factor of 2.5 is appropriate or not.

As discussed in the previous section, due to the relationship between EDE and fluence, this scaling factor is applied after generating a fluence, but before calculating the dose from the log-linear relationship. The result is that EDE is adjusted with respect to 1 AU, which increases a SPE EDE for transits closer to the Sun (Venus swing-by) and decreases the EDE the closer to Mars the vehicle is when a SPE. Specific applications and implications for future spaceflight missions from this scaling factor are presented in Section 5.3, which covers results from NASA reference missions.

4.4 Application of NASA Risk Assessment Methods

Since this research has NASA applications and was started with the intent of adding to the Integrated Medical Model (IMM), NASA's Handbook for Models and Simulations (*NASA* [2013]) was consulted during development. This handbook lists a number of considerations to account for and steps to take depending on the model or simulation including documentation, items to report, and factors for understanding results credibility. The most relevant portions at this stage of development (pre-NASA/individual research usage) are the factors for understanding results credibility. The other portions, especially NASA documentation standards will be completed as needed if this model is used for NASA applications in the future.

In order to understand results credibility, the handbook lists the following factors to consider:

A. Verification

B. Validation

C. Input pedigree

D. Results uncertainty

E. Results robustness

F. Use history

G. Model and simulation management

H. People qualifications

The first five listed are controlled at the developer level, while the last three involve keeping track of resources and people who interact with the model/simulation. As part of the development of the risk assessment model discussed in the previous sections, the developer factors were considered. As input pedigree was covered extensively in Sections 3.2-3.3, it will not be discussed below with verification, validation,

uncertainty, and robustness. These four are discussed below with comparisons and other tests that were completed to begin the process of model credibility assessment.

4.4.1 Verification

In order to determine if the risk assessment model represents the underlying functions and models for the intended use, tests were conducted for SPE occurrences, SPE EDEs, and orbital adjustment effect. The trend over the solar cycle for SPE occurrence rate was verified early in the process through demonstration that SPEs are more likely during solar maximum than minimum as the underlying model intends. SPEs were approximately five times more likely at solar maximum than minimum as demonstrated in Figure 4.4, showing that there was a significant difference between the parts of the solar cycle (1,000 iteration simulation execution to produce figure). Verification of the number of SPEs per transit is discussed in the validation section since there is not direct model data for comparison, and the occurrence rate was the most important to verify at this step.

The next aspect of verification was to check that the model provides the expected variation in the >60 MeV fluence compared to the data input to develop this segment of the model. Through evaluation of the Weibull distribution (2-factor) at various probabilities and fluence levels, the distribution performs as expected, producing values very close those expected. For example, the inverse Weibull was evaluated at probabilities designed to produce fluences at both high and low parts of the distribution, including 1 x 10^3 (model, 998), 1 x 10^4 (model, 9.99 x 10^3) and 1 x 10^9 (model, 1.01 x 10^9). This confirmed that the model was performing as intended within the SPE risk model.

Other verification tests included comparisons for orbital scaling factors and the effect of decreasing probability on dose. For the orbital scaling factors, the expected

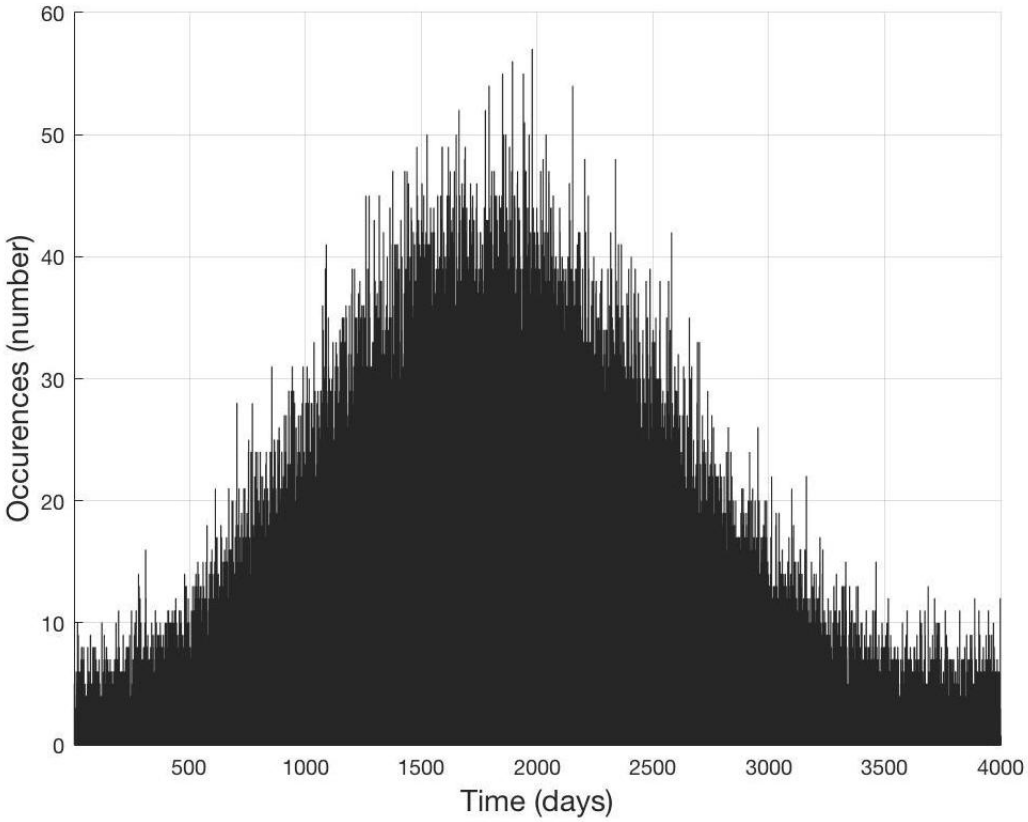

Figure 4.4: SPE probability variation over a non-specific solar cycle. For a 4,000-day solar cycle, the model built into the code generates a peak around mid-cycle before declining back to minimum probabilities.

transit dose for the Venus swing-by return was approximately 2.5 times as high as the GEO case. Also, the proportion of expected events at or above 1 Sv was similar at for the Venus return case compared to GEO, demonstrating that the rareness of the event has more of an impact than orbital location. Finally, the probability of a SPE occurrence at higher EDEs decreased with increasing EDEs, sometimes even having a median value of zero for a rarer event. These brief tests demonstrated that the SPE risk model is likely performing as intended from the perspective of the model design.

4.4.2 Validation

Validation tests completed for this risk model include comparison of GOES data SPE numbers, distribution results, and final model simulated Mars trips. All but the last one of these comparisons used the GEO test case since the original data were from satellites orbiting at this location.

The GEO test case was used to check that the risk model was representing the real-world data (GOES data). From the GOES SPE list (*NOAA* [2011b]), there are generally 6-12 SPEs per 6-months during solar maximum depending on the strength of the maximum. The model when executed in GEO for 6-month transits produced on average 6.5 SPEs, which is on the lower end of the range from historical data. Currently this may be acceptable considering that the current solar cycle is weaker and some experts believe the coming cycles may be less strong based on the observations during this current solar cycle [*Lockwood*, 2013; *Schwadron et al.*, 2014]. In addition, the higher end (12 SPEs/180 days) only occurred if a stronger solar cycle is predicted during the projected mission time, the parameters in the occurrence part of the model (Kim model *Kim et al.* [2009]) can be adjusted as necessary (see Section 2.3.1 for discussion of solar cycle prediction).

Also, the probability of expected doses was tested for the GEO case to eliminate orbital adjustments that might occur. For EDEs above 10 mSv and 100 mSv the proportion of events expected from the data was 13.3% and 3.89%, and the model proportions were 12.5% and 2.36% respectively for one of the test executions with 100,000 iterations. The model values are likely lower than the GOES data since the distribution is more spread out than the original data, which adds some probability for values that were not in the actual data such as for a dose of 1 Sv. As a result this model may underestimate the proportion of events for higher doses. But, since the

Sun may be less active in the future as discussed above, this model may be accurate for future solar cycles.

Finally, from the Earth-Mars transit of Curiosity, there were five SPEs recorded by RAD (Radiation Assessment Detector) during the 222 days of the transit that RAD was powered on [*Zeitlin et al.*, 2013]. According to *NOAA* [2016d], the time which RAD was recording SPEs (December 2011 to July 2012) was before the solar maximum, about three years into the solar cycle. In order to test the model with this case, the 217-day transit from Earth to Mars was considered with the transit occurring three years after the solar minimum. The full model recorded the average and median to be about six SPEs for this transit, which is a 20% difference compared to what was recorded by RAD (see Figure 4.5 for simulation results and Poisson fit). When the simulation SPE results were fit to a Poisson distribution, the cumulative probability function results in 0.400 for five SPEs and 0.560 for six SPEs. This indicates that a simulation result of five SPEs is fairly common and could be expected even without a low solar cycle. Since the current solar cycle had a much lower maximum than the past few before it, the occurrence portion of the model is likely to over estimate the number of SPEs for this solar cycle.

In addition, the model predicts an expected EDE of 52.9 mSv, while *Zeitlin et al.* [2013] report a "cruise" value of 24.7 mSv. This difference is likely due to the amount of shielding present around RAD compared to the amount in the model (RAD $\leq$10 g/cm^2, model 5 g/cm^2). From this comparison, the model predicts similar values to those measured by RAD, but there were too many differences between the environments to be more certain if this similarity adds credibility to the model.

As demonstrated in this section, with respect to model validation, the SPE risk model is close, but not as close necessarily as would be desired for future applications. With NASA's plans to go to Mars in the next couple of decades, it is likely that data

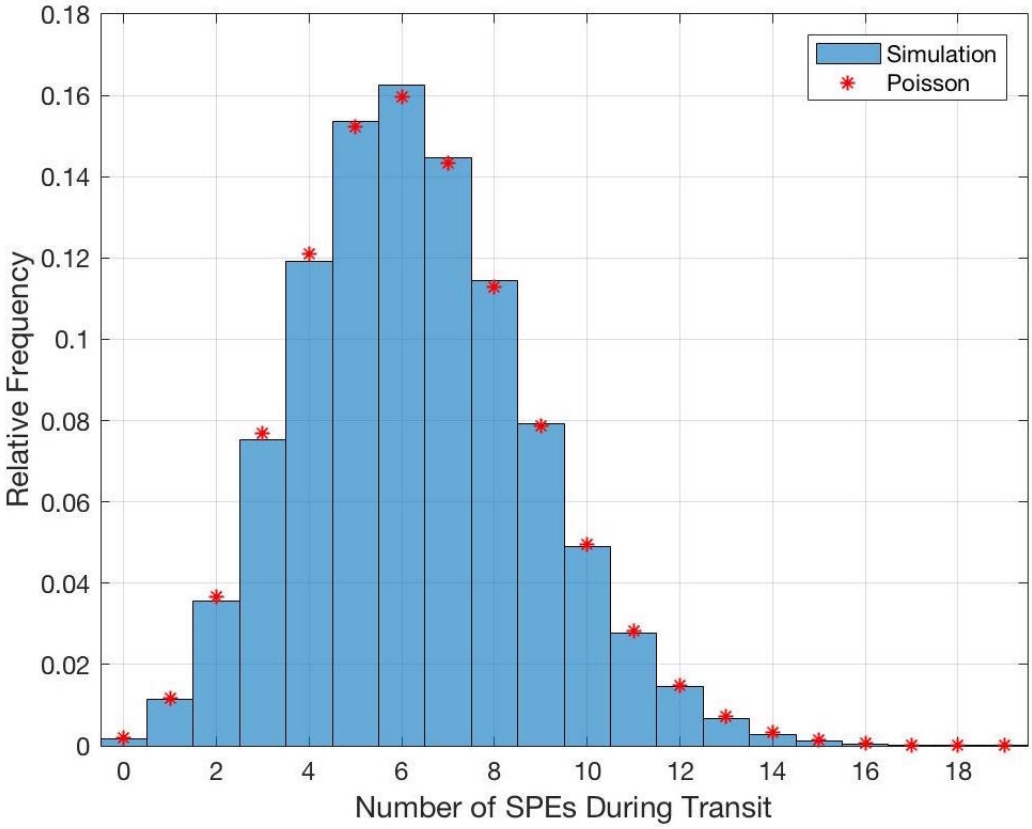

Figure 4.5: Curiosity transit simulation SPE number distribution.

will continue to be available and more models that can developed and updated, leading to more options for validation.

4.4.3 Sources of Uncertainty

For any Monte Carlo model results uncertainty is highly dependent on the number of iterations (n) during a model execution. In addition to the consideration of the number of iterations, there is also uncertainty sourced from the length of a solar cycle, the satellite data, and selected distributions that represent these data.

The largest possible source of uncertainty in this model is sourced from the length of a solar cycle. Since the Sun can be highly variable, the length of solar cycles can

vary within the 11-year average. Within the past five solar cycles (19-23, 24 has not ended yet) the length has varied from 3,653 to 4,262 days, which means that a 4,000-day solar cycle assumption is not necessarily valid [*Kim et al.*, 2009]. When examining risks at solar maximum or minimum, this will have little impact on results, but during the rise and fall of a cycle, the length will change the rate at which the probability changes for SPE occurrence.

Although these are not quantified at this time, the main possible sources of error for the GOES data include the measurements themselves and their later processing. Since the sensor measurements are corrected by NOAA, the assumption is that there is minimal uncertainty in these data points compared to other components of the SPE risk model. During data processing, the most probable sources of uncertainty are from the relatively low number of energy bins (seven) and filling the missing satellite data points through interpolation. Although the curve fits did not seem to be sensitive to the low number of energy bins, there can still be a source of uncertainty in these curves if the data are poorly fit. Some curves that had the worst fit were already excluded (as discussed in Sections 3.3 and 4.2), but those that were close to being excluded are possible uncertainty sources. Most of these events that were close to being excluded resulted in very small EDEs (less than 0.1 mSv) and the closest event exceeding 10 mSv was on December 13, 2006. This SPE is still nine orders of magnitude from being excluded based on the scaling parameter, and so for the larger events that matter for the final model, the uncertainty is likely lower from the fits derived from the GOES energy bins.

Missing data were accepted up to 10% for a total event and up to 24 data points in succession (represents about 8% of a day). Although these values are interpolated between known values, there is still a possibility for error, but it will depend on the amount of flux at the time compared to the overall flux values over the whole SPE. If

the missing data is not near a flux peak, then any data interpolation will have little effect, but if the converse, there could be larger effects, especially if part of a peak is missing. As a result, it is difficult to specify the amount of uncertainty since the flux changes with orders of magnitude. This implies that if a peak was obscured and the event was short, the calculated fluence could be below the actual value. These variations are assumed to have less impact over the 180 SPEs that were analyzed, with the most uncertainty related to other factors discussed below.

When generating the Weibull spectra fits (3-parameter) for each event and comparing the Weibull spectra fits to both literature and the processed data, there are sometimes widespread differences between these different sources. The most widely varying energy over the events evaluated seems to be the >30 MeV for the 180 SPEs evaluated, but when comparing literature values that are available for larger SPEs the largest differences are in the lower energy bins. The differences for individual events can exceed 100%, but on average around 20% or less, depending on the comparison. What is unknown is the impact that these differences have on calculated EDE since there are little data outside of transport codes to generate this information. Since the fluences and EDE vary in a logarithmic manner, these errors are small in context of the model, meaning that these differences likely have little impact on the model, especially with respect to sensitivity. Therefore, errors in this aspect of the model will not likely contribute highly to uncertainty, when the variance in the SPE size is much higher (range over five to six orders of magnitude for fluences in each energy bin).

For the EDE calculations, the transport code itself is assumed to have minimal uncertainty and that the distribution fit for the fluence and log relationship to EDEs is the larger source of uncertainty. As discussed in the validation section, there is a concern that there is a larger difference between the proportion of events at

higher EDEs between the model and GOES data compared to lower EDEs. This is a reflection on the model that may or may not adequately represent the real system, and only more data can determine the level of uncertainty for this part of the model.

Between all of the sources of uncertainty before executing the model and those after, this model is complex enough to consider the application of advanced statistical and mathematical methods as part of furthering model credibility (such as Bayesian or Markov chain methods). This step should be taken in the future as this model progresses closer to a specific need for NASA or others who are interested. The uncertainty quantification in this research as a result is focused on confidence levels related to iterations within the model, which is explained below.

In order to determine how many iterations were needed to be reasonably certain in the results (confidence levels), two approaches were used during model development. Both approaches assume that for large enough n, a variable of interest will follow a normal distribution and converge on a value.

The first approach was to execute the model for increasing numbers of iterations while recording a target variable that is likely to be a rare occurrence and/or have large errors associated with it. For this model, the expected number of events above 1 Sv was chosen since this is a relevant EDE for the start of possible acute radiation effects and has yet to occur during the space age. The transit of interest that should make this variable most rare is one of the shorter Earth-Mars or Mars-Earth transits since larger doses are mitigated through increasing distance from the Sun. In addition, the less time spent in deep space during the transit, the less chance of a SPE occurrence. This transit is compared with the GEO case, which does not have any of the orbital adjustments discussed earlier. Figure 4.6 below shows that the values for 1 Sv event number start to lose their variation in the 100,000's for n, which corresponds to execution times as little as a few minutes or as much as 30

minutes.

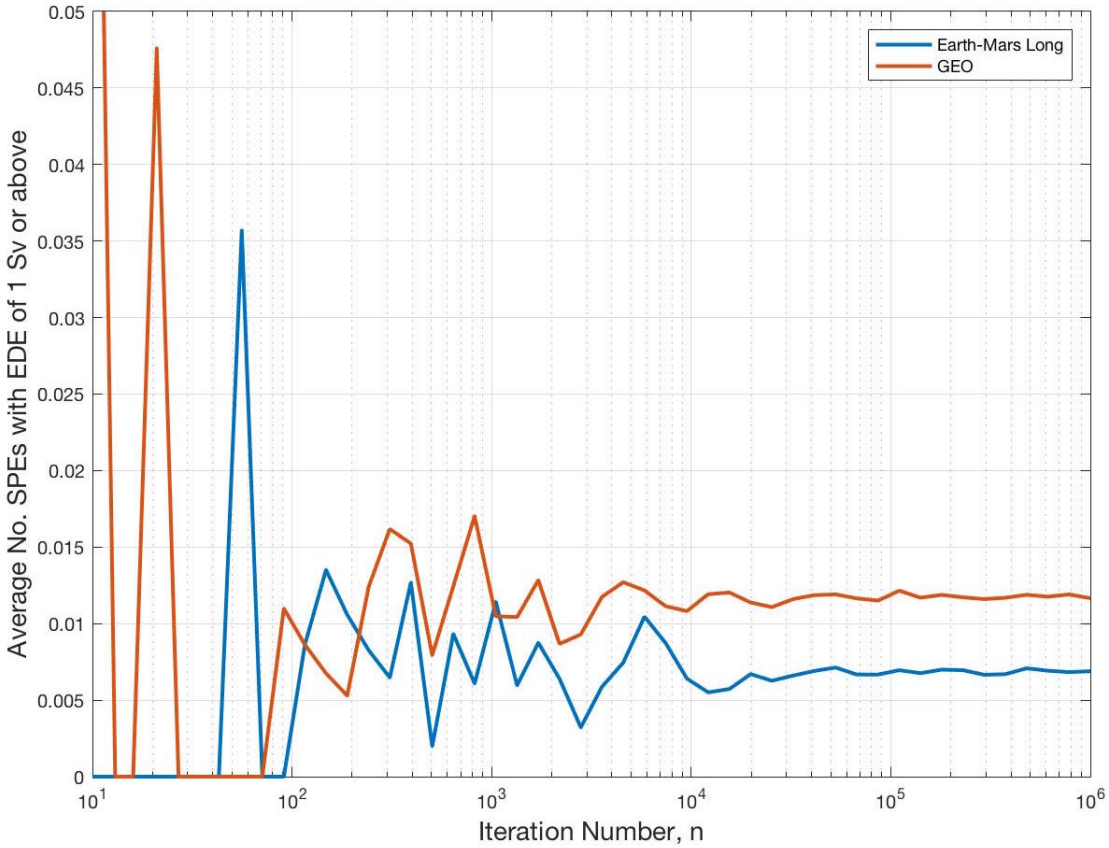

Figure 4.6: Convergence of average number of events for 1 Sv. Both cases shown here begin to lose their variation around 100,000 and a bit below that number as well.

In the second method, the number of iterations is calculated numerically based on the large n assumption. In addition, as n increases it can be assumed that the calculated mean and standard deviation from the model will approach the true mean and standard deviation. Therefore, Equation 4.5 can be used to estimate n for a specified error (E) and confidence level (with corresponding Z-value) (adapted from

Driels and Shin [2004], where S_x is the standard deviation and $\bar{x}$ is the mean).

$$n = \left[\frac{100ZS_x}{E\bar{x}}\right]^2 \tag{4.5}$$

For the GEO case, this resulted in n-values of 6.57 x 10^4 and 2.84 x 10^6 for 95% and 99% confidence levels respectively. The Earth-Mars transit case resulted in higher n-values of 2.23 x 10^5 and 9.63 x 10^6 for 95% and 99% confidence levels respectively.

Since the errors in the event fluence spectra and resulting error are likely greater than 1% due the other uncertainties mentioned earlier in this section, 95% confidence is a much more reasonable goal. This additionally requires a much smaller number of iterations, which helps reduce computational time. For future integration into IMMs complete model, reducing computational needs is highly desirable.

Between the two methods for determining n, the second method is more conservative and so to insure that the rarest outputs lose their variation, a minimum of 250,000 iterations should be used, reducing the uncertainty in the model results. For future applications this number may change, especially if newer propulsion systems can make the journey quicker, reducing the chance of SPEs during the transit.

4.4.4 Results Robustness

The last area applicable to this research is results robustness, which refers to the sensitivities in the model and how much is known about them [*NASA*, 2013]. In order to evaluate sensitivities, the variation in parameters must be known that will have the largest impact on the final results, and how much they match the sensitivities for the real world system that the model is seeking to represent. For this SPE risk model, the parameters that may have the capacity to significantly impact the model are:

- Mission length

- Orbital scaling factor
- Number of iterations
- Shielding

As seen through test model executions, the mission length has one of the largest impacts on results, which means that the model is sensitive to this factor. Fortunately, this factor is also a user input variable and so sensitivity is controlled. There is still a risk of the sensitivity impacting the model results if a user does not understand how mission length impacts the results in that longer missions will for example have on average more SPEs.

The orbital scaling factor is also a possible source of sensitivity as it can also have a large impact on the model. As discussed in Section 4.3, there is some sensitivity to specific energies and so this sensitivity may change in the future. Currently though, there is not much data or literature to support the choice of this value in comparison to others, and so the sensitivity is somewhat unknown.

Next, as explained in the uncertainty section, the number of iterations can also have a large impact on the system. If too low of a value is chosen, there can be wide, varying changes in variables of interest. Once a large enough n is chosen, the model becomes less sensitive to this choice with mission length and orbital scaling factor contributing the main reductions in model robustness.

Finally, the last factor that may contribute to model sensitivity is the level of shielding selected. This model currently is very dependent on the shielding selected, which drives the distribution fits. If the level of shielding were to change, about 50% of the model would need to be updated, and so this factor might be the highest source of sensitivity. If this factor is not changed, it becomes a fixed value for the model and does not contribute to sensitivity.

Other factors such as the Weibull distribution parameters (both two- and three-factor) do not contribute to sensitivity as much in the model. The Weibull distributions involve averaged data points and application over a large number, which decreases sensitivity overall, even if one SPE might be particularly sensitive due to poor distribution fit.

Overall the model is at an acceptable level of robustness for the current application, where most sensitivity is related to model inputs to execute the risk model, not the factors in the model itself. This assessment may change in the future, but for now the level of confidence in the model is high enough to generate initial results.

4.5 SPE Risk Model Overview

The SPE risk model presented follows the process shown below in Figure 4.7, which shows the progression from data and literature input to interpreting the results through the use of NASA risk assessment methods. In developing the model, the first consideration was to determine what the expected and/or desired types of input would be for the model. This risk model is designed to apply to a wide variety of missions throughout the inner heliosphere and risk changes depending on the timing of the solar cycle. So, both a heliospheric location and day within the solar cycle are needed. These inputs also fit well with researchers and engineers designing the mission transits as the common way to report orbit vectors includes a time and distance component, which are not difficult to convert to the day-location input for the risk model.

The next part of the risk model is the SPE likelihood component derived from *Kim et al.* [2009], which contains an adjusted beta distribution function (described in Section 4.1). When executed as part of the model, the probability for a SPE is determined based on the day within the solar cycle.

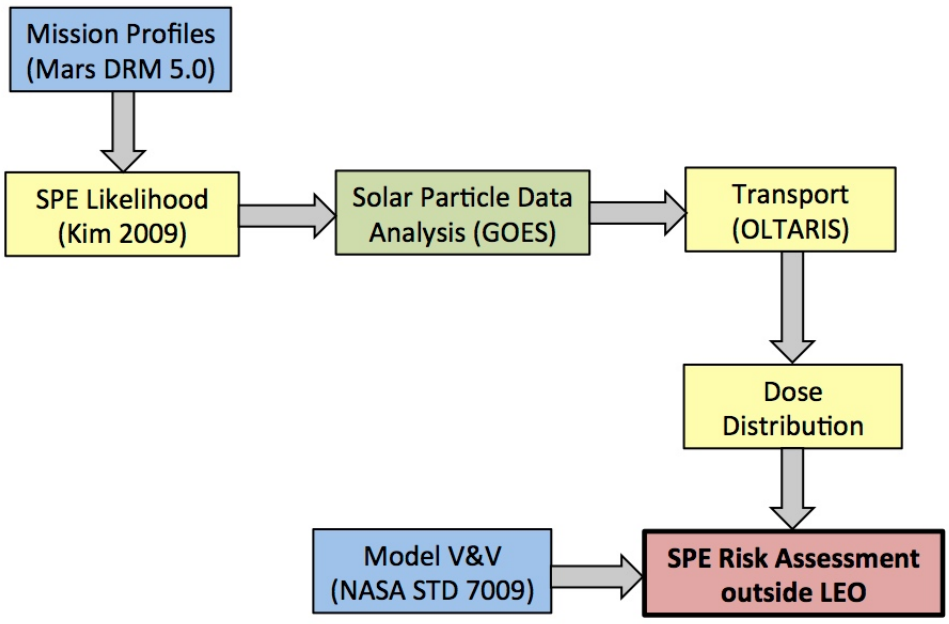

Figure 4.7: SPE risk model flowchart. All components in the diagram work together in the code to produce the complete SPE risk model. Blue indicates portions sourced from NASA design standards, yellow individual models, green for data analysis, and red for the model endpoint.

After the likelihood determination, the solar particle data analysis took place, identifying 180 SPEs, fitting them to a three-parameter Weibull, and using OLTARIS to calculate doses. Then the model uses the fluence Weibull distribution derived from the solar particle data analysis to generate a fluence value at >60 MeV to generate the selected model dose, EDE. These steps incorporate both the transport and dose distribution components as listed in Figure 4.7.

From applying these components multiple times in the probabilistic portions of the model, the expected number and distribution of SPEs for a transit can be estimated. In addition, the user can pick one dose threshold of interest to determine specific information with regards to that dose. This answers questions of how rare an event is for different missions and can be used for worst-case type modeling.

Finally, the risk model can be summarized as follows for any iteration that takes place during a model execution to determine if an SPE occurs and if so, its expected severity:

- SPE occurrence model called with generation of the first random number,
- Random number is compared with SPE probability for that day in the solar cycle to determine if SPE occurs,
- Once a SPE occurs, the second random number is generated for the Weibull fluence distribution,
- Random number is used as a probability for fluence magnitude at > 60 MeV,
- Fluence magnitude is adjusted by orbital scaling factor based on location with respect to the Sun,
- Fluence is converted to dose using the linear log fit derived,
- Event occurrence time and magnitude are noted, and model is executed for the number of iterations that remain.

More information regarding the MATLAB code for the risk model summarized above is given in Appendix B. Now with development of the risk model complete, different relevant mission transits can be examined for expected mission risk from radiation.

5. RISK PROFILES FOR LONG-DURATION MISSIONS

In evaluating acute radiation risk for long-duration missions, the most critical information is whether there will be a non-insignificant chance of a loss of crew or mission (LOC or LOM). Other levels of mission or crew health impact are also important to use in evaluation, allowing for better mission design, especially with respect to mass to reduce cost. To examine some of these possibilities with the SPE risk model presented in Sections 4.1-4.5 for future human spaceflight missions, NASA's Mars Design Reference Architecture (DRA) was selected [*Mars Architecture Steering Group and Drake*, 2009]. These mission profiles were selected additionally for evaluation since they represent the highest radiation risk scenario targeted currently for human spaceflight due to increased time, less warning, decreased shielding, and lack of quick return to Earth. As seen through the risk analysis results, there is an advantage for some of these missions in that the dose from SPEs decreases the farther from the Sun a mission takes place.

5.1 Mars Design Reference Missions

In Figure 5.1 the conceptual orbital transfers are shown with the long-stay case on the left and the short-stay case on the right. These mission profiles represent possible orbital transfers in the mid-2030's with conventional propulsion [*Drake*, 2008]. If propulsion capabilities increase, allowing for shorter transfers, the timing of missions will change. The Venus swing-by case may even be eliminated if enough of an increase in propulsive technology occurs.

For the transits shown in Figure 5.1, there are very similar outbound journeys with both long- and short-stay taking 210 and 217 days respectively. The long-stay return also takes 210 days as planned in *Drake* [2008], but the short-stay return

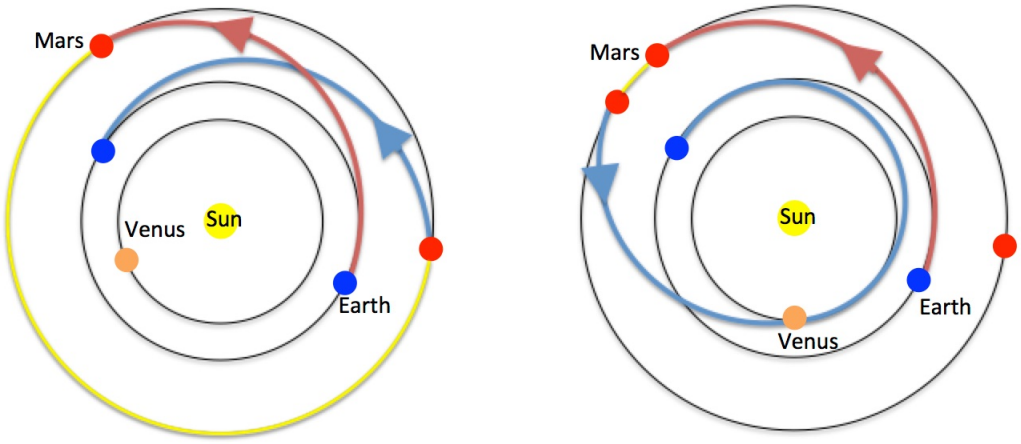

(a) Long-stay **(b)** Short-stay

Figure 5.1: Mars design reference architecture proposed mission orbital transfers. Outbound transits are depicted in red curves with an arrow, Mars stay in yellow curves, and inbound/return in blue curves with an arrow. Adapted from: *Drake* [2008].

takes 403 days due to the Venus swing-by. Surface stays are approximately 500 days for the long-stay and 30 days for the short-stay. For more details on the proposed Mars missions see *Drake* [2008], *Mars Architecture Steering Group and Drake* [2009] or the Addenda to these documents. Finally, a GEO case is included to simulate a mission in geosynchronous orbit for comparison to the different Mars transits so that the effect of different heliospheric locations can be understood.

5.2 Event Likelihood and Consequences

As mentioned in Section 4.1.2, the NASA Human System Risk Board (HSRB) Risk Matrix can be used to classify the level of risk from SPEs by likelihood and consequence as shown in the Human Research Roadmap [*NASA*, 2014]. The classifications are low ($\leq 0.1\%$), medium ($< 1\%$), and high ($\geq 1\%$) for likelihood, and very low (no impact), low (minimal impact), medium (significant impact), and high (LOC

or LOM) for consequences. As shown in Figure 5.2, these likelihood and consequence values are set in a grid to determine the level of risk, with the worst-case scenarios for high consequence and medium to high likelihood. Most SPEs fall in the lowest row with very low consequences, but the highest SPEs fall in the yellow part of the chart. These are highly unlikely SPEs, but could have medium to high consequences. An example of a historical high consequence, low likelihood SPE is the October 1989 event. Consequences will depend on the level of shielding, but risk is considered to be high for this type of SPE. This research focused on events such as these, using the SPE risk model to determine the probability of SPEs that result in higher doses (in addition to expected transit doses).

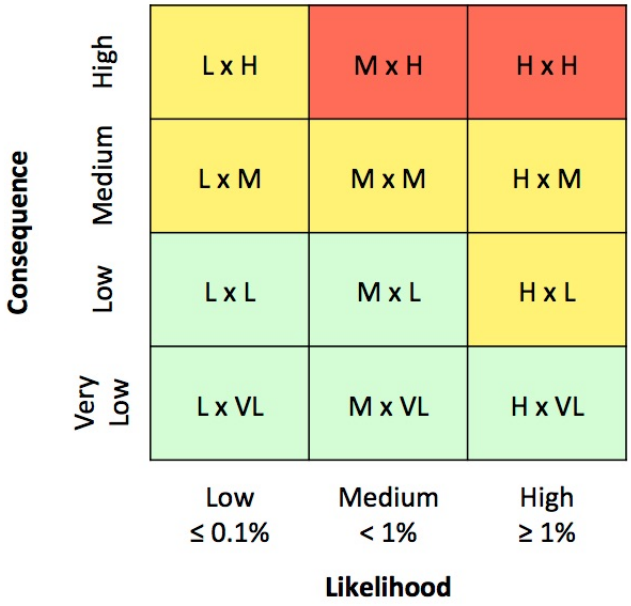

Figure 5.2: NASA risk matrix for consequence and likelihood. The red, yellow, and green highlighting indicate levels of risk with red being unacceptable, yellow being some risk, and green little to no risk [*NASA*, 2016c]. Adapted from *NASA* [2014].

Of the 180 historical SPEs analyzed, there were five events that produced an average effective dose equivalent above 250 mSv for whole body dose while shielded by 5 g/cm^2 of aluminum. This is less than 3% of the total events over 30 years of SPE data (or 3 x 10^{-4}% overall risk by day), and using the risk matrix, would be classified as low likelihood for any mission less than a year. The impact would likely be low to medium as this dose is not mission or crew endangering. If a crew member is more sensitive to radiation, the individual might have a temporary depression in lymphocytes and/or fatigue until their body recovers, but otherwise be healthy enough to continue their duties. The doses of concern for high consequence are above 1000 mSv (1 Sv), and, as discussed below are quite unlikely to occur for current Mars DRAs, especially when considering the current solar activity trend. For further information on NASA radiation risk classifications see the appendix of the "Human Research Program Requirements Document," which lists risk for different mission types (*NASA* [2015]).

5.3 Mission Transit Risk Assessments

In the following sections, results are presented from executions of the SPE risk model for each of the five selected transits. The results were as expected in terms of general trends with the highest dose and number of SPEs expected for the return with the Venus swing-by. The GEO case had the second highest dose since most other transits included only Earth-Mars segments, which reduces dose, although does not necessarily reduce the total number of SPEs. All results presented here are simulations executed with the minimum number of iterations (250,000) to produce the 95% confidence interval for the rarest model quantity (see Section 4.4.3 for details).

Additionally, all results are given for solar maximum, unless stated otherwise, since this constitutes the highest risk for SPEs. This is not necessarily the highest

total dose for a mission since GCRs must be considered in addition to SPEs. Solar minimum cases were examined, which yielded low doses and few SPEs as expected due to the reduction in probabilities for SPE occurrences. For a mission to Mars during solar minimum using the long-stay transit, on average one SPE is expected during the entire transit, which constitutes little risk (although GCR doses will be much higher). Table 5.1 shows the overall model results are given as average values for each model output.

Table 5.1: Mission transit risk assessment results for all cases at solar maximum.

Model Quantity	GEO	Earth-Mars (Long)	Mars-Earth (Long)	Earth-Mars (Short)	Mars-Earth (Short)
SPE No.					
All	6.48	7.56	7.55	7.81	14.4
>10 mSv	0.809	0.687	0.677	0.708	1.88
>100 mSv	0.153	0.110	0.109	0.113	0.381
>1 Sv	$1.20\text{x}10^{-2}$	$6.94\text{x}10^{-3}$	$6.94\text{x}10^{-3}$	$6.92\text{x}10^{-3}$	$3.30\text{x}10^{-2}$
SPE EDEs (mSv)					
Transit	94.4	65.9	65.1	67.6	246
Individual	14.6	8.77	8.62	8.64	17.1

When interpreting these results, the average transit and individual SPE EDEs should be interpreted with caution. In actuality, the transit EDE likely represents one or more larger SPE and some smaller events, with one or more insignificant events (as seen in historical data, not the averaged individual EDE given above). Since the average individual SPE EDE varies less than the transit SPE EDE with respect to heliospheric location, both are useful for examination of the variation between transits.

5.3.1 180-Day GEO

As shown in Table 5.1, the expected number of SPEs during a mission to GEO is about six events. Table 5.2 below shows further details for the GEO control case. As mentioned in the validation discussion (Section 4.4.2), the expected number of events for around solar maximum is lower than expected, but still within the number seen in historical data. These results could also be applied to the lunar orbit portion of a mission, although the severity would be lessened for surface operations due to partial shielding by the surface.

Table 5.2: 180-day GEO SPE number and dose results.

Model Quantity	Average	95%CI	Minimum	Maximum
SPE No.				
All	6.48	(6.47,6.49)	0	20
>10 mSv	0.809	(0.805,0.813)	0	7
>100 mSv	0.153	(0.151,0.155)	0	4
>1 Sv	$1.20\text{x}10^{-2}$	($1.16\text{x}10^{-2}$, $1.24\text{x}10^{-2}$)	0	2
SPE EDEs (mSv)				
Transit	94.4	(92.4,96.4)	0	$8.57\text{x}10^{4}$
Individual	14.6	(13.8,15.3)	0	$8.55\text{x}10^{4}$

From these results it can be seen that it is highly likely to have at least one 10 mSv SPE at solar maximum, with higher EDEs expected if there are more events during the transit. In historical data, this trend can be seen in solar maxima years in which there is rarely a set of six to seven SPEs without exceeding 10 mSv. In addition, the maximum number of SPEs expected by EDE cutoffs are generally around two to three events higher than what is seen in the worst-cases seen in the historical data

(i.e. none for 1 Sv, two for 100 mSv, and four for 10 mSv). This demonstrates that it may be possible, although highly unlikely to have a higher number of events with higher doses. Until the processes that cause SPEs are better understood, the bounds are unknown for events and so these maximum cases cannot necessarily be excluded.

The expected EDEs for the full transit and individual events also come close to historical data, but the maxima are much higher than what has been recorded in the space age. This was expected, as the occurrence of higher dose SPEs build up over the 250,000 iterations executed for this model (as compared to lower iteration executions that show fewer higher dose SPEs).

For future missions of longer duration, these results demonstrate that with the fast communication times possible at GEO and warning system, the risk of excess dose from SPEs is very low. These factors, combined with the additional shielding from the radiation belts, explain why risk is considered to be controlled for ISS missions within LEO [*NASA*, 2016d].

5.3.2 Mars Long-Stay

The Mars long-stay mission represents the most efficient orbital transfers (Hohmann transfers) that are available with current conventional propulsion. During a mission there would be a main engine burn to enter the transit to Mars from LEO and one from Mars orbit to enter the transit back to Earth. There would be correction burns as needed, but overall this mission design is the simplest, which makes it easier to predict mission requirements and possible risk. The surface stay is dictated by these transfers and the orbital alignment, which means that once astronauts are on Mars, there would be no return to Earth until the planets are positioned correctly. The longer surface stay compared to the shorter option discussed later can help to decrease radiation risk. Surface stay provides the advantages of a thin atmosphere,

which reduces the risk while on the surface, and the addition of some gravity may also reduce the risk of synergistic effects as well (if 3/8 of Earth's gravity is sufficient to negate the microgravity effects). Here the deep space orbital transfers are presented only, with each of the main segments discussed below for SPE risk.

5.3.2.1 Outbound

As discussed earlier, the transit to Mars for the long-stay scenario is 210 days long. As the astronauts travel from Earth to Mars, radiation risk decreases such that the expected number of events with higher doses decreases compared to GEO. In Table 5.3 below, the detailed results for the Mars long-stay outbound segment are presented, and text follows comparing these results to GEO.

Table 5.3: Mars long-stay outbound SPE number and dose results.

Model Quantity	Average	95%CI	Minimum	Maximum
SPE No.				
All	7.56	(7.55,7.57)	0	23
>10 mSv	0.687	(0.684,0.690)	0	7
>100 mSv	0.110	(0.109,0.111)	0	4
>1 Sv	6.94×10^{-3}	(6.61×10^{-3}, 7.27×10^{-3})	0	2
SPE EDEs (mSv)				
Transit	65.9	(64.5,67.3)	0	7.70×10^{4}
Individual	8.77	(8.25,9.29)	0	7.69×10^{4}

From these results it can be seen that not every transit is likely to have one event exceeding 10 mSv, but between the outbound and inbound segments (or two outbound transits), one event exceeding 10 mSv is likely. Compared to the GEO case, this is a decrease in severity of SPEs, which was expected based on the orbital

effect that SPEs decrease in fluence as distance from the Sun increases. The minima and maxima for the number of SPEs at all levels does not differ much compared to the GEO case due to the increased time spent in space. Although the likelihood of higher dose SPEs decreases, the additional time spent in space increases the overall number of SPEs.

The transit and individual EDEs reflect decreased values compared to GEO as expected due to the orbital effects. The minima and maxima are outside the expected values for a mission again here since the EDEs shown in the maxima have not been seen in the space age.

5.3.2.2 Inbound

The inbound portion of the long-stay scenario is also 210 days spent in deep space, which means that the risk of higher doses increases as astronauts approach Earth (approaching GEO risk levels). In Table 5.4 below, the detailed results for the Mars long-stay inbound segment are presented. Then, these results are compared to both GEO and the outbound transit cases.

Table 5.4: Mars long-stay inbound SPE number and dose results.

Model Quantity	Average	95%CI	Minimum	Maximum
SPE No.				
All	7.55	(7.54,7.56)	0	24
>10 mSv	0.677	(0.674,0.680)	0	7
>100 mSv	0.109	(0.107,0.110)	0	4
>1 Sv	6.94×10^{-3}	(6.61×10^{-3}, 7.27×10^{-3})	0	2
SPE EDEs (mSv)				
Transit	65.1	(63.6,66.7)	0	1.11×10^{5}
Individual	8.62	(8.08,9.16)	0	1.11×10^{5}

These results overall are nearly the same as the outbound case, which was expected due to the time and transit similarities. As with the outbound case, in comparing these results to the GEO case there is a decrease in severity of SPEs. The maxima and minima values only differ in the maximum number of expected SPEs, but this is only by about 4%, which is not significant for this probabilistic model.

The average transit and individual EDEs are slightly lower for the inbound case than for the outbound, which is likely due to fluctuations within the model itself. The EDEs differ by less than 2% for both individual and transit cases, and these differences are decreased as iteration number increases. For a simulation set to capture the 1 Sv severity case at 95% CI by iteration number, this is acceptable, although other applications may require smaller differences. In contrast, the maximum expected SPE EDE was much higher for this case, although this was due to only one of the three executions, which exceeded $1x10^5$ mSv, inflating the average. As mentioned earlier, the possibility of this high EDE is very low since it required 250,000 iterations to produce these high values.

Overall for a Mars long-stay mission scenario, the average mission expected EDE from SPEs while in deep space would be 131 mSv, which does not pose a high risk to astronauts. The concern is if during those transits, there are years such as 1989, 2000, or 2001, which would provide much higher EDEs, likely exceeding 500 mSv for just the larger events. Assuming 1 mSv/day from GCRs, the total mission dose could exceed 1 Sv for the transit segments alone, which may not be acceptable for future missions [*National Research Council*, 2008].

5.3.3 Mars Short-Stay

The Mars short-stay mission is a much different option than the conventional long-stay scenario presented above. The short stay can provide some propulsive

advantages among others, but of the two mission scenarios, it produces the highest risk from a radiation perspective. Since most of the mission is not spent on the surface and in orbit, the 30 days on the surface are short compared to the 217- and 403-day transits from a radiation risk perspective. In addition, traveling closer to the Sun increases expected fluence, which increases expected doses during the inbound portion of the mission. Each of the main segments are discussed below for the SPE risk during the transit to Mars and back, with comparisons to the long-stay Mars case.

5.3.3.1 Outbound

The outbound portion of the short-stay scenario is just a week longer than the long-stay outbound transit with 217 days in deep space. As with the long-stay case, radiation risk decreases as astronauts approach Mars compared to GEO. Table 5.5 below shows further details for the short-stay outbound case, and then discussion follows comparing these results to GEO and the long-stay cases.

Table 5.5: Mars short-stay outbound SPE number and dose results.

Model Quantity	Average	95%CI	Minimum	Maximum
SPE No.				
All	7.81	(7.80,7.83)	0	24
>10 mSv	0.708	(0.705,0.711)	0	7
>100 mSv	0.113	(0.112,0.115)	0	5
>1 Sv	6.92×10^{-3}	(6.59×10^{-3}, 7.25×10^{-3})	0	2
SPE EDEs (mSv)				
Transit	67.6	(66.4,68.9)	0	5.62×10^{4}
Individual	8.64	(8.46,8.82)	0	5.59×10^{4}

These results are very similar to the Mars long-stay transits presented above due to the similar mission times since this transit was only a week longer. Adding a week to the transit increases the number of SPEs expected at different EDEs slightly, but still on average at least two transits would be needed for exposure to one event exceeding 10 mSv. The maxima and minima values are also nearly the same as the two long-stay cases with differences in the total number of SPEs and the number exceeding 100 mSv. This difference likely occurred, since on average, the number exceeding 100 mSv is more often four for long-stay transits, but sometimes five and adding an additional week is enough to elevate it to five.

The average EDEs for transit and individual SPEs are also slightly higher due to the increased time spent in space, which allows for a higher number of events. The high variation in maximum EDEs is also continued into this transit case, but the values do not exceed $1x10^5$ mSv for this case. Although the model was executed for the same number of iterations for each case, the extremely high EDE SPEs are so unlikely that they can vary widely within the model.

5.3.3.2 Inbound

The inbound portion of the short-stay scenario is 403 days spent in deep space, including a Venus swing-by. This transit includes the Venus swing-by to provide a propulsive boost and make the short-stay mission possible based on orbital constraints. Due to the increased time spent in deep space with part of the transit spent closer to the Sun, this transit constitutes the highest radiation risk of the proposed Mars transits. This is demonstrated in Table 5.6 below, which shows increases in nearly all model quantities compared to other transits.

The number of SPEs expected at all EDE severity cases are increased by a factor of about two to three compared to the other Mars transits, except for the 1 Sv case,

Table 5.6: Mars short-stay inbound SPE number and dose results.

Model Quantity	Average	95%CI	Minimum	Maximum
SPE No.				
All	14.4	(14.4,14.4)	1	34
>10 mSv	1.88	(1.88,1.89)	0	11
>100 mSv	0.381	(0.379,0.384)	0	5
>1 Sv	$3.30\text{x}10^{-2}$	($3.23\text{x}10^{-2}$, $3.37\text{x}10^{-2}$)	0	2
SPE EDEs (mSv)				
Transit	246	(242,250)	$1.67\text{x}10^{-2}$	$2.60\text{x}10^{5}$
Individual	17.1	(16.0,18.1)	0	$2.60\text{x}10^{5}$

which is increased by a factor of around five. The number of those SPEs exceeding 1 Sv probably demonstrates the highest effect since the orbital effects have the most effect on the higher doses due to the scaling factor. The effect is lessened for the other cases as for all SPEs and the >10 mSv cases the number is increased by a little more than a factor of two, while >100 mSv is closer to three.

Similar trends are also seen in the EDEs for transit and individual SPEs, but the most interesting part is that the minimum transit dose is not zero here, which indicates that this transit is the most likely to receive doses from SPEs. But, as these results were generated from 250,000 iterations, the probability is quite low for this effect to only appear during the 403-day transit.

During a Mars short-stay mission scenario, the average mission expected EDE from SPEs while in deep space would be 314 mSv, which is nearly triple the amount for long-stay missions, and still may not pose a high risk to astronauts. If the inbound transit takes place during a year similar to 1989, 200, or 2001, the EDE from SPEs alone could exceed 1 Sv. Assuming 1 mSv/day for the dose from GCRs, the EDE may exceed 1.6 Sv, which is likely not acceptable for future missions [*National Research*

Council, 2008].

5.4 Discussion

For future long-duration spaceflight, the EDE of highest concern is the 1 Sv case as it could cause operational and health consequences depending on the mission and astronauts. As listed in Table 5.7, the chance of a 1 Sv case is highest as expected for the Venus swing-by case due to the closer approach to the Sun, which increases fluence, increasing dose. Even for the Venus swing-by case a 1 Sv SPE is much less probable than 0.1%, but a 1 Sv event would fall fairly high on the NASA risk matrix presented above, probably in the yellow of the matrix.

Table 5.7: Probability of 1 Sv or higher events during transit.

	GEO	Earth-Mars (L)	Mars-Earth (L)	Earth-Mars (S)	Mars-Earth (S,V)
>1 Sv	$1.20\text{x}10^{-2}$	$6.94\text{x}10^{-3}$	$6.94\text{x}10^{-3}$	$6.92\text{x}10^{-3}$	$3.30\text{x}10^{-2}$
Transit time (days)	180	210	210	217	403
% per day expected	$6.67\text{x}10^{-3}$	$3.30\text{x}10^{-3}$	$3.30\text{x}10^{-3}$	$3.19\text{x}10^{-3}$	$8.19\text{x}10^{-3}$

In the Human Research Roadmap (*NASA* [2016d]), the risks associated with acute radiation effects during operation are either labeled green (acute radiation syndrome) or yellow (central nervous system), which somewhat matches what this research has found. But, since these risks are dependent on transit choices, the risk may even drift into the yellow as demonstrated here for acute radiation syndrome. Although, it can be argued that since events greater than 1 Sv have not been observed in the space age, this risk is minimal unless the Sun dramatically changes over the next

cycles.

Examining the 1 Sv case in further detail for the short-stay return, the probability of greater than 1 Sv SPEs can be described as a Poisson distribution fit. As seen in Figure 5.3, the highest number of greater than 1 Sv SPEs during the transit was three for the 250,000-iteration case with only one transit having this occurrence. The Poisson fit appears to over estimate the frequency of three SPEs meeting the 1 Sv limit, but when executed for more iterations (1,000,000 instead of 250,000), the simulation converges to the distribution. Zero SPEs meeting this criterion during the transit are most common with a cumulative probability distribution value of 0.967.

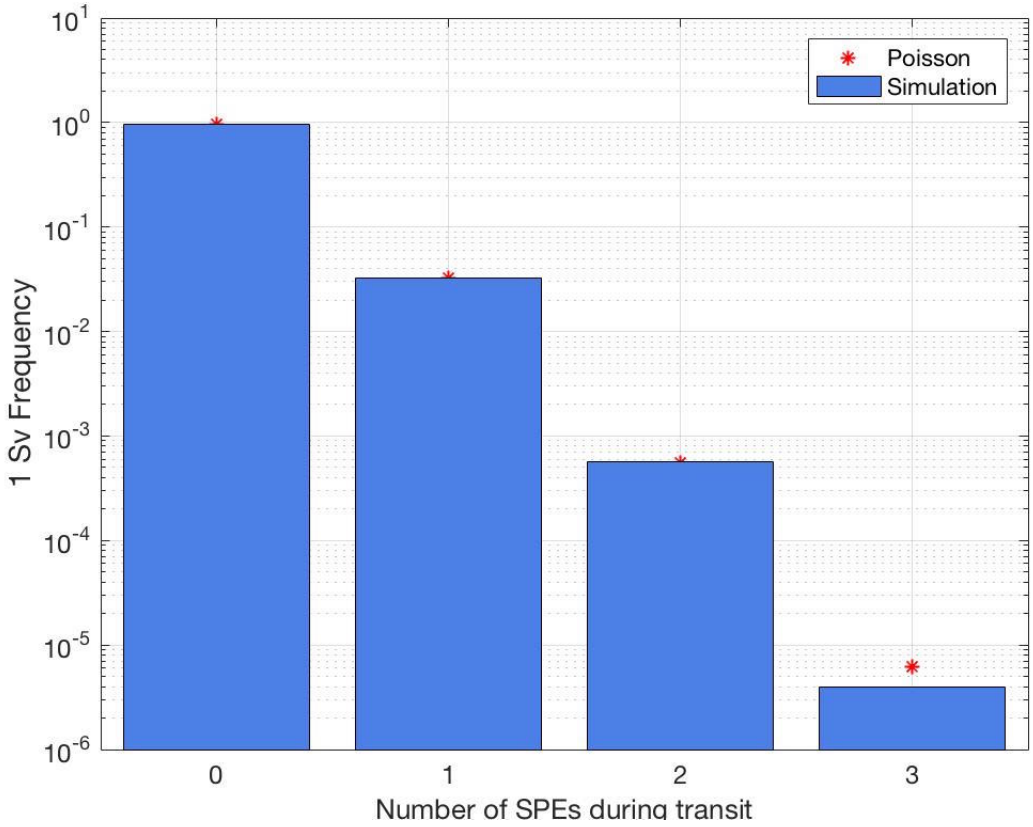

Figure 5.3: Short-stay return 1 Sv distribution. Nearly all of the transit iterations resulted in no SPEs greater than 1 Sv with a small portion of transits having at least one event meeting this criterion.

In addition, from fitting distributions to the transit dose for the short-stay return (as in Section 4.2.3 with fluences), the Normal distribution is the closest to the model results as seen in Figure 5.4. Other distributions over or underestimate the tails of the distribution and all tested distributions did not capture the full peak. The Normal distribution results in 95% of the transit doses being below 845 mSv, and 99% below 2.19 Sv. This implies that the maximum given earlier for this transit is quite rare and unlikely to occur, but greater than 1% of the top doses are above 1 Sv, which may require design changes depending on the mission.

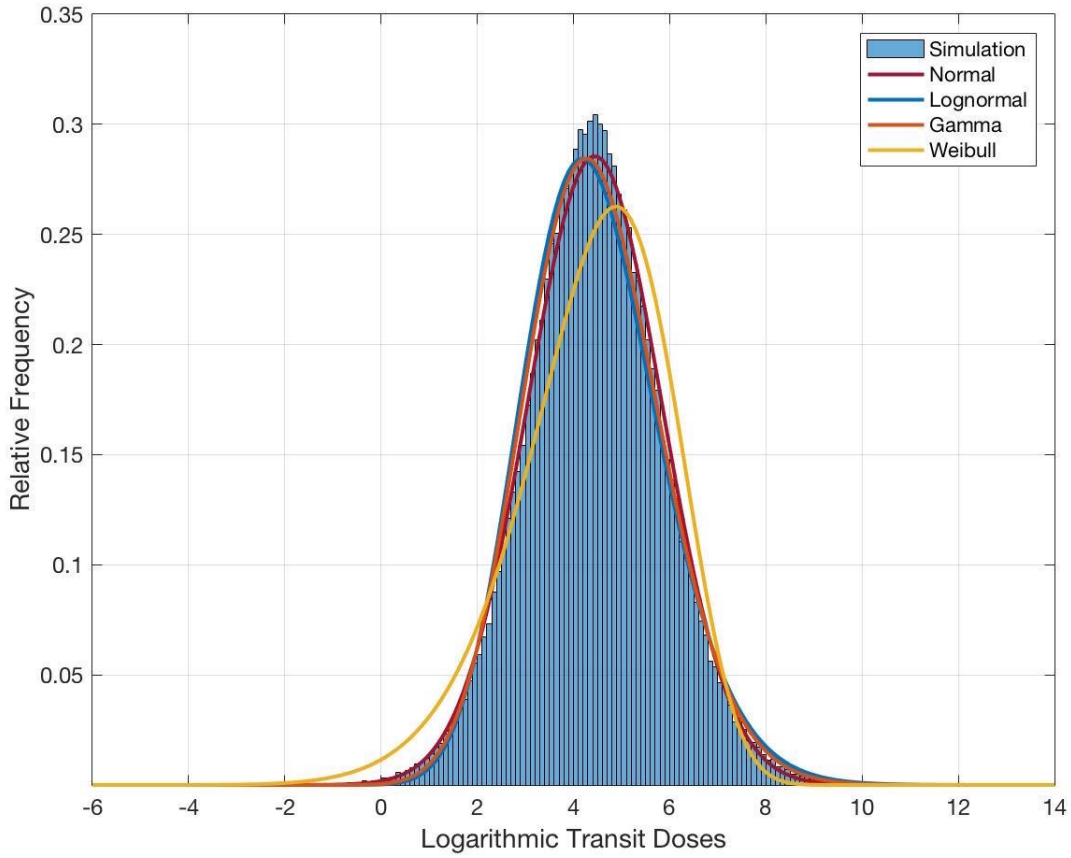

Figure 5.4: Short-stay return dose distribution. Doses are displayed in their logarithmic form for clarity in visualizing the distribution and fits.

The results presented above were given for a single choice of iteration number, but there are other evaluation methods to use in results interpretation. The choice by the user for iteration number will depend on the research application and two other possible methods that were investigated are presented here.

One option is to generate the number of iterations for any variable of interest with any selected confidence interval. When this approach is used to generate 95% CIs around the mean, the number of iterations varies from around 100 for the Venus swing-by total SPE number to over 400,000 for individual SPE EDE values. This results in unrealistic values between the maxima of the different model quantities with low SPE numbers and high EDEs due to the difference in iterations.

Also, another evaluation method is to generate a specific desired maximum or minimum for a particular variable. For instance, in order to keep within the historical SPE EDEs (at GEO), only around 50 iterations are required, which results in a confidence interval of around ±10-15 mSv (maximum SPE around 500-900 mSv, minimum SPE on the order of $1x10^{-5}$).

These other evaluation methods were not given in detail as they focus on specific model quantities and provide likely incorrect results for other quantities. Future users may find these other evaluation methods of interest for different applications.

The results presented above are a demonstration of the information that can be produced by this SPE risk model for applications outside of LEO. The results are not adjusted for uncertainties in the original data for reasons explained in Section 4.4.3, but may be added later with future iterations to improve model robustness. Even with this issue, these initial results seem to match well with historical data and the data from RAD on Curiosity. With additional model credibility assessment and outside review, this model will have the capability to accurately determine expected doses and probabilities for future long-duration missions.

6. CONCLUSIONS AND IMPLICATIONS FOR FUTURE RESEARCH

Currently with plans to send humans farther away from Earth into the solar system, it is important to understand how solar activity can affect human spaceflight for long-duration missions. Throughout the history of solar activity it has been observed that the Sun waxes and wanes over hundreds of years with local maxima every 11 years. When the Sun is more active, emissions such as flares and coronal mass ejections are more common, accelerating particles throughout the solar system. While there are observable quantities that can sometimes predict these events or warn that they are imminent, overall, solar events are probabilistic in nature, making it difficult to plan for their occurrence.

During the space age there have been a number of models for the space radiation environment and for characterizing solar particle events. Now with Mars as the next human spaceflight goal, there is interest in understanding how risks from solar events impact other risks in spaceflight, which may accumulate to make missions more dangerous.

6.1 SPE Risk Model Outside LEO

In order to develop a probabilistic risk model for SPEs useful for future Mars missions, past historical data and current models are integrated. Historical data can be from a number of sources, but satellite data, especially those of NOAA's GOES program are ideal. GOES has measured the space radiation environment at GEO for decades, allowing for numerous analyses and models to be developed. These data were analyzed and characterized by SPE for the past 30 years of data, which demonstrated the variety of SPEs occurrence and severity. MATLAB code files were

developed to process these data anew since NOAA has updated the data with new corrections within the past several years. Once SPEs were analyzed, one of NASA's space radiation risk tools, OLTARIS was used to calculate doses for each of the 180 SPEs from 1986 to 2016.

Through the use of an occurrence model combined with the satellite-based doses, a new model was developed to analyze the risk from SPEs within the inner heliosphere. This model allowed for choice of mission parameters, dose level of interest, and confidence level inputs. The SPE risk model was innovative in that it was written in MATLAB to enable integration with other spaceflight risks and utilizes a new process in determining doses. Previously, most SPE risk calculations were based on historical "worst-case" scenarios for planning, but now with this model, doses can be estimated for missions if the orbital vector with respect to the solar cycle is known. The overall model used a probabilistic risk analysis approach with SPE occurrence and severity distributions implemented to generate doses for a mission. This approach will help better design missions to mitigate expected doses, through efficient use of radiation protection methods.

Currently the SPE risk model is in its initial development and is in need of peer review to solidify the credibility. Other disadvantages include the singular level of shielding (5 g/cm^2 aluminum), simple fluence orbital scale factor application ($R^{-2.5}$ for all fluences), and the lack of uncertainty analysis for the initial model data. Even so, proposed mission transits were used to test the model and compare to relevant data in literature. The model was least accurate in the number of SPEs expected, but the doses may be realistic based on previous space missions. Future studies will help to clarify if the transit SPE number and doses measured by RAD were typical or not for a Mars transit of that type. Initial results demonstrated the disadvantages to choosing a mission with a Venus swing-by, which more than doubles expected

doses and the number of possible events. But, these doses are still not likely to cause LOC or LOM, although may be disruptive in other ways depending on the mission architecture. Since there are little data outside of LEO, it is hoped that this model can help to fill the gap, allowing for mission analysis from a radiation perspective and integrated with other health risks.

This research is unique in approach in that through using a common engineering software (MATLAB), the results can be integrated with other risk models unrelated to radiation. In addition, this research adds to solar event history through a new analysis of SPEs with a code developed that can be applied to past, present, and future SPEs. This combination of MATLAB modeling and new SPE analysis will be useful for numerous future applications and research for human spaceflight missions beyond LEO.

6.2 Opportunities for Further SPE Risk Assessment

In the current phase of development, the SPE risk assessment model can only be applied for general situations, but there are future possibilities that could help add to the capabilities of the model and to its inputs. These possibilities include:

- New code development in MATLAB to incorporate more risk model options (shielding levels),
- Investigation into the timing of SPEs,
- More detailed dose studies,
- Addition of a solar activity dependent GCR model,
- Inclusion of higher energy particles and alphas in SPE model,
- And advanced models for dose and heliospheric propagation.

First, through development of the model, it was demonstrated that there can be a strong correlation between fluence of a specific energy and effective dose equivalent.

This relationship is likely shielding specific and new relationships could be developed for different levels of shielding to open up possible modeling opportunities. Doses for the identified SPEs could be calculated for additional shielding levels through OLTARIS, and new models for different shielding levels generated. Another approach to dose calculations would be to use a transport code within the main model to add additional levels of shielding. This latter approach could also take different inputs instead of just a depth of aluminum. Within MATLAB it is possible to utilize subroutines for other coding languages such as Fortran or C/C++, and so, rewriting this risk model into another language would not be necessary. Through either of these options the risk model could have added capabilities for different levels of shielding.

One area in SPE research that has been of interest recently is investigating the timing of SPEs, comparing their start at the Sun, arrival at the target, and duration. Through the analysis code developed for SPE GOES data analysis, the beginning and end of SPEs are already noted, so developing the code further to examine SPE timing is possible. This would add a duration criterion to the model, which would mean that two events could happen simultaneously, with rises and falls noted in the SPE fluxes. Since SPEs differ in the flux even with similar integrated fluence, there would be a need to characterize events as (for example) long or short in duration with high or low flux over time. Future investigations outside this model development could help this through discoveries into what signatures or characteristics distinguish one SPE from another. Once a parameter is developed to characterize the rises and falls, complete duration can be included in the model that would be capable of determining the combined flux at any time from any number of events.

In addition, most NASA risk models that include whole body doses also include organ specific doses. Organ specific doses were not included in this research, but there are advantages to understanding the affect of a mission transit on organ dose.

Since space agencies have non-cancer dose limits that are organ specific, it could be important to compare the different organ doses. Through this comparison, it could be determined which part of the body is most at risk and may exceed limits first. It is unknown at this time whether there will be a correlation as observed with EDE for shielding, but presumably it is possible. Additionally, these organ doses were saved along with the EDE throughout the code development process, so less research is needed to begin to implement this idea compared to some of the others. Finally, there are standards for differing sized standard female and male bodies for dose studies, so EDEs and organ doses could be adjusted by expected astronaut size instead of only using CAF and CAM.

Next, since GCR dose for a mission depends on solar activity and this model already includes a solar cycle component, GCR dose could be added. This capability would provide the opportunity to conduct full mission dose analyses beyond the estimates that were given in the results through assumption of 1 mSv/day. Further implementation of this model could include use of models found in literature for GCRs, as well such as by *Badhwar and O'Neill* [1996] and their subsequent updates. This additional capability could also include an adjustment for solar cycle length to increase accuracy of dose calculations, since solar cycles do vary in length from the average 4,000-day cycle used in this research. The addition of GCRs would make the SPE risk model into an overall space radiation risk model, usable by more researchers in the future.

Although adding a transport code might be necessary to achieve SPE progression throughout the heliosphere, it is still desirable to increase the credibility in this portion of the model. This added development would likely greatly increase the complexity since magnetic flux tubes and other magnetohydrodynamics concepts are prominent in the theory behind the progression through the heliosphere [*Posner*

et al., 2013].

In the model presented in this document higher energy particles were excluded due to data availability issues, while alpha particles were not considered since SPE models generally include protons only. Depending on the mission these excluded particles could add to the total event doses and may need to be accounted for in the future. As more GOES data are collected, these particles may become candidates for further analysis as the medium energy protons were, which could allow for better characterization of SPEs from a particle standpoint.

Finally, the last aspect of research into SPEs that can be added (once available) is more historical data between Earth and other planets, moons, asteroids, and other solar system objects. This additional data would allow for more verification and validation testing that could lead to increased model usage and credibility. Without additional data, it is not known how accurate the model is for location other than GEO since the only data currently for destinations such as Mars are from Curiosity's RAD instrument.

SPE research over the space age has touched on all of the topics discussed in this document, and for manned spaceflight the risks are generally accepted for any mission. As this research has demonstrated, part of the risk to humans in space from radiation is due to the variety of energies and particles involved. This variety produces an even more varied set of possible biological responses, causing high uncertainties. Through research like this SPE risk model to quantify the expected probabilistic component of space radiation risk, future uncertainties can be reduced. Research in this area will eventually contribute to quantifying overall risk of a mission, allowing for better design, increased astronaut protection, and bring a new era of successful space travel beyond low Earth orbit.

REFERENCES

Adamczyk, A., M. Clowdsley, G. Qualls, S. Blattnig, K. Lee, et al. (2011). Full Mission Astronaut Radiation Exposure Assessments for Long Duration Lunar Surface Missions, in 2011 IEEE Aerospace Conference. Institute of Electrical and Electronics Engineers, Big Sky, MT. doi:10.1109/AERO.2011.5747250.

Adams, J. (2011). Probabilistic Solar Energetic Particle Models, in 23rd International Cosmic Ray Conference. Beijing, China.

Adams, J. H., M. Bhattacharya, Z. W. Lin, G. Pendleton, and J. W. Watts. (2007). The ionizing radiation environment on the moon. *Adv. Space Res.*, *40*, 338-341. doi:10.1016/j.asr.2007.05.032.

Badhwar, G. D., and P. M. O'Neill. (1996). Galactic Cosmic Radiation Model and Its Applications. *Adv. Space Res.*, *17*(2), 7-17. doi:10.1016/0273-1177(95)00507-B.

Bieber, J. W. (2014). University of Delaware Bartol Research Institute Neutron Monitor Program. http://neutronm.bartol.udel.edu/main.html, accessed on August 30, 2016.

Bieber, J. W., and P. Evenson. (1991). Determination of energy spectra for the large solar particle events of 1989, in 22nd International Cosmic Ray Conference. Dublin, Ireland.

Buckey, J. C. (2006). Radiation Hazards: Establishing a Safe Level, *in Space physiology*, 53–76. Oxford University Press, Oxford; New York, NY.

Burke, L. M., R. D. Falck, and M. L. McGuire. (2010). Interplanetary Mission Design Handbook: Earth-to-Mars Mission Opportunities 2026 to 2045. *Tech. Rep. NASA/TM-2010-216764*, National Aeronautics and Space Administration, Cleveland, OH.

Camenisch, C., K. M. Keller, M. Salvisberg, B. Amann, M. Bauch, et al. (2016). The early Spörer Minimum - a period of extraordinary climate and socio-economic changes in Western and Central Europe. *Climate of the Past Discussions*, 1–33. doi:10.5194/cp-2016-7.

Carnell, L., S. Blattnig, S. Hu, J. Huff, M.-H. Kim, R. Norman, Z. Patel, L. Simonsen, and H. Wu. (2016). Evidence Report: Risk of Acute Radiation Syndromes Due to Solar Particle Events. *Tech. Rep. JSC-CN-35747*, National Aeronautics and Space Administration, Houston, TX.

Christian, E., and A. Davis. (2012). Advanced Composition Explorer (ACE) Mission Overview. ACE Science Center. http://www.srl.caltech.edu/ACE/ace_mission.html, accessed on August 30, 2016.

Cooper, C. (2013). The Structure of Our Sun, *in Our Sun: biography of a star*, 43–81. Race Point Publishing, New York, NY. ISBN 1627880763.

Crosby, N., D. Heynderickx, P. Jiggens, A. Aran, B. Sanahuja, et al. (2015). SEPEM: A tool for statistical modeling the solar energetic particle environment. *Space Weather*, *13*, 406-426. doi:10.1002/2013sw001008.

Cucinotta, F. (2010). Radiation Risk Acceptability and Limitations. National Aeronautics and Space Administration. https://three.jsc.nasa.gov/articles/AstronautRadLimitsFC.pdf, accessed on November 29, 2016, date posted: December 21, 2010.

Dayeh, M. A., M. I. Desai, K. Kozarev, N. A. Schwadron, L. W. Townsend, M. PourArsalan, C. Zeitlin, and R. B. Hatcher. (2010). Modeling proton intensity gradients and radiation dose equivalents in the inner heliosphere using EMMREM: May 2003 solar events. *Space Weather*, *8*, S00E07. doi:10.1029/2009sw000566.

Devore, J. (2012). Continous Random Variables and Probability Distributions, *in Probability and Statistics for Engineering and the Sciences*, 137–192. Brooks/Cole,

Boston, MA.

Drake, B. G. (2008). Mars Design Reference Architecture 5.0 Study: Executive Summary. *Tech. Rep. NTRS-20090010571*, National Aeronautics and Space Administration.

Dreschhoff, G. A., and E. J. Zeller. (1990). Evidence of individual solar proton events in Antarctic snow. *Solar Physics*, *127*, 333-346.

Driels, M. R., and Y. S. Shin. (2004). Determining the number of iterations for Monte Carlo simulations of weapon effectiveness. *Tech. Rep. NPS-MAE-04-005*, Naval Postgraduate School, Monterey, CA.

Duderstadt, K. A., J. E. Dibb, C. H. Jackman, C. E. Randall, N. A. Schwadron, S. C. Solomon, H. E. Spence, and V. A. Yudin. (2016). Nitrate ions spikes in ice cores are not suitable proxies for solar proton events. *J. Geophys. Res. Atmospheres*, *121*(6), 2994-3016.

Falconer, D., A. F. Barghouty, I. Khazanov, and R. Moore. (2011). A tool for empirical forecasting of major flares, coronal mass ejections, and solar particle events from a proxy of active-region free magnetic energy. *Space Weather*, *9*, S04003. doi:10.1029/2009sw000537.

Feynman, J., T. Armstrong, L. Dao-Gibner, and S. Silverman. (1990). Solar proton events during solar cycles 19, 20, and 21. *Solar Physics*, *126*, 385-401.

Feynman, J., A. Ruzmaikin, and V. Berdichevsky. (2002). The JPL proton fluence model: an update. *Journal of Atmospheric and Solar-Terrestrial Physics*, *64*, 1679-1686. doi:10.1016/S1364-6826(02)00118-9.

Feynman, J., G. Spitale, J. Wang, and S. Gabriel. (1993). Interplanetary proton fluence model: JPL 1991. *J. Geophys. Res.*, *98*(A8), 13281-13294.

Frahm, R. A., J. R. Sharber, J. D. Winningham, H. A. Elliott, T. A. Howard, C. E. DeForest, D. Odstrĉil, E. Kallio, S. McKenna-Lawlor, and S. Barabash. (2013).

Solar energetic particle arrival at Mars due to the 27 January 2012 solar storm, in Thirteenth International Solar Wind Conference. AIP Publishing LLC, Big Island, HI. doi:10.1063/1.4811068.

Freier, P., and W. Webber. (1963). Exponential rigidity spectrums for solar-flare cosmic rays. *J. Geophys. Res.*, *68*(6), 1605-1629.

Gerontidou, M., A. Vassilaki, H. Mavromichalaki, and V. Kurt. (2002). Frequency distributions of solar proton events. *Journal of Atmospheric and Solar-Terrestrial Physics*, *64*, 489-496.

Goswami, J. N., R. E. McGuire, R. C. Reedy, D. Lal, and R. Jha. (1988). Solar-Flare Protons and Alpha-Particles during the Last 3 Solar-Cycles. *J. Geophys. Res.*, *93*(A7), 7195-7205. doi:10.1029/JA093iA07p07195.

Grayzeck, E. (2016). IMP-J. National Aeronautics and Space Administration. http://nssdc.gsfc.nasa.gov/nmc/masterCatalog.do?sc=1973-078A, accessed on November 5, 2016.

Hassler, D. M., C. Zeitlin, R. F. Wimmer-Schweingrubber, B. Ehresmann, S. Rafkin, et al. (2014). Mars Surface Radiation Environment Measured with the Mars Science Laboratorys Curiosity Rover. *Science*, *343*, 1-6.

Hathaway, D. H. (2010). The Solar Cycle. *Living Reviews in Solar Physics*, *7*(1), 1-65.

Hathaway, D. H. (2016a). Solar Cycle Prediction. National Aeronautics and Space Administration. http://solarscience.msfc.nasa.gov/predict.shtml, accessed on August 30, 2016.

Hathaway, D. H. (2016b). The Sunspot Cycle. National Aeronautics and Space Administration. http://solarscience.msfc.nasa.gov/SunspotCycle.shtml, accessed on August 30, 2016.

Heynderickx, D., B. Quaghebeur, J. Wera, E. J. Daly, and H. D. R. Evans. (2004).

New radiation environment and effects models in the European Space Agency's Space Environment Information System (SPENVIS). *Space Weather*, *2*, S10S03. doi:10.1029/2004sw000073.

Jiggens, P. T., S. B. Gabriel, D. Heynderickx, N. Crosby, A. Glover, and A. Hilgers. (2011). ESA SEPEM project: peak flux and fluence model, in 12th European Conference on Radiation and Its Effects on Components and Systems (RADECS). Institute of Electrical and Electronics Engineers.

Jun, I., R. T. Swimm, A. Ruzmaikin, J. Feynman, A. J. Tylka, and W. F. Dietrich. (2007). Statistics of solar energetic particle events: Fluences, durations, and time intervals. *Adv. Space Res.*, *40*, 304-312. doi:10.1016/j.asr.2006.12.019.

Kennedy, A. R. (2014). Biological Effects of Space Radiation and Development of Effective Countermeasures. *Life Sciences in Space Research*, *1*, 10-43. doi:10.1016/j.lssr.2014.02.004.

Kim, M.-H. Y., M. J. Hayat, A. H. Feiveson, and F. A. Cucinotta. (2009). Prediction of Frequency and Exposure Level of Solar Particle Events. *Health Phys.*, *97*(1), 68-81.

Kim, M.-H. Y., S. Hu, H. N. Nounu, and F. A. Cucinotta. (2010). Development of Graphical User Interface for ARRBOD (Acute Radiation Risk and BRYNTRN Organ Dose Projection). *Tech. Rep. NASA/TP-2010-216116*, National Aeronautics and Space Administration, Houston, TX.

Kim, M.-H. Y., J. W. Wilson, and F. A. Cucinotta. (2004). An Improved Solar Cycle Statistical Model for the Projection of Near Future Sunspot Cycles. *Tech. Rep. NASA/TP-2004-212070*, National Aeronautics and Space Administration, Langley, VA.

King, J. (1974). Solar Proton Fluences for 1977-1983 Space Missions. *Journal of Spacecraft and Rockets*, *11*(6), 401-408.

Knipp, D., A. Ramsay, E. Beard, A. Boright, W. Cade, I. Hewins, R. McFadden, W. Denig, L. Kilcommons, and M. Shea. (2016). The May 1967 Great Storm and Radio Disruption Event: Extreme Space Weather and Extraordinary Responses. *Space Weather*, *14*, 1-20. doi:10.1002/2016SW001423.

Knipp, D. J. (2015). Forward to space weather collection on geomagnetically induced currents: commentary and research. *Space Weather*, *13*, 742-746. doi:10.1002/2015sw001318.

Knipp, D. J., and eds., M. McQuade, and D. Kirkpatrick. (2011a). The Active Interplanetary Medium: Conduit for Space Weather, *in Understanding Space Weather and the Physics Behind It*, 445–490. Space Technology Series. McGraw-Hill, Boston, MA.

Knipp, D. J., and eds., M. McQuade, and D. Kirkpatrick. (2011b). The Active Sun and Other Stars: Sources of Space Weather, *in Understanding Space Weather and the Physics Behind It*, 399–444. Space Technology Series. McGraw-Hill, Boston, MA.

Knipp, D. J., and eds., M. McQuade, and D. Kirkpatrick. (2011c). Earth's Quiescent Magnetosphere: Its Role in the Space Environment and Weather, *in Understanding Space Weather and the Physics Behind It*, 293–346. Space Technology Series. McGraw-Hill, Boston, MA.

Knipp, D. J., and eds., M. McQuade, and D. Kirkpatrick. (2011d). Near-Earth Is a Place... with Susceptible Hardware and Humans, *in Understanding Space Weather and the Physics Behind It*, 589–652. Space Technology Series. McGraw-Hill, Boston, MA.

Knipp, D. J., and eds., M. McQuade, and D. Kirkpatrick. (2011e). The Quiescent Solar Wind: Conduit for Space Weather, *in Understanding Space Weather and the Physics Behind It*, 199–242. Space Technology Series. McGraw-Hill, Boston, MA.

Knipp, D. J., and eds., M. McQuade, and D. Kirkpatrick. (2011f). The Quiescent Sun and Its Interaction with Earth's Atmosphere, *in Understanding Space Weather and the Physics Behind It*, 93–148. Space Technology Series. McGraw-Hill, Boston, MA.

Knipp, D. J., and eds., M. McQuade, and D. Kirkpatrick. (2011g). Space Is a Place... with Weather, *in Understanding Space Weather and the Physics Behind It*, 1–42. Space Technology Series. McGraw-Hill, Boston, MA.

Knipp, D. J., and eds., M. McQuade, and D. Kirkpatrick. (2011h). Understanding Space Weather and the Physics Behind It. Space Technology Series. McGraw-Hill, Boston, MA.

Kruglanski, M. (2013). SPENVIS: Solar Particle Models. European Space Agency. https://www.spenvis.oma.be/help/background/flare/flare.html, accessed on May 29, 2015.

Kruglanski, M., N. Messios, E. D. Donder, E. Gamby, S. Calders, L. Hetey, H. Evans, and E. Daly. (2009). Last upgrades and development of the space environment information system (SPENVIS), in 2009 European Conference on Radiation and Its Effects on Components and Systems (RADECS), 563–565. IEEE, Bruges, Belgium. doi:10.1109/RADECS.2009.5994715.

Lario, D., A. Aran, N. Agueda, and B. Sanahuja. (2007). Radial dependence of proton peak intensities and fluences in SEP events: Influence of the energetic particle transport parameters. *Adv. Space Res.*, *40*, 289-294. doi:10.1016/j.asr.2007.01.057.

Lockwood, M. (2013). Reconstruction and Prediction of Variations in the Open Solar Magnetic Flux and Interplanetary Conditions. *Living Reviews in Solar Physics*, *10*(4), 1-88. doi:10.12942/lrsp-2013-4.

Mars Architecture Steering Group, and B. G. Drake. (2009). Human Exploration of Mars: Design Reference Architecture 5.0. *Tech. Rep. NASA/SP-2009-566*, Na-

tional Aeronautics and Space Administration, Houston, TX.

McCracken, K., D. Smart, M. Shea, and G. Dreschhoff. (2001a). 400 years of large fluence solar proton events, in 27th International Cosmic Ray Conference, vol. 8. Hamburg, Germany.

McCracken, K. G., G. A. M. Dreschhoff, E. J. Zeller, D. F. Smart, and M. A. Shea. (2001b). Solar cosmic ray events for the period 1561-1994 1. Identification in polar ice, 1561-1950. *J. Geophys. Res.*, *106*(A10), 21585-21598. doi:10.1029/2000ja000237.

McGuire, R. E. (2002). Welcome to the Home Page of the IMP-8 Goddard Medium Energy (GME). National Aeronautics and Space Administration. http://spdf.gsfc.nasa.gov/imp8_GME/GME_home.html, accessed on April 25, 2016.

McPhee, J. C., and J. B. Charles, eds. (2009). Human Health and Performance Risks of Space Exploration: Evidence reviewed by the NASA Human Research Program. *Tech. Rep. NASA/SP-2009-3405*, National Aeronautics and Space Administration, Houston, TX.

Meyer, J., G. Wibberenz, and M.-B. Kallenrode. (1993). Time-development of proton energy spectra in solar energetic particle events. *Adv. Space Res.*, *13*(9), 363-366.

Miroshnichenko, L., and R. Nymmik. (2014). Extreme fluxes in solar energetic particle events: Methodological and physical limitations. *Radiation Measurements*, *61*, 6-15.

Morgan, J. L. L., L. E. Ritchie, B. E. Crucian, C. Theriot, H. Wu, C. Sams, S. M. Smith, N. D. Turner, and S. R. Zwart. (2014). Increased dietary iron and radiation in rats promote oxidative stress, induce localized and systemic immune system responses, and alter colon mucosal environment. *FASEB J.*, *28*, 1486-1498. doi:10.1096/fj.13-239418.

Mottl, D., and R. Nymmik. (2007). The issues of reliability of solar ener-

getic proton flux databases and models. *Adv Space Res*, *39*(8), 1355-1361. doi:10.1016/j.asr.2007.01.055.

Myers, J. G., B. E. Lewandowski, J. E. Brooker, and A. S. Weaver. (2011). Assessing the likelihood of rare medical events in astronauts, in Annual Reliability and Maintainability Symposium. Lake Buena Vista, FL. doi:10.1109/RAMS.2011.5754508.

NASA. (1996). GOES I-M DataBook. *Tech. Rep. S-415-19*, Greenbelt, MD.

NASA. (1999). The GOES Program. National Aeronautics and Space Administration. http://goes.gsfc.nasa.gov/text/history/goes/, accessed on September 1, 2016.

NASA. (2001). International Space Station Integrated Medical Group (IMG) Medical Checklist: ISS - All Expeditions. *Tech. Rep. JSC-48522-E4*, National Aeronautics and Space Administration, Houston, TX.

NASA. (2003a). IMP 7. National Aeronautics and Space Administration. https://heasarc.gsfc.nasa.gov/docs/heasarc/missions/imp7.html, accessed on November 5, 2016.

NASA. (2003b). Update on the Solar Storm - Tuesday/Wednesday Solar Punch. http://www.nasa.gov/centers/goddard/news/topstory/2003/1028soho.html, accessed on September 4, 2016.

NASA. (2013). NASA Handbook for Models and Simulations: An Implementation Guide for NASA-STD-7009. *Tech. Rep. NASA/HDBK-7009*, National Aeronautics and Space Administration, Washington, DC.

NASA. (2014). Human Research Roadmap: Human Research Program Architecture. National Aeronautics and Space Administration. https://humanresearchroadmap.nasa.gov/architecture/, accessed on July 8, 2016.

NASA. (2015). Human Research Program Requirements Document: Human Research Program, Revision G. *Tech. Rep. HRP-47052*, National Aeronautics and

Space Administration, Houston, TX.

NASA. (2016a). About the SDO Mission. http://sdo.gsfc.nasa.gov/mission/, accessed on August 30, 2016.

NASA. (2016b). Coordinated Data Analysis Web: IMP (All), Particles (space). NASA Goddard Spaceflight Center. http://cdaweb.sci.gsfc.nasa.gov/index.html/, accessed on November 5, 2016, updated weekly.

NASA. (2016c). Human Research Program Integrated Research Plan, Revision H. *Tech. Rep. HRP-47065*, National Aeronautics and Space Administration, Houston, TX.

NASA. (2016d). Human Research Roadmap: Explore. National Aeronautics and Space Administration. https://humanresearchroadmap.nasa.gov/explore/, accessed on November 28, 2016.

NASA. (2016e). Integrative Risk Models Toolkit. National Aeronautics and Space Administration. https://spaceradiation.jsc.nasa.gov/irModels/, accessed on September 16, 2016.

NASA. (2016f). OLTARIS: On-Line Tool for the Assessment of Radiation In Space. National Aeronautics and Space Administration. https://oltaris.nasa.gov, accessed on January 14, 2016.

NASA. (2016g). SOHO: Solar and Heliospheric Observatory. http://sohowww.nascom.nasa.gov/home.html, accessed on August 30, 2016.

National Research Council. (2008). Managing Space Radiation Risk in the New Era of Space Exploration. The National Academies Press, Washington, DC. ISBN 0-309-11384-9.

NCRP. (2006). Information Needed to Make Radiation Protection Recommendations for Space Missions Beyond Low-Earth Orbit. *Tech. Rep. No. 153*, National Council on Radiation Protection and Measurements, Bethesda, MD.

Nealy, J. E., S. A. Striepe, and L. C. Simonsen. (1992). MIRACAL: A Mission Radiation Calculation Program for Analysis of Lunar and Interplanetary Missions. *Tech. Rep. NASA/TP-1992-3211*, National Aeronautics and Space Administration, Hampton, VA.

Nemiroff, R., and J. Bonnell. (1999). Astronomy Picture of the Day: March 16, 1999. National Aeronautics and Space Administration. http://apod.nasa.gov/apod/ap990316.html, accessed on October 2, 2016.

Nichols, T. F. (2009). Forecasting Dose and Dose Rate from Solar Particle Events Using Locally Weighted Regression Techniques. Ph.D. thesis, University of Tennessee, Knoxville.

NOAA. (2011a). GOES SEM Data: New Averages, GOES 6-15. National Centers for Environmental Information. http://satdat.ngdc.noaa.gov/sem/goes/data/new_avg/, accessed on August 1, 2016, updated monthly.

NOAA. (2011b). Solar Proton Events Affecting the Earth Environment : January 1976 - present. U.S. Dept. of Commerce, NOAA, Space Weather Prediction Center,. ftp://ftp.swpc.noaa.gov/pub/indices/SPE.txt, accessed on May 5, 2016, updated monthly.

NOAA. (2016a). Access to GOES SEM data. National Centers for Environmental Information (NCEI). http://www.ngdc.noaa.gov/stp/satellite/goes/dataaccess.html, accessed on August 1, 2016.

NOAA. (2016b). GOES History. National Oceanic and Atmospheric Administration. http://www.goes-r.gov/mission/history.html, accessed on November 7, 2016.

NOAA. (2016c). GOES Space Environment Monitor: Data describing the environment at geosynchronous orbit. National Centers for Environmental Information. http://www.ngdc.noaa.gov/stp/satellite/goes/index.html, accessed on August 1, 2016.

NOAA. (2016d). Solar Cycle Progression. National Oceanic and Atmospheric Administration. http://www.swpc.noaa.gov/products/solar-cycle-progression, accessed on August 30, 2016.

NOAA. (2016e). Space Weather Enthusiasts Dashboard. National Oceanic and Atmospheric Administration, Space Weather Prediction Center. http://www.swpc.noaa.gov/communities/space-weather-enthusiasts, accessed on September 10, 2016.

NOAA, and NASA. (2009). GOES N Series Data Book, Rev D. *Tech. Rep. CDRL PM-1-1-03*, Greenbelt, MD.

Núñez, M. (2011). Predicting Solar Energetic Proton Events (E > 10 MeV). *Space Weather*, *9*, S07003.

Parihar, V. K., B. Allen, K. K. Tran, T. G. Macaraeg, E. M. Chu, et al. (2015). What happens to your brain on the way to Mars. *Science Advances*, *1*(4), 1-6. doi:10.1126/sciadv.1400256.

Posner, A. (2007). Up to 1-hour forecasting of radiation hazards from solar energetic ion events with relativistic electrons. *Space Weather*, *5*, S05001. doi:10.1029/2006sw000268.

Posner, A., D. Odstrĉil, P. MacNeice, L. Rastaetter, C. Zeitlin, B. Heber, H. Elliott, R. A. Frahm, J. J. E. Hayes, and T. T. von Rosenvinge. (2013). The Hohmann-Parker effect measured by the Mars Science Laboratory on the transfer from Earth to Mars: Consequences and opportunities. *Planetary and Space Science*, *89*, 127-139.

Reames, D. V. (1999). Particle Acceleration at the Sun and in the Heliosphere. *Tech. Rep. NTRS-19990032186*, National Aeronautics and Space Administration, NASA Technical Reports Server.

Rodriguez, J. V., J. C. Krosschell, and J. C. Green. (2014). Intercalibra-

tion of GOES 8-15 solar proton detectors. *Space Weather*, *12*(1), 92-109. doi:10.1002/2013sw000996.

Rodriguez, J. V., T. G. Onsager, and J. E. Mazur. (2010). The east-west effect in solar proton flux measurements in geostationary orbit: A new GOES capability. *Geophys. Res. Lett.*, *37*(7), L07109. doi:10.1029/2010gl042531.

Rosenzweig, J. A., O. Abogunde, K. Thomas, A. Lawal, Y. U. Nguyen, A. Sodipe, and O. Jejelowo. (2010). Spaceflight and modeled microgravity effects on microbial growth and virulence. *Applied Microbiology and Biotechnology*, *85*, 885-891. doi:10.1007/s00253-009-2237-8.

Sanahuja, B., A. Aran, D. Lario, and eds., J. Lilensten, A. Belehaki, M. Messerotti, R. Vainio, J. Watermann, and S. Poedts. (2008). SOLPENCO. The background physics, *in COST 724: Developing the scientific basis for monitoring, modeling and predicting Space Weather*, 217–221. European Science Foundation, Brussels, Belgium.

Sandberg, I., P. Jiggens, D. Heynderickx, and I. A. Daglis. (2014). Cross calibration of NOAA GOES solar proton detectors using corrected NASA IMP-8/GME data. *Geophys. Res. Lett.*, *41*(13), 4435-4441. doi:10.1002/2014gl060469.

Sauer, H. H. (1993). GOES observations of energetic protons to E $>$ 685 MeV: Description and data comparison, in D. A. Leahy, R. B. Hickws, and D. Venkatesan, eds., 23rd International Cosmic Ray Conference, vol. 3. Alberta, Canada.

Schrijver, C. J., J. Beer, U. Baltensperger, E. W. Cliver, M. Güdel, et al. (2012). Estimating the frequency of extremely energetic solar events, based on solar, stellar, lunar, and terrestrial records. *J. Geophys. Res. Space Physics*, *117*, A08103. doi:10.1029/2012ja017706.

Schwadron, N., C. Goodrich, H. Spence, L. Townsend, F. Cucinotta, et al. (2006). Earth-Moon-Mars Radiation Environment Module (EMMREM), in Aerospace

Conference, IEEE 2007. Institute of Electrical and Electronics Engineers, Big Sky, MT.

Schwadron, N. A., J. B. Blake, A. W. Case, C. J. Joyce, J. Kasper, et al. (2014). Does the worsening galactic cosmic radiation environment observed by CRaTER preclude future manned deep space exploration? *Space Weather*, *11*, 622-632. doi:10.1002/2014sw001084.

Schwadron, N. A., L. Townsend, K. Kozarev, M. A. Dayeh, F. Cucinotta, et al. (2010). Earth-Moon-Mars Radiation Environment Module framework. *Space Weather*, *8*, S00E02. doi:10.1029/2009sw000523.

Shea, M., and D. Smart. (1990). A summary of major solar proton events. *Solar Physics*, *127*, 297-320.

Shea, M., and D. Smart. (1993). History of energetic solar protons for the past three solar cycles including cycle 22 update, *in Biological Effects and Physics of Solar and Galactic Cosmic Radiation*, 37–71. Springer US, Boston, MA. ISBN 978-1-4615-2916-3.

Shea, M., and D. Smart. (1994). Significant proton events of solar cycle 22 and a comparison with events of previous solar cycles. *Adv. Space Res.*, *14*(10), 631-638.

Shea, M., and D. Smart. (1995). A comparison of energetic solar proton events during the declining phase of four solar cycles (cycles 1922). *Adv. Space Res.*, *16*(9), 37-46.

Shea, M. A., and D. F. Smart. (2006). Geomagnetic cutoff rigidities and geomagnetic coordinates appropriate for the Carrington flare Epoch. *Adv. Space Res.*, *38*, 209-214. doi:10.1016/j.asr.2005.03.156.

Singleterry, J., Robert C., S. R. Blattnig, M. S. Clowdsley, G. D. Qualls, C. A. Sandridge, et al. (2010). OLTARIS: On-Line Tool for the Assessment of Radiation in Space. *Tech. Rep. NASA/TP-2010-216722*, National Aeronautics and Space

Administration, Hampton, VA.

Slaba, T. C., S. R. Blattnig, M. S. Clowdsley, S. A. Walker, and F. F. Badavi. (2010). An Improved Neutron Transport Algorithm for HZETRN. *Tech. Rep. NASA/TP-2010-216199*, National Aeronautics and Space Administration, Hampton, VA.

Smart, D., and M. Shea. (1999). Comment on the use of GOES solar proton data and spectra in solar proton dose calculations. *Radiation Measurements*, *30*, 327-335.

Smart, D., and M. Shea. (2002). A review of solar proton events during the 22nd solar cycle. *Adv. Space Res.*, *30*(4), 1033-1044.

Smart, D. F., and M. A. Shea. (1989). Solar proton events during the past three solar cycles. *Journal of Spacecraft and Rockets*, *26*(6), 403-415. doi:10.2514/3.26086.

Steward, G. A., V. V. Lobzin, P. J. Wilkinson, I. H. Cairns, and P. A. Robinson. (2011). Automatic recognition of complex magnetic regions on the Sun in GONG magnetogram images and prediction of flares: Techniques for the flare warning program Flarecast. *Space Weather*, *9*, S11004. doi:10.1029/2011sw000703.

Stoker, P. (1995). Relativistic solar proton events. *Space Science Reviews*, *73*, 327-385.

Tapping, K. F. (2013). The 10.7 cm solar radio flux (F10.7). *Space Weather*, *11*, 394-406. doi:10.1002/swe.20064.

The University of New Hampshire Space Science Center. (2016). What is Prediccs? http://prediccs.sr.unh.edu/#what, accessed on August 30, 2016.

Townsend, L. W., and E. N. Zapp. (1999). Dose uncertainties for large solar particle events: input spectra variability and human geometry approximations. *Radiation Measurements*, *30*, 337-343.

Tylka, A. J., and W. F. Dietrich. (2009). A new and comprehensive analysis of proton spectra in ground-level enhanced (GLE) solar particle events, in 31th International Cosmic Ray Conference. Lodz, Poland.

Usoskin, I. G. (2013). A History of Solar Activity over Millennia. *Living Reviews in Solar Physics*, *10*, 1-94. doi:10.12942/lrsp-2013-1.

Usoskin, I. G., and G. A. Kovaltsov. (2012). Occurrence of Extreme Solar Particle Events: Assessment from Historical Proxy Data. *The Astrophysical Journal*, *757*, 1-6. doi:10.1088/0004-637x/757/1/92.

Usoskin, I. G., S. K. Solanki, and G. A. Kovaltsov. (2007). Grand minima and maxima of solar activity: New observational constraints. *Astronomy & Astrophysics*, *471*, 301-309.

Wilson, J. W., S. Y. Chun, F. F. Badavi, L. W. Townsend, and S. L. Lamkin. (1991). HZETRN: A Heavy Ion/Nucleon Transport Code for Space Radiations. *Tech. Rep. NASA/TP-3146*, National Aeronautics and Space Administration, Hampton, VA.

Wolff, E. W., M. Bigler, M. A. J. Curran, J. E. Dibb, M. M. Frey, M. Legrand, and J. R. McConnell. (2012). The Carrington event not observed in most ice core nitrate records. *Geophys. Res. Lett.*, *39*, L08503. doi:10.1029/2012gl051603.

Xapsos, M. A., J. Barth, E. Stassinopoulos, E. A. Burke, and G. Gee. (1999). Space environment effects: model for emission of solar protons (ESP): cumulative and worst case event fluences. *Tech. Rep. NASA/TP-1999-209763*, National Aeronautics and Space Administration, Greenbelt, MD.

Zapp, E. N., C. R. Ramsey, L. W. Townsend, and G. D. Badhwar. (1999). Solar particle event dose and dose-rate distributions: parameterization of dosetime profiles, with subsequent dose-rate analysis. *Radiation Measurements*, *30*, 393-400.

Zeitlin, C., D. M. Hassler, F. A. Cucinotta, B. Ehresmann, R. F. Wimmer-Schweingruber, et al. (2013). Measurements of energetic particle radiation in transit to Mars on the Mars Science Laboratory. *Science*, *340*, 1080-1084. doi:10.1126/science.1235989.

Zell, H., ed. (2016). Missions Supporting the Study of the Sun-Earth Connection:

Heliophysics. National Aeronautics and Space Administration. https://www.nasa.gov/mission_pages/sunearth/missions/index.html, accessed on August 30, 2016.

APPENDIX A

FULL SOLAR PARTICLE EVENT LISTING

This appendix contains information as to the supplemental files in .xlsx format, which document both the integrated fluences for SPEs from 1986 to present and missing data points filled as part of the analysis by month and satellite. These files contain the direct output from the code listed in Appendix B, which have been combined over multiple runs. After generating these files, the SPE fluences were minimally processed, just combined where necessary when events had longer tails that read as another event. As discussed in the main text, there was not a way to avoid this, but it was optimized so that it occurred as little as possible. When running the data analysis code it is important to note that this does occur and to consult with an SPE listing (such as *NOAA* [2011b]) to interpret the results correctly.

Those interested in being notified of events beyond mid-2016 can subscribe to NOAA's SWPC (Space Weather Prediction Center) daily "Solar and Geophysical Activity Summary," which sends subscribers a daily email with energetic events, particle counts, and other measures of space weather activity.

A.1 Integrated Fluences

The file titled "GOESspecMAIN.xlsx" contains the integrated fluences for all events analyzed in this research. The first column is the GOES number (i.e. 6 = GOES-6) and the next two columns list event start and end date and time if applicable. The cases where these are listed as "N/A" can be explained through reading the "Code" column and in most cases N/A is marked with "d" to indicate that the satellite data for that month was expected to have an event, but did not

have any data points meeting the cutoff. The next seven columns are the integrated fluences in p/cm^2 for each energy bin and if not listed can also be explained through the "Code" column (see below for full listing). The columns following the integrated fluence listings contain other information about the event that was processed. The first of these is the number of missing data points filled. If an event is fully analyzed, this will be a number, if not it will read "N/A" such as for events that did not meet the cutoff or had too many missing points to fill based on the 10% criterion explained in Section 3.3.2. Next is the "Code" column as briefly discussed above and fully explained below. This was created so that a user would know why an event did not get processed and what possible problems occurred during processing.

a = no points missing or filled

b = some points missing or filled

c = too many missing data points overall or in succession for event

d = month did not have any points that met the 10 pfu at $>$ 10 MeV cutoff

e = error, if occurs, contact author

f = event could not be completed due to missing next month of data (event overlaps between months)

The last column is "Note," which has information with regards to whether a SPE recorded was actually part of another event right before it or not. If the additional event was past the flux peak listed by NOAA in *NOAA* [2011b], then it was considered to be part of the tail not meeting the cutoff, but sometimes this was added on. The phrases "Not past event peak" and "Past event peak" indicate whether the SPE on that line was added to the previous line or not respectively.

Finally, it should also be noted that in this file although one satellite was analyzed after another by month, sometimes the data has one month combined with another due to events taking place at the end of the month. A user should make sure they

are reading the data correctly by the dates.

A.2 Filled Flux Points

This file is named "GOESfilledMAIN.xlsx" and contains a listing of all missing data points filled for events for those that were filled or an indication otherwise. Events that did not meet the NOAA 10 pfu criterion are not listed in this file as they were in the integrated fluences file. Like "GOESspecMAIN.xlsx" this file contains the GOES number in the first column and is organized by month and GOES number, with the same ordering note as mentioned previously where months may be analyzed together for one satellite before moving on to the next. The next column, "Event Start" lists the date and time of event start for reference for the following column, "Missing Times Filled." This column either lists line by line the date and time filled or "N/A" to designate that there was no need to list these values. The final column provides explanation of the times filled by stating:

- "none missing" - no data points missing from event
- "some filled" - a number of data points were filled, but were under the 10% limit
- "too many overall" - limit reached during event for 10% of data for event missing
- "too many in succession" - did not occur during the SPEs analyzed here since they met the overall case first, but is for if 24 lines (2 hours) in succession are missing

Finally, note that some events may have what seems like a large number of data points that needed to be filled, but these were larger events and the missing data points therefore have less of an impact and is why a percentage criterion was selected instead of a fixed number.

APPENDIX B

MATLAB CODE FILES

This appendix contains the code files and information about them used to generate the SPE listing attached in the Excel files. These files fall under the copyright of this document and credit must be given to the author if used in publications. A summary of the SPE risk model code files is provided, but not listed in full here. Until the model has outside credibility assessment (peer review), the model will not be ready for research and/or design use - if interested in assisting with this process, contact the author. Code files can be obtained upon request from the author via email to: sarah.e.over@gmail.com.

Important notes about the code files:

- Final code was tested and run in MATLAB version 2016a for Mac (OSX 10.11.6).
- On a Windows version of MATLAB, the Excel output files will need to be changed to the original MATLAB function (xlswrite) file since this built-in file is not fully compatible with OSX for MATLAB 2016a.
- For Mac users, the Excel output file, "xlwrite" written by Alec de Zegher can be obtained through the MATLAB file exchange.
- The code below was formatted through use of the "M-code LaTeX Package" written by Florian Knorn, which can also be obtained through the file exchange as well.

B.1 Data Processing

Below code is listed in full that was used to process NOAA data .csv files, generating event listings and missing data listings. The code is organized by sections with the main files listed first which call all other files to process data. The starter input file is called "xlsGOESmain.m" and once called, this file will ask the user to input file names of GOES data to process (which must be in MATLAB's path to process). The next set of files are those used to convert data from NOAA .csv files to matrices and date-time format during processing. Special case files are listed next, which cover events extending from one month the next (i.e. event starts on a 30th/31st and does not finish till the 1st/2nd) and events containing missing data points due to loss of satellite coverage. Finally, the last file listed is used to generate Weibull parameters for processed events and is designed to take data directly copied from a spreadsheet for one or more events. This file also optionally includes the creation of a plot to view the Weibull curve fits generated.

B.1.1 Primary SPE Calculation and Output

The files listed in this section are those that are always called to perform data processing and are the minimum necessary to determine SPE fluence for events. Other files that are called conditionally are listed in the next few sections and their purpose explained.

[**xlsGOESmain.m**] - user runs all the rest of the code for data analysis with this file, user inputs number of months desired to evaluate in each run and questions will be asked throughout the run to continue to progress through the data files

```
1  % File for processing any GOES satellite proton data for no's ...
       06-15.  Data
2  % inputs are 5 minute integrated flux averages in a [n,7] matrix ...
       plus an
3  % [n] vector containing time stamps for the integrated flux.
4
5  % When run, it converts the Excel files to matricies to process ...
       based on
6  % specific satellite data used.  User must have Excel files set ...
       and ready
7  % for processing.
8
9  % Note, integrated flux units: protons/(ster*cm^2) for energies of
10 %           1, 5, 10, 30, 50, 60, and 100 MeV
11 % Also, another approach was considered, requiring user to input ...
       expected
12 % event timings from NOAA list, but for the sake of user time ...
       required to
```

```
13 % process events, this was disregarded.  The only rationale was ...
      to avoid
14 % events being combined that might indeed be separate because of ...
      drops
15 % within and outside of event occurrences, which can be ...
      processed manually
16 % if needed. As of 9/24/16, this only occurs two times in the ...
      data from
17 % 1986-present and so time is better spent processing these ...
      manually than
18 % slowing down the whole process.  Finally, it is possible that ...
      events
19 % might be too close together to resolve (overlapping 10x10), so ...
      neither
20 % the considered or current process would be able to resolve these.
21
22 % Created: 8/12/16
23 % Last modified: 9/26/2016 - added satellite designator for ...
      GOES13-15
24 % Last verified: 9/27/2016 - 2001 data
25
26
27 % Files called when running routine and subroutines:
28 % xls0607read, xls0812read, xls1315read,
29 % xlsGOESproc, extraGOESdata, xlsGOESspec, missGOESdata
30
31 % Files generated: GOESspec.xlsx, GOESfilled.xlsx
32 %   which contain individual satellite spectra for each event ...
      and missing
33 %   data filled documentation categorized by year
34
```

```
35
36 clear
37 clc
38
39 %%%%%%%%% Needed to load at beginning to make Excel output work ...
       (and setup
40 %%%%%%%%% headers at the same time)
41 %% Initialisation of POI Libs
42 % Add Java POI Libs to matlab javapath
43 javaaddpath('poi_library/poi-3.8-20120326.jar');
44 javaaddpath('poi_library/poi-ooxml-3.8-20120326.jar');
45 javaaddpath('poi_library/poi-ooxml-schemas-3.8-20120326.jar');
46 javaaddpath('poi_library/xmlbeans-2.3.0.jar');
47 javaaddpath('poi_library/dom4j-1.6.1.jar');
48 javaaddpath('poi_library/stax-api-1.0.1.jar');
49
50 % Setup headers in Excel files
51 xlsFiles;
52
53 specexst = 3;
54 missst = 2;
55
56
57 % Loop for additional file inputs so that can run one month for all
58 % satellites at the same time
59     % Setup loop criterion
60 ques_m = 'How many months would you like to analyze?\n';
61 loopno = input(ques_m);
62
63     % Loop for each month
64 for i = 1:1:loopno
```

```
65      fprintf('\nHow many satellites covered month %d?',i)
66      ques_sat = '\n';
67      satno = input(ques_sat);
68      for j = 1:1:satno
69          fprintf('\nEnter name of file for satellite %d, month ...
                %d',j,i);
70          stm = ' (filename.csv):\n';
71          fname = input(stm,'s');
72          GOESn = str2num(fname(2:3)); %#ok<ST2NM> %not needed
73          % Pass to appropriate xls read file
74          if (GOESn == 6) || (GOESn == 7)
75              [coldt,colMeV] = xls0607read(fname);
76              des = 0;
77              [specexend,missend] = ...
78                  xlsGOESproc(coldt,colMeV,GOESn,specexst,missst,des);
79          elseif (GOESn == 8) || (GOESn == 9) || (GOESn == 10) ||...
80                  (GOESn == 11) || (GOESn == 12)
81              [coldt,colMeV] = xls0812read(fname);
82              des = 0;
83              [specexend,missend] = ...
84                  xlsGOESproc(coldt,colMeV,GOESn,specexst,missst,des);
85          elseif (GOESn == 13) || (GOESn == 14) || (GOESn == 15)
86              % Read 1st set - called "B"
87              [coldt,colMeV] = xls1315Bread(fname);
88              des = 1;
89              [specexend,missend] = ...
90                  xlsGOESproc(coldt,colMeV,GOESn,specexst,missst,des);
91              specexst = specexend;
92              missst = missend;
93              % Read other direction - called "A"
94              [coldt,colMeV] = xls1315Aread(fname);
```

```
95              des = 2;
96              [specexend,missend] = ...
97                  xlsGOESproc(coldt,colMeV,GOESn,specexst,missst,des);
98          end
99
100         % Run analysis function to generate analysis information
101
102
103         % Reset Excel line fillers and skip line to create space
104         if j == satno      % want extra space to divide months
105             specexst = specexend + 1;
106             missst = missend + 1;
107         else
108             specexst = specexend;
109             missst = missend;
110         end
111
112
113
114
115     end
116
117 end
```

[**xlsGOESproc.m**] - file looks through each month of data for possible events, applying criteria as discussed in Section 3.3 to separate out SPE segments to pass to another file (xlsGOESspec.m) for individual event processing

```
1  % Function file for prepping data to be analyzed for each event ...
       and sets up
2  % critera by which an event may not be recorded other than too ...
       much missing
3  % data (covered in missGOESdata.m)
4
5  % For more information on data that is being processed, see main ...
       file
6  % (xlsGOESmain.m)
7
8  % Created: 8/11/2016
9  % Last modified: 9/27/2016 - fixed check for missing data at end ...
       of month
10 % to accomodate an entire missing data month (i.e. G11, 2001-12)
11 % Last verified: 9/27/2016 - 2001 all months
12
13 % Current setting is for a cutoff pfu (cpfu) for the end of ...
       events to be
14 % 3.33 pfu, with 6.66 pfu (bpfu) for cases where events occur ...
       close to one
15 % another, user can change these values below.
16
17
18 function [excend,filed] = ...
       xlsGOESproc(coldt,colMeV,GOESn,excstart,filst,des)
19
```

```
% Set event tail cutoff value
% cpfu = 1;
cpfu = 3.33;
% cpfu = 5;
bpfu = 6.66;

% Generate size of inputs and setup 10 MeV column for testing
s_month = size(coldt);
len = s_month(1);
c10MeV = colMeV(:,3);

% Check for event at end of month spilling over to next
end_month = c10MeV(len);
repld = 0;
warn = 'Data ok at end of month';
while end_month < 0 % run till find non-missing point
    repldchk = len - repld;
    if repldchk == 0
        warn = 'Entire month missing data';
        break
    else
        end_month = c10MeV(len-repld);
        repld = repld + 1;
        warn = 'Missing data at end of month - caution';
    end
end
fprintf('%s\n\n',warn)

while end_month ≥ cpfu  % Will run till month occurs without ...
    event towards end
    [coldt,colMeV,echk] = extraGOESdata(coldt,colMeV,GOESn,des);
```

```
50      if echk == 1
51          break
52      else
53          s_monthx = size(coldt);
54          len = s_monthx(1);
55          c10MeV = colMeV(:,3);
56          end_month = c10MeV(len);
57      end
58  end
59
60
61  % Generate test vector for when events might be occurring ...
        (meeting 10x10
62  % criterion)
63  evtest = zeros(len,1);
64  for i = 1:1:len
65      if c10MeV(i) ≥ 10
66          evtest(i) = 1;
67      end
68  end
69
70  % Check for events occuring and process if so
71  % Initialize loop variables
72  evn = 0;
73  sum_evtest = sum(evtest);
74
75
76  if sum_evtest == 0
77      % no events, no pts over 10x10 cutoff
78      fprintf('No events this month recorded with this satellite.\n')
79      eventdt_tr = 0;
```

```
80      eventE_tr = [0 0 0 0 0 0 0];
81      [excend,filed] = ...
82              xlsGOESspec(eventdt_tr,eventE_tr,...
83              GOESn,excstart,filst,des);
84  else % Events probably occurring
85      while sum_evtest > 0
86          % Find start of event and set new vectors
87
88          % Ignore if start of month is a hangover from previous ...
                (over 10
89          % pfu) - took out - see text file for previous ...
                implementation
90
91
92          % Find start of first new event
93          chk0 = find(c10MeV>0);    % Exclude missing data points
94          s_chk0 = size(chk0);
95          l_chk0 = s_chk0(1);
96          % Loop through non-missing data points to find set of 3 ...
                consecutive
97          % points above 10x10
98          if l_chk0 < 3
99              % looking at end of month, not usable and cannot ...
                    determine if
100             % event starts or not (need rise + 10x10)
101             ev_start = [];
102         else
103             for g = 1:1:l_chk0
104                 if evtest(chk0(g)) == 1   % start
105                     if evtest(chk0(g+1)) == 1   % 2nd point
106                         if evtest(chk0(g+2)) == 1  % 3rd point
```

```
107                             ev_start = chk0(g);
108                             break
109                         end
110                     else
111                         % not long enough to meet 3 @ 10x10, do ...
                               nothing
112                         ev_start = [];
113                     end
114                 else
115                     % not true event, just random increase in data
116                     ev_start = [];
117                 end
118             end
119         end
120
121         % Take out false event data and find end of event:
122         stchk = isempty(ev_start);
123         if stchk == 1
124             % No more events
125             sum_evtest = 0;
126             excend = excstart;
127             filed = filst;
128             fprintf('No more events this month\n')
129         else
130             % Event occurs
131             EventStartdt = coldt(ev_start);
132             EventStartst = datestr(EventStartdt);
133             fprintf('Event start at: %s \n',EventStartst)
134             eventdt = coldt(ev_start:end);
135             eventE = colMeV(ev_start:end,:);
136             ev_c10MeV = eventE(:,3);
```

```
137             % find drop off after end
138             ev_chk0 = find(ev_c10MeV>0);    % Exclude missing ...
                   data points
139             sev_chk0 = size(ev_chk0);
140             lev_chk0 = sev_chk0(1);
141             % Loop through non-missing data points after start ...
                   to find
142             % where drop off is
143
144             % Ask if close to another event and process ...
                   differently if so
145             fprintf('Does this event occur close to another event')
146             askclose = '? 1 = yes, 0 = no\n';
147             refchk = input(askclose);
148             % do refined check to make sure do not combine events
149             if refchk == 1
150                 for m = 1:1:lev_chk0
151                     if ev_c10MeV(ev_chk0(m)) < bpfu
152                         EventPastdt = eventdt(ev_chk0(m));
153                         EventPaststr = datestr(EventPastdt);
154                         fprintf('Poss past end at %s ...
                               \n',EventPaststr)
155                         fprintf('Is the time above close to ...
                               another event')
156                         qend = '? 0 = yes, 1 = no\n';
157                         qendans = input(qend);
158                         if qendans == 0
159                             ev_endpret = ev_chk0(m);
160                             break
161                         else
162                             % not end yet, keep looking and ...
```

```
                                process as usual
163                             if ev_c10MeV(ev_chk0(m)) < cpfu
164                                 if ev_c10MeV(ev_chk0(m+1)) < 10
165                                     ev_endpret = ev_chk0(m);
166                                     break
167                                 else
168                                     % erroneous drop (never ...
                                        quite that rapid)
169                                 end
170                             else
171                                 ev_endpret = [];
172                             end
173                         end
174                     end
175
176                 end
177             else
178                 % Process assuming event flux will drop completely
179                 for m = 1:1:lev_chk0
180                     if ev_c10MeV(ev_chk0(m)) < cpfu
181                         if ev_c10MeV(ev_chk0(m+1)) < 10
182                             ev_endpret = ev_chk0(m);
183                             break
184                         else
185                             % erroneous drop (never quite that ...
                                rapid)
186                         end
187                     else
188                         ev_endpret = [];
189                     end
190                 end
```

```
191             end
192
193
194             % Test for case of data not existing to fill end of ...
                    month, or
195             % continue to process
196             test_endpt = isempty(ev_endpret);
197             if test_endpt == 1
198                 sum_evtest = 0;
199                 eventdt_tr = eventdt(1);
200                 eventE_tr = [];
201                 [excend,filed] = ...
202                     xlsGOESspec(eventdt_tr,eventE_tr,GOESn,...
203                     excstart,filst,des);
204                 excstart = excend;
205                 filst = filed;
206             else
207                 % Find actual end
208                 for j = ev_endpret:-1:1
209                     if evtest(j+ev_start-1) == 0
210                         % do nothing, not end
211                     else
212                         ev_end = j;    % Need + 1 b/c of working ...
                                backwards
213                         break
214                     end
215                 end
216
217                 % Trim data to start and stop points
218                 eventdt_tr = eventdt(1:ev_end);
219                 eventE_tr = eventE(1:ev_end,:);
```

```
220
221                 % Pass to spectrum file or declare as 1 line event
222                 ev_finish = ev_start + ev_end;
223                 % Pass information to next file to generate data ...
                        to fill
224                 % into Excel files
225                 [excend,filed] = ...
226                     xlsGOESspec(eventdt_tr,eventE_tr,GOESn,...
227                     excstart,filst,des);
228                 evn = evn + 1; % event counter for testing
229
230                 % Replace test vector for part used in event and ...
                        reset for
231                 % next loop
232                 if ev_end == 1
233                     evtest(ev_start) = 0;
234                 else
235                     for k = 1:1:ev_finish
236                         evtest(k) = 0;
237                     end
238                 end
239                 sum_evtest = sum(evtest);
240                 excstart = excend;
241                 filst = filed;
242             end
243         end
244     end
245 end
```

[**xlsGOESspec.m**] - calculates integrated fluences and assigns codes telling the user information about the processed SPE

```
% Function file for usual processing of GOES data for an event:
    % Takes trimmed event data as input
    % Checks for missing data (calls missGOESdata.m) and fills ...
       as possible
    % Sums resulting data
    % Prints results to spectra file

% Created: 8/20/2016
% Last modified: 9/26/2016 - swapped 'd' and 'e' designations ...
    since took
% out 1-line cases
% Last verified: 9/27/2016 - 2001 data

function [exced,edfil] = ...
    xlsGOESspec(eventdt_tr,eventE_tr,GOESn,excst,stfil,des)

% Generate information and check for missing data, filling as ...
    needed and if
% clauses to check for various endings
edatl = size(eventdt_tr);
e_len = edatl(1);
test_dt = isa(eventdt_tr,'numeric');
test_E = isempty(eventE_tr);

% Run through 1-line cases: missing data at end of month, 1-line ...
    event, and
% no events -- not all applies after taking out 1-event case in
```

```
% xlsGOESproc.m, but helpful for debugging
if e_len == 1
    if test_E == 1
        % do not look for missing data - missing data to ...
           complete event at
        % end of month or flux did not fall below cutoff
        chk = 5;
        pt_fill = 0;
    elseif test_dt == 1
        % no event meeting 10x10 criteria
        chk = 4;
        pt_fill = 0;
    else
        % 1-line valid event, no points filled
        chk = 3;
        pt_fill = 0;
    end
    edfil = stfil;
else
    [chk,specMeVfil,pt_fill,edfil] = ...
        missGOESdata(eventdt_tr,eventE_tr,GOESn,e_len,stfil,des);
end

% Sum and store information in text files
if chk == 0
    % store information that the event was no good
    e_fspec = [NaN NaN NaN NaN NaN NaN NaN];
    code = 'c';
    no_fil = 'N/A';
    dtstart = eventdt_tr(1);
    ev_dtst = {datestr(dtstart)};
```

```
54      dtend = eventdt_tr(e_len);
55      ev_dted = {datestr(dtend)};
56  elseif (chk == 1) || (chk == 2)
57      % sum and store values for event that had some filled or none
58      e_fspec = sum(specMeVfil).*1200.*pi();
59      if chk == 1
60          code = 'b';
61          no_fil = pt_fill;
62      elseif chk == 2
63          code = 'a';
64          no_fil = 0;
65      end
66      dtstart = eventdt_tr(1);
67      ev_dtst = {datestr(dtstart)};
68      dtend = eventdt_tr(e_len);
69      ev_dted = {datestr(dtend)};
70  elseif chk == 3;
71      % case of 1-line event
72      e_fspec = eventE_tr.*1200.*pi();
73      code = 'e';
74      no_fil = 0;
75      dtstart = eventdt_tr;
76      ev_dtst = {datestr(dtstart)};
77      dtend = 'N/A';
78      ev_dted = {dtend};
79  elseif chk == 4;
80      % case of no event meeting 10x10 cutoff
81      e_fspec = [NaN NaN NaN NaN NaN NaN NaN];
82      code = 'd';
83      no_fil = 'N/A';
84      dtstart = 'N/A';
```

```
85      ev_dtst = {dtstart};
86      dtend = 'N/A';
87      ev_dted = {dtend};
88  elseif chk == 5;
89      % case of event missing data to complete from next month
90      e_fspec = [NaN NaN NaN NaN NaN NaN NaN];
91      code = 'f';
92      no_fil = 'N/A';
93      dtstart = eventdt_tr;
94      ev_dtst = {datestr(dtstart)};
95      dtend = 'N/A';
96      ev_dted = {dtend};
97  end
98
99  % Print to Excel file
100 % Set up ranges
101 row1 = excst;
102 chr1 = int2str(row1);
103 Rg1 = ['A',chr1];
104 Rg2 = ['B',chr1];
105 Rg3 = ['C',chr1];
106 Rg4 = ['D',chr1];
107 Rg5 = ['K',chr1];
108 Rg6 = ['L',chr1];
109
110 % Specify outputs and convert to cell for proper output
111 Efluspec = num2cell(e_fspec); % may not need to convert to cell
112 no_fil = {no_fil};
113 code = {code};
114
115 if des == 0
```

```
116     Gndes_pre = int2str(GOESn);
117 elseif des == 1
118     desch = 'B';
119     GOESnch = int2str(GOESn);
120     Gndes_pre = [GOESnch,desch];
121 elseif des == 2
122     desch = 'A';
123     GOESnch = int2str(GOESn);
124     Gndes_pre = [GOESnch,desch];
125 end
126 Gndes = {Gndes_pre};
127 
128 % Write to Excel file (note need sheet specifier, otherwise tries
129 % to use range as sheet)
130 xlwrite('GOESspec.xlsx',Gndes,'Sheet1',Rg1);
131 xlwrite('GOESspec.xlsx',ev_dtst,'Sheet1',Rg2);
132 xlwrite('GOESspec.xlsx',ev_dted,'Sheet1',Rg3);
133 xlwrite('GOESspec.xlsx',Efluspec,'Sheet1',Rg4);
134 xlwrite('GOESspec.xlsx',no_fil,'Sheet1',Rg5);
135 xlwrite('Goesspec.xlsx',code,'Sheet1',Rg6);
136 
137 % Reset values for next loop
138 exced = excst + 1;
139 edfil = edfil + pt_fill;
```

[**xlsFiles.m**] - generates Excel output setup with column and row titles

```
% File for setting up Excel sheets with headers for both the ...
    filled and
% spectra sheets

% Created: 08/24/2016
% Last Modified: 08/24/2016 - creation
% Last Verified: 08/24/2016 - 1986/1987 data


% Initialize variables to be used in setting Excel location ...
    placement and
% start files

% Spectra File Setup
Rg1a = ['A','2'];
Rg2a = ['B','2'];
Rg3a = ['C','2'];
Rg4a = ['D','1'];
Rg4a1 = ['D','2'];
Rg5a = ['K','2'];
Rg6a = ['L','2'];

colA = {'GOES No.'};
colB = {'Event Start'};
colCa = {'Event End'};
colDa = {'Event Spectra'};
colDa1 = {'1 MeV','5 MeV','10 MeV','30 MeV','50 MeV','60 ...
    MeV','100 MeV'};
```

```
26 colKa = {'No. Miss. Filled'};
27 colLa = {'Code'};
28
29 xlwrite('GOESspec.xlsx',colA,'Sheet1',Rg1a);
30 xlwrite('GOESspec.xlsx',colB,'Sheet1',Rg2a);
31 xlwrite('GOESspec.xlsx',colCa,'Sheet1',Rg3a);
32 xlwrite('GOESspec.xlsx',colDa,'Sheet1',Rg4a);
33 xlwrite('GOESspec.xlsx',colDa1,'Sheet1',Rg4a1);
34 xlwrite('GOESspec.xlsx',colKa,'Sheet1',Rg5a);
35 xlwrite('Goesspec.xlsx',colLa,'Sheet1',Rg6a);
36
37
38 % Filled missing points setup
39 Rg1b = ['A','1'];
40 Rg2b = ['B','1'];
41 Rg3b = ['C','1'];
42 Rg4b = ['D','1'];
43
44 colA = {'GOES No.'};
45 colB = {'Event Start'};
46 colCb = {'Missing Times Filled'};
47 colDb = {'Info'};
48
49 xlwrite('GOESfilled.xlsx',colA,'Sheet1',Rg1b);
50 xlwrite('GOESfilled.xlsx',colB,'Sheet1',Rg2b);
51 xlwrite('GOESfilled.xlsx',colCb,'Sheet1',Rg3b);
52 xlwrite('GOESfilled.xlsx',colDb,'Sheet1',Rg4b);
```

B.1.2 Satellite Data Setup

All of the files in this section take GOES .csv 5-minute averaged flux files as inputs and convert the data to matrix form to be processed in MATLAB. GOES-13 and GOES-15 both have sensors pointing opposite directions and are labeled either "A" and "B" or "East" and "West" depending on the researcher. The orientation is not unchanging throughout the year due to the "flip" that those satellites perform once or twice a year. These two directions have slightly different processing needs and so are split into two files.

[xls0607read.m] - GOES-6 and GOES-7 .csv files

```
1  % Function for reading and converting data formatted under the ...
       GOES 06 and
2  % 07 satellite files
3
4
5  % Created: 8/10/16
6  % Last modified: 8/12/16 (simplifying to just converting data)
7
8
9  function [dtcol,Ecol] = xls0607read(fname)
10
11 % Define #header rows since changes based on month
12 month = str2num(fname(16:17)); %#ok<ST2NM>
13 if (month == 1) || (month == 3) || (month == 5) || (month == 7) ...
       ||...
14          (month == 8) || (month == 10) || (month == 12)
```

```
15      hL = 430;
16  elseif (month == 4) || (month == 6) || (month == 9) || (month == 11)
17      hL = 429;
18  elseif month == 2
19      year = str2num(fname(12:15)); %#ok<ST2NM>
20      fyear = rem(year,4);
21      if fyear == 0
22          hL = 428;
23      else
24          hL = 427;
25      end
26  end
27
28  % Convert data from csv file
29  fulldata = readtable(fname,'Delimiter',',','HeaderLines',hL);
30
31  dtcol = datetime(cellstr(table2cell(fulldata(:,1))),...
32      'InputFormat','yyyy-MM-dd HH:mm:ss.SSS');
33  Ecol = table2array(fulldata(:,23:29));
```

[**xls0812read.m**] - GOES-8 through GOES-12 .csv files

```
% Function for reading and converting data formatted under the ...
    GOES 08
% through GOES 12 satellites


% Created: 9/26/16
% Last modified: 9/26/16


function [dtcol,Ecol] = xls0812read(fname)

% Define #header rows since changes based on month
month = str2num(fname(16:17)); %#ok<ST2NM>
if (month == 1) || (month == 3) || (month == 5) || (month == 7) ...
    ||...
        (month == 8) || (month == 10) || (month == 12)
    hL = 454;
elseif (month == 4) || (month == 6) || (month == 9) || (month == 11)
    hL = 453;
elseif month == 2
    year = str2num(fname(12:15)); %#ok<ST2NM>
    fyear = rem(year,4);
    if fyear == 0
        hL = 452;
    else
        hL = 451;
    end
end
```

```
27
28 % Convert data from csv file
29 fulldata = readtable(fname,'Delimiter',',','HeaderLines',hL);
30
31 dtcol = datetime(cellstr(table2cell(fulldata(:,1))),...
32     'InputFormat','yyyy-MM-dd HH:mm:ss.SSS');
33 Ecol = table2array(fulldata(:,25:31));
```

[**xls1315Aread.m**] - GOES-13 and GOES-15 .csv files, “A” direction

```
% Function for reading and converting data formatted under the ...
    GOES 13-15
% satellites designated "A" (i.e. labeled "West" in data file) ...
    based on
% previous databases


% Created: 9/26/16
% Last modified: 9/26/16


function [dtcol,Ecol] = xls1315Aread(fname)

% Define #header rows since changes based on month
month = str2num(fname(25:26)); %#ok<ST2NM>
if (month == 1) || (month == 3) || (month == 5) || (month == 7) ...
    ||...
        (month == 8) || (month == 10) || (month == 12)
    hL = 718; %457 ==> 454  %721 ==> 718
elseif (month == 4) || (month == 6) || (month == 9) || (month == 11)
    hL = 717; %one less than above
elseif month == 2
    year = str2num(fname(12:15)); %#ok<ST2NM>
    fyear = rem(year,4);
    if fyear == 0
        hL = 716; %one less than above
    else
        hL = 715; %one less than above
```

```
26      end
27  end
28
29  % Convert data from csv file
30  fulldata = readtable(fname,'Delimiter',',','HeaderLines',hL);
31
32  dtcol = datetime(cellstr(table2cell(fulldata(:,1))),...
33      'InputFormat','yyyy-MM-dd HH:mm:ss.SSS');
34  Ecolwq = table2array(fulldata(:,16:29));
35  Ecol = ...
        [Ecolwq(:,2),Ecolwq(:,4),Ecolwq(:,6),Ecolwq(:,8),Ecolwq(:,10),...
36      Ecolwq(:,12),Ecolwq(:,14)];
```

[**xls1315Bread.m**] - GOES-13 and GOES-15 .csv files, “B” direction

```
% Function for reading and converting data formatted under the ...
    GOES 13-15
% satellites designated "B" (i.e. labeled "East" in data file) ...
    based on
% previous databases


% Created: 9/26/16
% Last modified: 9/26/16


function [dtcol,Ecol] = xls1315Bread(fname)

% Define #header rows since changes based on month
month = str2num(fname(25:26)); %#ok<ST2NM>
if (month == 1) || (month == 3) || (month == 5) || (month == 7) ...
    ||...
        (month == 8) || (month == 10) || (month == 12)
    hL = 718; %457 ==> 454  %721 ==> 718
elseif (month == 4) || (month == 6) || (month == 9) || (month == 11)
    hL = 717; %one less than above
elseif month == 2
    year = str2num(fname(12:15)); %#ok<ST2NM>
    fyear = rem(year,4);
    if fyear == 0
        hL = 717; %one less than above
    else
        hL = 716; %one less than above
```

```
26      end
27  end
28
29  % Convert data from csv file
30  fulldata = readtable(fname,'Delimiter',',','HeaderLines',hL);
31
32  dtcol = datetime(cellstr(table2cell(fulldata(:,1))),...
33      'InputFormat','yyyy-MM-dd HH:mm:ss.SSS');
34  Ecolwq = table2array(fulldata(:,2:15));
35  Ecol = ...
        [Ecolwq(:,2),Ecolwq(:,4),Ecolwq(:,6),Ecolwq(:,8),Ecolwq(:,10),...
36      Ecolwq(:,12),Ecolwq(:,14)];
```

B.1.3 Special Cases

These files are only needed if the data from a satellite has missing points or has an event close to the end of a month, which both require extra steps in order to calculate integrated fluence for an event.

[**extraGOESdata.m**] - function to add next month's data to the end of the current month being analyzed, process repeats till an event does not occur close to the end of a month

```
% See xlsGOESmain.m for details on what this file does as it ...
    does the same
% process, but only for one month, adding on data for events ...
    that run over
% into the next month.

% Created: 8/20/16
% Last modified: 9/26/2016 - fixed GOES no's...
% Last verified: 8/29/2016 - ran 1989 months that go over into ...
    the next,
% checking for missing file and wrong GOES no.

function [coldtx,colMeVx,echk] = ...
    extraGOESdata(coldt,colMeV,GOESn,des)

% Ask for next month
fnask = ['\nEnter file name for next month'...
    '(fname.csv)\n if no file exists, enter nothing\n'];
fname2 = input(fnask,'s');
```

```
16
17 % Separate out case of event not having a corresponding file for the
18 % next month with the same satellite
19 nofile = isempty(fname2);
20 if nofile == 1
21     echk = 1;
22     coldtx = coldt;
23     colMeVx = colMeV;
24     fprintf('Do not use last event of month\n\n')
25 else    % file present
26     echk = 0;
27     GOESnt = str2num(fname2(2:3)); %#ok<ST2NM> %not needed
28     testGn = isequal(GOESnt,GOESn);
29     if testGn == 0
30         fnask2 = ['\nRe-enter file name for next month, GOES'...
31             'number does not match\n if no file exists, enter ...
                nothing\n'];
32         fname2 = input(fnask2,'s');
33         nofile2 = isempty(fname2);
34         if nofile2 == 1
35             echk = 1;
36             coldtx = coldt;
37             colMeVx = colMeV;
38             fprintf('Do not use last event of month\n\n')
39         else
40             % Pass to appropriate xls read file
41             if des == 0
42                 if (GOESn == 6) || (GOESn == 7)
43                     [coldtx,colMeVx] = xls0607read(fname2);
44                 elseif (GOESn == 8) || (GOESn == 9) || (GOESn == ...
                        10) ||...
```

```
45                          (GOESn == 11) || (GOESn == 12)
46                      [coldtx,colMeVx] = xls0812read(fname2);
47                  end
48              elseif des == 1
49                  % Read 1st set - called "B"
50                  [coldtx,colMeVx] = xls1315Bread(fname2);
51              elseif des == 2
52                  % Read other direction - called "A"
53                  [coldtx,colMeVx] = xls1315Aread(fname2);
54              end
55              coldtx = [coldt; coldtx];
56              colMeVx = [colMeV; colMeVx];
57
58              % Update test vector
59              s_month = size(coldtx);
60              len = s_month(1);
61              c10MeV = colMeVx(:,3);
62
63              ev_testx = zeros(len,1);
64              for i = 1:1:len
65                  if c10MeV(i) ≥ 10
66                      ev_testx(i) = 1;
67                  end
68              end
69          end
70      else
71          % Pass to appropriate xls read file
72          if des == 0
73              if (GOESn == 6) || (GOESn == 7)
74                  [coldtx,colMeVx] = xls0607read(fname2);
75              elseif (GOESn == 8) || (GOESn == 9) || (GOESn == 10) ...
```

```
                ||...
76                  (GOESn == 11) || (GOESn == 12)
77                [coldtx,colMeVx] = xls0812read(fname2);
78            end
79        elseif des == 1
80            % Read 1st set - called "B"
81            [coldtx,colMeVx] = xls1315Bread(fname2);
82        elseif des == 2
83            % Read other direction - called "A"
84            [coldtx,colMeVx] = xls1315Aread(fname2);
85        end
86        coldtx = [coldt; coldtx];
87        colMeVx = [colMeV; colMeVx];
88
89        % Update test vector
90        s_month = size(coldtx);
91        len = s_month(1);
92        c10MeV = colMeVx(:,3);
93
94        ev_testx = zeros(len,1);
95        for i = 1:1:len
96            if c10MeV(i) ≥ 10
97                ev_testx(i) = 1;
98            end
99        end
100
101    end
102 end
```

[**missGOESdata.m**] - function to find and replace missing/erroneous data points in the satellite data due to connectivity problems or any number of other satellite data availability issues, and function also generates an Excel file listing the times in the data that points were filled

```
% Function file created to look for missing data in NOAA GOES proton
% spectra and fill in as appropriate.

% File set such that if around 10% of data overall or 24/288 in ...
    succession
% is missing, then event is declared "no good." From ...
    observations of data
% when processing manually, these seemed to be appropriate since ...
    over 10%
% of data missing generally indicates other issues (data ...
    chopping in and
% out) and 24/288 is 2 hours worth of data missing in which ...
    events can
% change dramatically (and keeps events for analysis that NOAA ...
    has listed).
% If different values are desired, user can edit first lines where
% constants occur: misspart = overall metric, missucc = ...
    succession metric

% Created: 8/11/2016
% Last modified: 9/27/2016 - fixed GOES no outputs
% Last verified: 9/27/2016 - 2001 data checked

% Next actions - sensitivity studies on missing data cutoffs
```

```
18
19 % Inputs:
20 % ev_specMeV = input event spectrum
21 % ev_dt = input date and time corresponding with spectrum
22 % ev_len = number of lines in event
23 % stfil = where starting to fill in Excel file (from previous edfil)
24 % Outputs:
25 % chk = test value for if too much missing data (0 indicates ...
       cannot use
26 %       event, 1 means filled some, 2 means no missing data)
27 % specMeVfil = filled spectrum with no more missing data points
28 % edfil = keeping track of where file is filled to for returning ...
       to it
29 % later
30
31
32 function [chk,specMeVfil,ptfil,edfil] = ...
33     missGOESdata(ev_dt,ev_specMeV,GOESn,ev_len,stfil,des)
34
35 % Initalize vectors for recording missing and filled data
36 misspart = 10;
37 missucc = 24;
38 % misspart = 5;
39 miss = zeros(ev_len,1);
40 missdt = ev_dt(1);      % 1st pt - never used or replaced, ...
       should never
41                         % have missing data
42 txtstart = stfil;
43
44 % Check for missing data in all columns
45 for i = 1:1:ev_len
```

```
46      if ev_specMeV(i,1) < 0
47          miss(i) = -1;
48      elseif ev_specMeV(i,2) < 0
49          miss(i) = -1;
50      elseif ev_specMeV(i,3) < 0
51          miss(i) = -1;
52      elseif ev_specMeV(i,4) < 0
53          miss(i) = -1;
54      elseif ev_specMeV(i,5) < 0
55          miss(i) = -1;
56      elseif ev_specMeV(i,6) < 0
57          miss(i) = -1;
58      elseif ev_specMeV(i,7) < 0
59          miss(i) = -1;
60      end
61  end
62
63  %-------------------------
64  % Edit missing data to be averages of before and after event
65
66  % Create while loop IC
67  miss_sum = sum(miss);
68  dt = 0;      % (no. of filled points)
69  test_many = -100*sum(miss)/ev_len;
70
71  % Continue till all missing data filled or too many missing points
72  if miss_sum == 0
73      % no missing points, no changes in energy matrix
74      specMeVfil = ev_specMeV;
75      chk = 2;
76      code = 'none missing';
```

```
77      dt = dt + 1;
78  elseif test_many > misspart
79      % More than misspart% of data missing
80      specMeVfil = ev_specMeV;
81      chk = 0;
82      code = 'too many overall';
83      dt = dt + 1;
84  else
85      while miss_sum < 0
86          miss_st = find(miss<0,1);    % Find first missing line
87          for j = miss_st:1:ev_len     % Find last missing line
88              if miss(j) == 0
89                  miss_end = j - 1;
90                  break
91              end
92          end
93
94          % Check if too many missing points (represents about 10% ...
                of day
95          % missing)
96          l_ck = miss_end - miss_st;
97          if l_ck ≥ missucc
98              miss_sum = 0;
99              chk = 0;
100             code = 'too many in succession';
101             dt = dt + 1;
102         else
103             % If not, then average and fill
104             ev_specfil = (ev_specMeV(miss_st-1,:) + ...
105                 ev_specMeV(miss_end+1,:))./2;
106             for k = miss_st:1:miss_end
```

```
107                 for m = 1:1:7
108                     ev_specMeV(k,m) = ev_specfil(m);
109                 end
110                 dt = dt + 1;
111                 missdt(dt) = ev_dt(k);
112                 % replace vector of filled data times
113                 miss(k) = 0;
114             end
115                 % reset values for looping again or exiting
116             miss_sum = sum(miss);
117             % fprintf('Miss sum = %f\n',miss_sum); % used to ...
                    check loop
118             chk = 1;
119             code = 'some filled';
120         end
121     end
122     % Save new output of energy matrix with missing points filled
123     specMeVfil = ev_specMeV;
124 end
125
126 % Set number of filled points
127 ptfil = dt;
128
129 % fil10chk = 100*ptfil/ev_len;
130 % if fil10chk > 5
131 %     chk = 0;
132 %     code = 'too many overall';
133 % else
134 %     % do nothing
135 % end
136
```

```
137
138 %-------------------------
139 % Print to text file with start of event as first line
140 % Setup ranges based on previous
141 row1 = txtstart;
142 chr1 = int2str(row1);
143 Rg1 = ['A',chr1];
144 Rg2 = ['B',chr1];
145 Rg3 = ['C',chr1];
146 Rg4 = ['D',chr1];
147
148 % Specify outputs and convert to cell for proper output
149 ev_dt1a = {datestr(ev_dt(1))};
150 if chk == 1
151     missdt_out = cellstr(datestr(missdt));
152 else
153     missdt_out = {'N/A'};
154 end
155 c_id = cellstr(code);
156
157 if des == 0
158     Gnodes_pre = int2str(GOESn);
159 elseif des == 1
160     desch = 'B';
161     GOESnch = int2str(GOESn);
162     Gnodes_pre = [GOESnch,desch];
163 elseif des == 2
164     desch = 'A';
165     GOESnch = int2str(GOESn);
166     Gnodes_pre = [GOESnch,desch];
167 end
```

```
168 Gno = {Gnodes_pre};
169
170
171 % Write to Excel file (note need sheet specifier, otherwise ...
       tries to
172 % use range as sheet)
173 xlwrite('GOESfilled.xlsx',Gno,'Sheet1',Rg1);
174 xlwrite('GOESfilled.xlsx',ev_dt1a,'Sheet1',Rg2);
175 xlwrite('GOESfilled.xlsx',missdt_out,'Sheet1',Rg3);
176 xlwrite('GOESfilled.xlsx',c_id,'Sheet1',Rg4);
177
178 %xlswrite('GOESfilled.xlsx',xls_outm,cRange) Does not work on a ...
       Mac...
179
180 %--------------------------
181 % Reset end to pass back to main file
182 % txtend = txtstart + dt;
183 edfil = txtstart;
```

B.2 Probabilistic Risk Code Files Content

The SPE probabilistic risk analysis model presented in this document includes several MATLAB code files and of them, the main files comprising the risk model are summarized here in order of use in the model during execution of the model. The model itself is in the third version, with the second version completed in January 2016 , and the original iteration in July 2014.

SPE Data file: Includes the test orbital vectors in [day, radius] form where day is the day within the solar cycle, not of a particular year and radius is the distance from the Sun in AU on any given day of the mission

Run Orbits D - 2016: This is the main call function to run a risk analysis and takes orbital vector, number of iterations, threshold dose, and confidence level percent as inputs. This file also asks for inputs during execution as to if the user wishes to save the results to a text file and if so, asks for relevant information about the run to be added to the results. The outputs of this file include a histogram plot for the SPEs during a mission and basic statistics (mean, median, confidence interval, minimum, maximum) on the:

- Number of SPEs
- Number of SPEs at the given threshold or above
- Proportion of SPEs out of the total meeting the threshold or above
- Transit dose
- Individual event doses

Run Orbits Print D: This file transfers the results of the model to a text file which is named based on the date and time it was produced.

SPE Time Dose Orbit: This file is called from the main run file (Run Orbits D - 2016) and contains the code to determine if a SPE occurs on a specific day (hazard function file called) and then if so, records the information and calls the function file that determines the dose and any orbital effects for that SPE.

SPE Hazard Function - 2016: Contains the adjusted beta distribution for characterizing the probability of an event during any day in the solar cycle. The probability is returned to the time dose orbit file to determine if a SPE occurs or not.

SPE Dose Prob F: This file is called from the time dose orbit file to determine the dose of an event through the procedures outlined in the main text of this document. Once these values are obtained, the values are passed back to the call file, and added to the vectors with this information.

All other files involved in this risk model were generated to understand the results or are now outdated in this third iteration.